Titre: Title:	Numerical modeling of the deformation in polymer blends under shear flow
Auteur: Author:	Azadeh Shahshahani
Date:	2005
Type:	Mémoire ou thèse / Dissertation or Thesis
Référence: Citation:	Shahshahani, A. (2005). Numerical modeling of the deformation in polymer blends under shear flow [Mémoire de maîtrise, École Polytechnique de Montréal]. PolyPublie. https://publications.polymtl.ca/7679/

UNIVERSITÉ DE MONTRÉAL

NUMERICAL MODELING OF THE DEFORMATION IN POLYMER BLENDS UNDER SHEAR FLOW

AZADEH SHAHSHAHANI
DÉPARTEMENT DE MATHÉMATIQUES ET DE GÉNIE INDUSTRIEL
ÉCOLE POLYTECHNIQUE DE MONTRÉAL

MÉMOIRE PRÉSENTÉ EN VUE DE L'OBTENTION
DU DIPLÔME DE MAÎTRISE ÈS SCIENCES APPLIQUÉES (M.Sc.A.)
(MATHÉMATIQUES DE APPLIQUÉES)
DÉCEMBRE 2005

Your file Votre référence
ISBN: 978-0-494-16853-0
Our file Notre référence
ISBN: 978-0-494-16853-0

UNIVERSITÉ DE MONTRÉAL

ÉCOLE POLYTECHNIQUE DE MONTRÉAL

Ce mémoire intituled :

NUMERICAL MODELING OF THE DEFORMATION
IN POLYMER BLENDS UNDER SHEAR FLOW

présenté par : SHAHSHAHANI Azadeh
en vue de l'obtention du diplôme de : Maîtrise ès science appliquées
a été dûment accepté par le jury d'examen constitué de :

M. AUDET Charles, Ph.D., président ;
M. DUFOUR Steven, Ph.D., directeur de recherche;
Mme HEUZEY Marie-Claude, ing. Ph.D., codirectrice de recherche;
M. BERTRAND François, Ph.D., membre.

To my dear son "Navid".

ACKNOWLEDGMENTS

I would like to extend my sincerest gratitude to my advisor Dr. Steven Dufour for his support, technical and professional guidance and patience throughout my study at "École Polytechnique de Montréal". He has always been available to answer my questions and discuss problems with me. Without his encouragement and help this work would not have been possible. I would like also to thank my co-advisor Dr. Marie-Claude Heuzey for her guidance and support at all levels. I feel honoured to have been their student.

Many thanks to the members of my master defence committee: Dr. Charles Audet and Dr. François Bertrand. Their suggestions during my master defence made this experience a professional and rewarding one.

I would also like to thank Dr. Ahamadi Malidi in our research group. He devoted much time to help me understand and modify the code. I am very grateful to my co-workers in the computer lab for their help and cooperation. To all, I would like to thank them for their great friendship and support.

I would also like to thank my parents, and my brother. No matter how far I was from Tehran, Iran, they always made me feel close to them and an important member of the family. I will always be grateful for their moral support, especially to my mother, for all those encouraging phone calls when she was far and for all the days that she was there for me. I would like to thank my life-partner for his constant encouragement and support. I would also like to thank my son Navid since he is one of the most important persons in my life. With them all, I'm truly blessed.

Last but not least, I would like to thank Dr. Pierre Carreau and the members of the NATEQ research team on microporous membranes, for the financial support that made this research possible.

RÉSUMÉ

Nous proposons un modèle numérique pour l'étude de la déformation d'une phase dispersée dans un mélange polymère, soumise à un écoulement cisaillé. Une méthodologie numérique transitoire, dans le cadre de la méthode des éléments finis, est utilisée pour la discrétisation des équations de conservation, de l'équation de transport de la variable utilisée pour la capture des surfaces libres et des équations constitutives. Nous considérons les fluides newtoniens et viscoélastiques. Pour ce qui est des fluides viscoélastiques, le modèle Oldroyd-B est utilisé. Les surfaces libres sont capturées à l'aide d'une stratégie eulérienne sur maillage fixe. La tension superficielle fait aussi partie de notre modèle afin d'étudier son influence sur la topologie des interfaces. Des techniques de mise-à-jour sont utilisées afin d'éliminer les oscillations et la diffusion numériques dans la solution discrète, pour d'obtenir une discrétisation précise des surfaces libres. Cette méthodologie est vérifiée et validée à l'aide de l'étude de plusieurs problèmes, tels qu'un écoulement de Poiseuille viscoelastique, le transport d'une goutte viscoélastique dans un écoulement de Poiseuille, la déformation d'une goutte viscoélastique dans un écoulement cisaillé et la déformation et la coalescence de gouttelettes dans une matrice viscoélastique.

ABSTRACT

A numerical model for studying the deformation of a dispersed phase in polymer blends under simple shear flow is presented. A transient numerical methodology, in the finite element framework, is used to discretize the conservation equations, the transport equation of the free surface capturing marker variable and the constitutive equations. Newtonian fluid and viscoelastic fluid are considered. In the case of a viscoelastic fluid, the Oldroyd-B model is considered. Interfaces are captured using an Eulerian fixed mesh strategy. Interfacial tension is also included in the numerical model in order to study its influences on the topology of interfaces. Post-processing techniques are applied to eliminate the numerical oscillations and diffusion in the discrete numerical, in order to have an accurate discretization of free surfaces. This methodology is verified and validated by studying a viscoelastic Poiseuille flow, the transport of a viscoelastic single drop in a Poiseuille flow, the deformation of a viscoelastic drop in a shear flow, and finally, the deformation and coalescence of drops in a shear flow.

CONDENSÉ EN FRANÇAIS

Les mélanges polymères sont reconnus comme étant une avenue intéressante pour produire de nouveaux matériaux possédant des propriétés spécifiques. Les mélanges polymères peuvent être miscibles ou immiscibles. Ceci dépend des interactions qui existent entre les chaînes moléculaires. Les mélanges polymères immiscibles qui mènent à des mélanges multiphases possèdent des propriétés différentes des polymères constituants, et ces propriétés sont aussi reliées à la morphologie du mélange. La morphologie d'un système multiphase évolue de façon complexe pendant le procédé de mélange, et lorsqu'en écoulement, la structure de ce mélange polymère immiscible sera modifiée. Une morphologie biphase est généralement formée de gouttelettes immergées dans une matrice polymère. Soumise à un écoulement en cisaillement simple, la morphologie biphase évolue de telle sorte que les gouttelettes s'allongent et coalescent. Un mélange polymère immiscible à morphologie co-continue peut ainsi être produit. En extrayant une des phases, à l'aide d'un solvant approprié, une membrane poreuse co-continue est produite, et celle-ci peut avoir une multitude d'applications dans divers procédés de séparation.

L'*objectif principal* de ce mémoire est la modélisation numérique des changements morphologiques des mélanges polymères immiscibles résultant d'un écoulement. Le design de nouveaux mélanges polymères, avec des propriétés spécifiques, est lié au contrôle de la morphologie du système multiphase. Les composantes du mélange sont habituellement immiscibles et par conséquent, le mélange obtenu a une morphologie biphase. Des situations plus complexes peuvent survenir lorsque plus de deux polymères sont mélangés ensemble. De plus, puisque les mélanges polymères sont utilisés dans des

applications industrielles, et puisque qu'une compréhension fondamentale du procédé n'est pas toujours possible, plusieurs produits obtenus par cette approche sont élaborés à l'aide d'une procédure d'essais et erreurs. Dans le but de contrôler ces procédés, et afin de prédire les propriétés du mélange polymère résultant, un point de départ simple est de considérer la déformation et le bris d'une seule gouttelette immergée dans un liquide, dans un écoulement bien défini, et par la suite d'étendre l'étude à une population de gouttelettes.

La difficulté principale rencontrée lors de la modélisation numérique d'écoulements multifluides est de déterminer de façon précise la position des surfaces libres, qui est inconnue a priori. Une autre difficulté est que les propriétés des fluides, qui influencent directement la dynamique des surfaces libres, tels la densité et la viscosité, sont souvent discontinues aux interfaces. De plus, l'influence de la tension interfaciale ne peut être négligée, afin d'être en mesure d'obtenir une représentation précise de la topologie des surfaces libres.

Plusieurs stratégies numériques sont proposées dans la littérature, pour la modélisation des écoulements à surfaces libres. La capture eulérienne de surfaces libres est populaire pour la modélisation des écoulements multifluides complexes, puisque cette méthode est facile à mettre en oeuvre et qu'elle peut aussi être utilisée pour traiter les écoulements à surfaces libres complexes, avec des interfaces qui se brisent et qui entrent en contact entre elles. Cependant, cette méthode est moins précise que les méthodes lagrangiennes puisque dans l'approche eulérienne les interfaces infiniment minces sont remplacées par une région de transition définie à l'aide d'une variable qui identifie la région occupée par chaque fluide. Cette variable est alors transportée par le champ de vitesse des fluides en résolvant une équation de transport. Cependant, si la stratégie

numérique globale n'est pas bien choisie, la capture des surfaces libres peut être imprécise à cause de l'incertitude inhérente à l'utilisation de la région de transition pour localiser les interfaces. Des problèmes d'oscillations et de diffusion numérique sont aussi observés avec les méthodes de capture d'interfaces. Ceci peut mener à une déformation de la région de transition de la variable transportée et par conséquent, à des problèmes de conservation de la masse. Ces imprécisions sont causées par la discrétisation de l'équation de transport, par les schémas d'intégration en temps et par le type de maillage utilisé. Il est alors important de choisir la bonne stratégie numérique afin d'être en mesure de faire un transport précis des surfaces libres, sans créer ou perdre de la masse artificiellement. Ce travail sera donc basé sur la méthode de la pseudo-concentration, qui consiste à transporter une variable discontinue (la pseudo-concentration). Le saut de cette variable est alors utilisé pour identifier la position des surfaces libres. Cette pseudo-concentration est advectée dans le domaine de calcul en résolvant une équation de transport à l'aide d'une méthode d'éléments finis stabilisée.

La simulation numérique d'écoulements de fluides viscoélastiques est toujours un problème difficile. Le choix du modèle qui décrit le comportement viscoélastique des fluides est central dans la stratégie de résolution du problème. Même s'il est bien connu qu'aucun modèle n'est parfait, certains modèles sont plus réalistes que d'autres. Dans cette étude, les résultats numériques seront obtenus à l'aide du modèle Oldroyd-B, puisqu'il s'agit d'un des modèles différentiels linéaires transitoires les plus simples, bien qu'il ne soit pas le plus représentatif du comportement des polymères fondus. Les composantes qui font que la simulation d'écoulements visccoélastiques est difficile, lorsque comparée aux problèmes newtoniens, sont présentes dans ce modèle. Les nombre

adimensionnels tels que le nombre de Weissenberg (pour les écoulements stationnaires) et le nombre de Deborah (pour les écoulements transitoires) sont utilisés pour quantifier le caractère viscoélastique des écoulements. Un des principaux défis des chercheurs est de prédire la comportement de ces fluides pour de grands nombres de Deborah. Au cours des dernières années consacrées à l'étude numérique des problèmes d'écoulements viscoelastiques à l'aide de la méthode des éléments finis, un problème de convergence a été observé, même pour de petites valeurs du nombre de Weissenberg. Plusieurs auteurs avancent qu'une cause possible de ce problème est numérique (un mauvais choix des conditions limites, la nature hyperbolique des équations, l'inaptitude de la méthode des éléments finis à bien discrétiser les singularités, etc). Le développement de nouvelles techniques de discrétisation éléments-finis, tout particulièrement pour les problèmes hyperboliques, a permis de résoudre partiellement le problème du « haut nombre de Weissenberg ». Par conséquent, le projet actuel sera basé sur la méthode de Galerkin discontinue pour la discrétisation des équations constitutives, afin d'éviter les limitations bien connues de la méthode de Galerkin, qui est sujette à des oscillations numériques lorsqu'elle est utilisée pour résoudre des équations hyperboliques.

Il est bien connu que la modélisation numérique de problèmes d'écoulements viscoélastiques est très coûteuse. Dans les géométries bidimensionnelles, il est nécessaire de discrétiser deux composantes en vitesse, la pression et les trois composantes du tenseurs symétrique des extra-contraintes. Cette situation devient plus compliquée dans le cadre d'applications tridimensionnelles, où le tenseur des extra-contraintes contient 6 inconnues et le vecteur de vitesses 3 composantes. Par conséquent, il est important de choisir une discrétisation appropriée pour les différentes variables afin de minimiser la

taille du système discret. De plus, la discrétisation des équations de conservation, de l'équation de transport de la pseudo-concentration et des équations constitutives mènent à un système global d'équations algébriques non linéaires. Il est alors nécessaire de construire une matrice jacobienne de grande taille. Ce système non linéaire doit alors être résolu à l'aide d'une méthode itérative performante. Une des méthodes les plus populaires est la méthode de Newton, étant donné l'ordre de convergence quadratique et sa robustesse lorsqu'une condition initiale suffisamment près de la solution analytique est utilisée.

Ce projet peut avoir plusieurs répercussions au niveau industriel. Une des applications les plus répandues des mélanges polymères est la production de membranes utilisées dans des procédés de séparation tels l'osmose inverse, la séparation de gaz à l'aide de membranes et l'ultra-filtration, selon la taille des pores. Les simulations numériques peuvent aider à prédire la morphologie de ces membranes haute performance avant de les produire, puisqu'elles nécessitent une quantité importante de temps de fabrication, d'énergie et de matériel. La méthodologie numérique développée pour ce projet peut être utilisée pour étudier d'autres types d'écoulements à surfaces libres complexes. Les résultats de ce projet peuvent être appliqués à différents matériaux afin de produire d'autres types de membranes possédant des propriétés diverses, pour différentes applications.

Dans le but de satisfaire notre objectif principal, nous proposons donc une méthodologie numérique transitoire, dans le cadre de la méthode des éléments finis. Cette méthodologie est constituée de la discrétisation des équations de conservation de la masse et de la quantité de mouvement à l'aide de la méthode de Galerkin, l'équation de transport de la pseudo-concentration est

discrétisée à l'aide de la méthode SUPG et les équations constitutives du modèle Oldroyd-B sont discrétisées à l'aide de la méthode de Galerkin discontinue.

Les interfaces sont capturées à l'aide d'une stratégie eulérienne sur un maillage fixe. Afin d'obtenir une modélisation précise de ces problèmes d'écoulements multifluides, il est important d'utiliser une technique de mise-à-jour afin de calculer une discrétisation précise de la fonction de pseudo-concentration. Plusieurs techniques ont été étudiées lors de ce travail, telles que la technique de mise-à-jour locale par moindres-carrés, l'utilisation du terme d'absorption non linéaire de Layton et Polman, la technique de filtration de Devals et al. et la régularisation par produit de convolution. Nous avons appliqué ces techniques afin d'améliorer la précision de la solution calculée, et pour éliminer les oscillations et la diffusion numériques qui sont produites par la discrétisation de l'équation de transport hyperbolique. Ces techniques peuvent éliminer la plupart des oscillations numériques. Nous avons observé que la technique de Devals et al. générait une région de transition de la pseudo-concentration qui est trop abrupte pour le modèle CSF. Ceci nous a mené à utiliser une technique de régularisation par produit de convolution. Nous avons alors observé qu'avec cette technique, il y a une relation entre le rayon du support du noyau et la taille des éléments du maillage. Si nous changeons la taille des éléments du maillage, le rayon du support du noyau doit être modifié afin d'obtenir des résultats précis. Nous ne savons toujours pas comment déterminer cette quatité de façon automatique. Plus de travail sera nécessaire afin de bien comprendre cette relation. L'approche de Layton et Polman n'a pas donné les résultats escomptés. Nous avons finalement choisi la technique de mise-à-jour locale par moindres-carrés. Même si cette technique n'est pas parfaite, elle nous a permis d'obtenir les meilleurs résultats pour les problèmes

étudiés. Il y a toujours un besoin pour une technique de mise-à-jour locale qui performe mieux. Il s'agit donc d'un problème ouvert.

Pour ce qui est de la discrétisation des équations constitutives, nous avons opté pour la formulation de Brown et al. Nous avons obtenu des résultats pour des nombres de Deborah relativement petits. Le terme de transport du tenseur vitesse-de-déformation doit cependant être calculé lorsque cette formulation est utilisée, ce qui implique le calcul des dérivées secondes de la vitesse discrète. Ce calcul est délicat. Une façon de contourner ce problème est de faire une intégration par parties pour éliminer cette dérivée seconde, ce qui peut aider à atteindre des nombres de Deborah un peu plus importants. Il aurait aussi été possible d'utiliser la formulation de Guénette et Fortin, qui devrait permettre d'atteindre des nombres de Deborah encore plus grands. Nous prévoyons utiliser cette formulation dans le futur.

La tension interfaciale a été incluse dans le modèle numérique afin d'en étudier l'influence sur la topologie des interfaces. Puisque la modélisation de la tension interfaciale nécessite le calcul des dérivées de la pseudo-concentration, afin d'obtenir les normales et la courbure des surfaces libres, la région de transition de la pseudo-concentration doit être abrupte mais régulière. Par conséquent, il serait nécessaire de raffiner le maillage afin de modéliser de façon précise la physique interfaciale, ce qui permettrait de considérer de plus grandes valeurs du coefficient de tension interfaciale pour en étudier son influence sur la topologie des interfaces. Une meilleure technique de mise-à-jour pour réinitialiser la pseudo-concentration, afin d'obtenir une transition abrupte mais régulière, serait aussi nécessaire.

L'approche numérique développée dans le cadre de ce travail a été validée à l'aide d'un problème d'écoulement de Poiseuille viscoélastique, et du transport d'une gouttelette viscoélastique dans un écoulement de Poiseuille. Une comparaison entre le problème d'écoulement de Poiseuille viscoélastique stationnaire et le problème d'écoulement de Poiseuille viscoélastique transitoire nous a permis de vérifier les schémas d'intégration en temps pour discrétiser les termes transitoires des équations de Stokes, de l'équation de transport de la pseudo-concentration et des équations constitutives. L'étude du transport d'une gouttelette viscoélastique dans un fluide newtonien a aussi permis de vérifier le transport de la pseudo-concentration et des composantes des contraintes viscoélastiques.

Ces travaux ont mené à l'étude de la déformation d'une gouttelette, et de plusieurs gouttelettes, dans un écoulement en cisaillement. La déformation d'une gouttelette viscoélastique, immergée dans un fluide newtonien cisaillé, a aussi été investiguée. Pour deux valeurs du nombre capillaire, nous avons observé que la plus grande valeur mène à une plus grande déformation de la gouttelette viscoélastique. Les mêmes résultats ont été obtenus par Yue et al. Les composantes des contraintes viscoélastiques ont été analysées pour différentes valeurs du temps de relaxation. Nous avons observé que de plus grandes valeurs du temps de relaxation (donc, un caractère élastique plus important) produisent de plus grandes valeurs des contraintes viscoélastiques dans la gouttelette. Finalement, la coalescence a été étudiée pour deux mélanges de polymères avec des concentrations différentes. Nous avons observé que le taux de coalescence est plus élevé pour le mélange avec la concentration la plus élevée. La concentration et la déformation totale semblent être les facteurs principaux qui

régissent le taux de coalescence. Ces observations sont en accord avec les résultats de Lyu et al.

Le plan du présent document est le suivant: dans le premier chapitre, une revue des fluides viscoélastiques et des méthodes qui sont utilisées pour la simulation numérique de l'écoulement de ces fluides est présentée. Le deuxième chapitre est dédié à la description du système d'équations aux dérivées partielles, incluant les équations constitutives pour les fluides viscoélastiques, aux méthodes de capture de surfaces libres et à la modélisation de la tension interfaciale. Le troisième chapitre est dédié à la discrétisation des équations aux dérivées partielles pour la modélisation des écoulements à surfaces libres de fluides viscoélastiques incluant la tension interfaciale. Les diverses méthodes d'éléments finis sont décrites, tels les méthodes de Galerkin et de Galerkin discontinue (GD). Quelques méthodes de stabilisation, tels les méthodes «streamline-upwind» (SU) et «streamline-upwind/Petrov-Galerkin» (SUPG), sont aussi présentées. Le quatrième chapitre contient une revue des techniques itératives utilisées pour résoudre les systèmes d'équations algébriques non linéaires, telle que la méthode de Newton. Une approche découplée pour la modélisation numérique d'un écoulement multifluide viscoélastique de type Oldroyd-B est aussi introduite. Dans le cinquième chapitre, quelques techniques utilisées pour contrôler les solutions numériques, provenant de la résolution de l'équation de transport de la pseudo-concentration, sont présentées. Les derniers chapitres sont consacrés à la vérification et à la validation de la méthodologie proposée, et à la modélisation de la déformation des mélanges polymères soumis à un écoulement en cisaillement.

TABLE OF CONTENTS

LIST OF FIGURES

LIST OF SYMBOLS AND ABBREVIATIONS

Geometries quantities:

Ω	: computational domain	18
Ω_1	: section of the domain occupied by fluid 1	27
Ω_2	: section of the domain occupied by fluid 2	27
$\partial\Omega$	: boundary of the computational domain	18
Γ	: boundary of the computational domain	18
Γ_0	: solid boundary of the domain	45
Γ^-	: inlet of the domain	45
Γ^+	: outlet of the domain	45
$\Gamma_{D\vec{u}}$	: boundary with Dirichlet condition on velocity	20
$\Gamma_{N\vec{u}}$	: boundary with Neumann condition on velocity	20
Σ	: free surface	27
$\vec{n}$	: external normal vector to Γ	20
$\vec{n}_\Sigma$	: normal vector to free surface	28
$\vec{\delta}_\Sigma$	: Dirac delta function defined on Σ	33
$\vec{u}_\Sigma$	: velocity of the free surface	28
κ	: local curvature of the free surface	31
$F(\vec{x})$	: pseudo-concentration in stationary problems	29
$F(\vec{x},t)$	: pseudo-concentration in transient problems	29
$\vec{x}$	: point inside the domain with coordinates (x,y)	29
R_1, R_2	: local radii of curvature of the interface	31
ΔS	: unit area	33
ΔV	: unit volume	33

Physical quantities:

$\vec{u}$	: velocity field of the fluid (u,v)	18
$\vec{u}_{D\vec{u}}$	:Dirichlet condition on velocity	20
$\vec{t}_{N\vec{u}}$	: Neumann condition on velocity	20
$\vec{u}_1$	: velocity of fluid 1	28
$\vec{u}_2$	: velocity of fluid 2	28
$\vec{u}_i$	: velocity on the i^{th} node of an element	37
$\vec{\varphi}_i$	: interpolation function	37
p	: hydrostatic pressure	19
p_1	: hydrostatic pressure of fluid 1	32
p_2	: hydrostatic pressure of fluid 2	32
$\bar{\bar{\sigma}}$	: Cauchy stress tensor	18
$\bar{\bar{\sigma}}_1$	: Cauchy stress tensor of fluid 1	31
$\bar{\bar{\sigma}}_2$	: Cauchy stress tensor of fluid 2	31
$\bar{\bar{\tau}}$	: extra-stress tensor	19
τ_{11}	: component 11 of the extra-stress tensor	31
τ_{22}	: component 22 of the extra-stress tensor	31
τ_{12}	: component 12 of the extra-stress tensor	31
$\bar{\bar{\tau}}_s$	: solvent contribution of the extra-stress tensor	20
$\bar{\bar{\tau}}_v$	: viscoelastic contribution of the extra-stress tensor	20
$\bar{\bar{\dot{\gamma}}}(\vec{u})$	: rate-of-strain tensor	21
$\dot{\gamma}_{wall}$	: shear rate at the solid wall of the domain	24
ρ	: density of the fluid	18
$\eta(\bar{\bar{\dot{\gamma}}})$	: viscosity of the fluid	21

η_0	: reference viscosity	22
$\eta_s(\dot{\bar{\bar{\gamma}}})$	: solvent viscosity for a polymer solution	21
$\eta_v(\dot{\bar{\bar{\gamma}}})$	: viscoelastic viscosity for a polymer solution	21
η_1	: viscosity of fluid 1	30
η_2	: viscosity of fluid 2	30
$\eta(F)$	: viscosity of the interface	30
$\vec{f}$	: external body force	18
n	: dimensionless parameter for the rheological models	22
$\vec{f}_s$	: surface capillary force	33
$\vec{f}_v$	: *volumic* capillary force	33
λ	: relaxation time of the fluid	23
ε	: dimensional material parameter	25
α	: interfacial tension coefficient	31
t	: time	19

Discrete quantities:

Ω_h	: discrete computational domain (mesh)	37
V_h	: discrete space in velocity	37
Q_h	: discrete space in pressure	37
W_h	: discrete space in pseudo-concentration	43
Φ_h	: discrete space for the viscoelastic stresses	48
K	: an element	37
K_1	: previous element	46
K_2	: current element	46

∂K_2^-	: inflow of element K_2	46
∂K_1^+	: outflow of element K_1	46
$\vec{u}_h$	: discrete approximation of the velocity	37
$\vec{v}_h$	: discrete test function for velocity	37
p_h	: discrete approximation of the pressure	38
q_h	: discrete test function for pressure	38
F_h	: discrete approximation of the pseudo-concentration	43
w_h	: discrete test function for pseudo-concentration	43
$\vec{\vec{\tau}}_{vh}$	: discrete approximation of the stresses	49
$\vec{\vec{\varphi}}_h$	: discrete test function for stresses	49
$P_2^+ - P_1$	: Crouzeix-Raviart element	39

Spaces:

V	: functional space for velocity	35
Q	: functional space for pressure	35
W	: functional space for pseudo-concentration	35
Φ	: functional space for stresses	35
$L^2(\Omega)$	: space of square integrable functions on Ω	35
$L^2(\Omega)^n$	: vectorial version of $L^2(\Omega)$	36
$H^1(\Omega)$	: Sobolev space defined on Ω	36
$H^1(\Omega)^n$	: vectorial version of $H^1(\Omega)$	36
$H^1_{D\vec{u}}(\Omega)^n$	: functions of $H^1(\Omega)^n$ with zero values on $\Gamma_{D\vec{u}}$	36
$W(\Omega)$	: functional space for studying transport problems	36
$L^2_{\vec{u}}(\Gamma)$	: space defined on the border of Ω for transport problems	36

$W_{\Gamma^-}(\Omega)$	: functions of $W(\Omega)$ with zero values on $\Gamma^-(\Omega)$	36

Matrices and vectors:

A	: viscous diffusion matrix	38
B	: divergence matrix	38
C	: convection matrix	43
$\vec{U}$	: vector containing the degrees of freedom in velocity	38
$\vec{P}$	: vector containing the degrees of freedom in pressure	38
$\vec{F}$	: vector containing the degrees of freedom in pseudo-concentration	43
$\vec{G}$	: related vector to the body force	38

Reference quantities and dimensionless numbers:

Re	: Reynolds number	24
We	: Weissenberg number	24
De	: Deborah number	24
U	: characteristic velocity of the flow	24
L	: characteristic length of the flow	24
Ca	: capillary number	96

Other symbols:

$\vec{\nabla}$	: gradient operator	18

$\bar{\bar{I}}$	: unit tensor	19
$\| \|$	: vectorial or tensorial norm	33
$[\ ]$	: jump of a quantity	46

Abbreviations:

FEM	: finite element method	12
PTT	: Phan-Thien and Tanner	25
CSF	: Continum Surface Force	32
LBB	: Ladyzhenskaya-Babuska-Brezzi	13
SU	: streamline-upwind	14
SUPG	: streamline-upwind Petrov-Galerkin	14
DG	: discontinuous Galerkin	14
LU	: matrix factorization	57
EEME	: explicitly elliptic momentum equation	15
EVSS	: elastic-viscous stress splitting	15
EVSS – G	: elastic-viscous split-stress Galerkin	15
DEVSS	: discrete elastic viscous stress splitting	16
GMRES	: generalized minimal residual	17
BDF2	: second order backward differentiation formula	39
IMR	: implicit midpoint rule	44
TR	: trapezoid rule	44
VOF	: volume-of-fluid	64

INTRODUCTION

Polymers blending is known as an attractive technique to produce new materials with desirable properties. Polymer blends can be miscible or immiscible. This depends on the specific interactions existing between the polymer chains. However, immiscible polymer blends leading to multiphase blends have characteristics of both polymers and is related to the morphology of the blend. The morphology of a multiphase system evolves in a complex manner during melt processing. Moreover, under an applied flow, this complex structure of immiscible polymer blends will also change. A two-phase morphology consists of drops that are immersed in a polymeric fluid. Under a simple shear flow, the two-phase morphology evolves in a way that makes the drops elongate and coalesce. Consequently, a co-continuous immiscible polymer blend can be produced. By extracting one of these phases, using a suitable solvent, a co-continuous porous membrane is produced, which can have a wide range of applications in various separation processes.

The *main objective* of this thesis is the numerical modeling of flow-induced morphological changes in immiscible polymer blends. The design of new polymer blends, with specific properties, is essentially related to the control of the morphology of the multiphase system. The components of the blend are usually immiscible and therefore the resulting blend has a two-phase morphology. More complex situations can arise when more than two polymers are mixed together. Moreover, since polymer blends are used in industrial applications, and an exact understanding of the process is not always possible, many of the related industrial products are designed and manufactured through an unsatisfactory process of trial and error. In order to

control these processes, and to predict the properties of the polymeric mixture, one valid starting point is to consider the deformation and breakup of a single drop within another liquid in a well-defined flow field.

The principal difficulty in performing the numerical modeling of multifluid flows is to accurately determine the position of free surfaces, which is *a priori* unknown. Another difficulty is that some of the physical properties of the fluids, which directly influence the dynamics of free surfaces, such as density and viscosity, are often discontinuous at the interfaces. Moreover, the influence of interfacial tension cannot be neglected, in order to obtain an accurate representation of the topology of the free surfaces.

Numerous numerical strategies are available in the literature for modeling free surface flows. Eulerian free surface capturing is popular with regard to the modeling of complex multifluid flows, since this method is easy to implement and it can also be used to tackle complex free surface flows, with interface splitting and reconnection. However, this method is known to be less accurate in comparison with the Lagrangian approach since the zero thickness interface used in the Lagrangian method is replaced by a transition zone through the use of a marker variable. This variable is then transported by the velocity field of the fluids by solving a transport equation. However, if the overall numerical strategy is not well chosen, free surface capturing can be inaccurate due to the uncertainty inherent in the use of the transition region to locate interfaces. Free surface capturing methods also suffer from numerical oscillations and diffusion. This can lead to the deformation of the region of transition of the marker variable, and consequently, to mass-conservation problems. These inaccuracies come from the discretization of the transport

equation, the time integration scheme and the mesh size. It is therefore important to choose the correct numerical strategy in order to perform an accurate transport of the free surfaces, without artificially losing or creating mass. This work will be based on the pseudo-concentration technique, which consists in transporting a discontinuous marker variable (the pseudo-concentration). The jump of this variable is then used to identify the location of the free surfaces. This pseudo-concentration is advected in the computational domain by solving a transport equation using a stabilized finite element method such as the SUPG method.

The numerical simulation of viscoelastic fluid flow problems remains a challenging task for researchers. The choice of a model for the viscoelastic behavior of the fluids is a decisive factor in an overall solution strategy. Although it is generally accepted that no existing model is perfect, some models are more realistic than others. In this study, the numerical results for the Oldroyd-B model will be used since it is one of the simplest nonlinear, time-dependent differential model. The characteristics that make a viscoelastic flow calculation challenging, when compared to a Newtonian problem, are present in this model. Non-dimensional numbers such as the Weissenberg number (for stationary flows) and the Deborah number (for transient flows) are used to quantify the viscoelastic character of the flows. One of the key concern for researchers is to predict the behavior of these fluids for high values of the Deborah number. The past years devoted to the numerical study of viscoelastic fluid flow problems, using the finite element method, have demonstrated a loss of convergence, even for small values of the Weissenberg number. It is more or less agreed on that the cause for these failures are purely numerical (improper boundary conditions, the hyperbolic nature of the

equations, inability of the standard finite element method to deal with singularities, etc...). The development of new finite element discretization techniques, especially with regard to hyperbolic problems, has led to a partial solution of the "high Weissenberg number problem." Consequently, the present project will draw on the discontinuous Galerkin method to discretize the constitutive equations in order to avoid the known limitations of the Galerkin method, which is known to be subject to numerical oscillations when solving hyperbolic equations.

It is well known that the numerical modeling of viscoelastic fluid flow problems is very costly. In two-dimensional geometries, we have to discretize two velocity components, the pressure, and three components of the symmetric extra-stress tensor. This situation is considerably more complicated for three-dimensional applications, where the extra-stress tensor has six unknown components. As a result, it is of the foremost importance to choose an appropriate method for the discretization of the different variables in order to minimize the size of the resulting global discrete system. Moreover, the discretization of the conservation equations, the transport equation of the pseudo-concentration and the constitutive equations will lead to a global system of nonlinear algebraic equations. This will require the computation of large Jacobian matrices. This nonlinear system must be solved through the use of an efficient iterative method. One of the most popular method is Newton's method due to its reliability and quadratic order of convergence, once an initial solution has been chosen sufficiently close to the real solution.

This project has a number of important implications, especially from an industrial standpoint. One of the most widespread application of polymer

blends is the production of membranes that are used in separation processes such as reverse osmosis, membrane gas separation, ultra-filtration and micro-filtration, depending on the pore size. Numerical simulations can help to predict the morphology of these membranes, before producing them, since it requires considerable time, energy and materials. The numerical methodology developed for this project can be used to study other types of complex free surface flows. The results of this project can be applied to a variety of materials in order to make different kinds of membranes with a wide range of properties, and for various purposes.

The plan of this work is as follows: In the first chapter, a review of viscoelastic fluids and the methods that are commonly used in the numerical simulation of the flow of these fluids are described. The second chapter is dedicated to a description of the system of governing equations and of some differential constitutive equations for viscoelastic fluids, to free surface capturing and to interfacial tension modeling. The third chapter is devoted to the discretization of the system of partial differential equations used for modeling viscoelastic free surface flows with interfacial tension. This chapter will seek to explain the finite element discretization methods, such as the Galerkin and discontinuous Galerkin (DG) methods. Some stabilization techniques, such as the streamline-upwind (SU) technique and the streamline-upwind/Petrov-Galerkin (SUPG) technique will be discussed as well. Chapter four will review the iterative procedures employed for solving the nonlinear algebraic system of equations, such as Newton's method. An uncoupled approach for the numerical modeling of an Oldroyd-B viscoelastic multifluid flow is also presented as well. In the fifth chapter, some techniques used to control numerical oscillations and diffusion, resulting from solving the

transport equation, are presented. The last chapters are devoted to the verification and the validation of the proposed methodology, and to the modeling of the deformation of polymer blends under shear flow.

CHAPTER 1

THE NUMERICAL MODELING OF VISCOELASTIC FREE SURFACE FLOWS AND POROUS MEMBRANES

1.1 Polymer Blends

Blending polymers produce new materials, which can have numerous properties that will be obtained by an appropriate choice of the initial components. This technique seems to be an economical choice for synthesizing new polymers. Polymer blends can be miscible or immiscible, and they are completely determined by the specific interactions existing between the polymer chains. During melt processing, the microstructure of the multiphase blend develops in a very complex manner. When a multiphase system is submitted to an external solicitation, some phenomena such as deformation, break-up, and coalescence of the dispersed phase can take place [1]. It is well known that by mixing a small amount of a given polymer to a common bulk polymer, a new material with desirable properties can be produced [2]. The final properties of this product are dependent on the morphology of the dispersed phase, such as the size, shape and orientation of droplets. Therefore, the permeability of the membranes obtained from the resulting product can be tailored by controlling the blend morphology.

There are many factors that influence the morphology of a multiphase blend: the viscosity ratio, viscoelasticity, interfacial tension, the blend composition and the flow type. The influence of these parameters on the morphology of the material has been described by Favis [3], and by Utracki

and Shi [4]. Martin et al. [1] studied the deformation of dispersed high-density polyethylene immersed in a matrix of polystyrene under shear flow. In the range of small shear rates, these polymers can be assumed to be Newtonian fluids. They reported that the morphological changes in this polymer blend is due to coalescence, and not to break-up, which shows that the influence of interfacial tension is important. The evolution of the morphology of the dispersed phase of immiscible polymer blends in simple shear and elongational flows has been studied in details by Lacroix et al. [5]. They have shown that the flow conditions can considerably affect the morphology. The influence of these factors is not completely understood, and controlling the microstructure of immiscible polymer blends is therefore still difficult to achieve. Furthermore, since flow conditions cannot be completely controlled, and a direct observation of the blending process is not always possible, only qualitative relations between morphology and processing conditions have been proposed so far.

1.2 Methods for Studying Morphology Evolution

In order to follow the evolution of the morphology of multiphase polymer systems during processing, different techniques have been developed. Martin et al. [1] have reported that the first technique used was direct observation by way of optical microscopy. This approach was successful and has been used by many scientists between the years 1980 and 1998. Since most of the commercial blends at high concentrations of the dispersed phase are not transparent, this technique is not very practical. Another technique is the light scattering method, which can be used for investigating multi-drop

systems. But this technique is also limited to very low concentrations of the dispersed phase.

In order to study the changes in the morphology of multiphase polymer systems, scientists focused their attention on isolated drops submitted to large deformations leading to breakup, without considering coalescence and drop-drop interactions. Some indirect techniques have been proposed between the years 1997 and 1999 for studying concentrated systems and the importance of coalescence and breakup [1]. In these cases, the deformation of the blend morphology was not studied in real time. The flow was stopped when a steady-state microstructure was reached and then the samples were allowed to relax. The blends were then analyzed using optical devices, or cooled down in order to freeze the microstructure and then they were analyzed by electron microscopy. Important information about drops deformation and the evolution of the size of the dispersed phase could be obtained by using this method. Unfortunately, because of the interfacial tension, the deformed drops would recover their equilibrium shape during the relaxation process. Highly deformed drops would also break into droplets. The real morphology of the blend could not be obtained using this technique.

Martin et al. [1] presented a new indirect method to determine the shear-induced morphology of highly concentrated polymer blends. The morphology of the sample is frozen at constant stress between the parallel plates of a rheometer. This method makes it possible to understand the morphology/rheology/processing interrelationship in multiphase systems.

1.3 Porous Membranes

Porous membranes are one of the most useful products that can be obtained from immiscible polymer blends. These membranes are used for different separation processes, such as reverse osmosis, membrane gas separation, ultra-filtration and micro-filtration, depending on the pore size. Many techniques are available in order to produce these kinds of membranes such as the casting technique and the track-etching technique, which are described in Riscanu et al. [6].

There are two major categories of immiscible blend morphologies. One of them is the dispersed phase/matrix morphology and the other one is the co-continuous morphology. When both immiscible components are completely continuous throughout the blend system, it produces a co-continuous morphology. Solvent extraction of one of the component of a co-continuous blend results in the complete removal of that specific phase [7]. By extracting one of the two phases in a co-continuous blend, a well-controlled high volume porous structure with continuous pores in the micro-filtration region can be obtained [6].

1.4 Characteristics of Viscoelastic Fluids

The most outstanding non-Newtonian effects are exhibited by polymers or their mixtures. These effects differ qualitatively from the behavior of Newtonian fluids. To understand the source of these effects, a more detailed understanding of rheology is necessary.

1.4.1 The Weissenberg Effect

When Newtonian fluids, such as water or oil, are stirred at high velocity, the fluid is flung away from the rotating rod because of inertia. Non-Newtonian fluids, however, do not flow to the outer wall of the bowl when stirred at high velocity. They climb the rotating rod due to viscoelastic forces. This effect is known as the Weissenberg effect, and it cannot be explained through the relationships that govern Newtonian fluids. Therefore, it is essential to use rheological constitutive equations in order to capture these nonlinear effects.

1.4.2 Fluid Memory

When a stress is applied to Newtonian fluids, they deform and flow. When the stress is removed, the flow stops immediately and the total deformation remains unchanged. Viscoelastic fluids submitted to a stress also deform, but when the stress is removed, only a part of the deformation is recovered over some time. For these fluids, the internal molecular configuration can release the stored energy. The relaxation time, or the time over which the deformation is recovered, differs widely among different materials.

1.4.3 Die Swell

Polymers exhibit die swell, which means that as the polymer exits a die, the diameter of the liquid stream increases. Die swell is caused by the relaxation of extended polymer coils as the stress in a polymeric liquid

reduces from the top to the bottom. In the case of Newtonian fluids, swelling is observed, but it is not as important as in the case of viscoelastic fluids, and it is only due to the velocity profile rearrangement at the exit of the die.

1.5 Key Problems in the Simulation of Viscoelastic Fluid Flows

The numerical simulation of viscoelastic fluid flows remains a significant challenge for researchers. During the past few decades, the simulation of viscoelastic fluid flows, using finite element methods and finite volume methods, progressed considerably. As mentioned previously in the introduction, the most important problem is the loss of convergence of almost all numerical schemes for high values of the Weissenberg number. Researchers have found that because of the hyperbolic nature of the constitutive equations, the traditional Galerkin FEM is not practical for addressing problems where even small amounts of viscoelasticity are involved. This problem concerns the convection term $(\vec{u}\cdot\vec{\nabla}\bar{\bar{\tau}})$, arising from the viscoelastic nature of the fluid. As the Weissenberg number is raised, the influence of the convective term increases significantly, and the traditional Galerkin FEM, which suffers from oscillations, can no longer give reliable results. This is known as the "high Weissenberg number problem". The Weissenberg number corresponds to the Deborah number in transient flows.

Another possible cause for this problem is due to the rheological models that characterize the viscoelastic fluids. Even though these models can describe most of the behaviors of viscoelastic fluids, they are singular close to boundary singularities. A number of constitutive equations have been suggested during the last years [24]. The choice of suitable constitutive

equations and the determination of rheological constants is a critical step in numerical simulations. The constitutive equations should at least give adequate predictions in simple rheometrical flows. Computing solutions of viscoelastic fluid flow problems is very costly since, in two-dimensional geometries, two velocity components, the pressure and three components of the extra-stress tensor, have to be discretized. That is to say, except for simulations with integral models, most of the simulations in the literature consider simple and not realistic differential models, such as the Oldroyd-B or the Phan-Thien and Tanner constitutive equations, with only one relaxation time. It is worth mentioning that a multi-mode model is a generalization of the one-mode model. In a multi-mode model, a spectrum of relaxation times are used instead of using only one relaxation time, which is the case in a one-mode model. Using a spectrum of relaxation times allows more realistic fitting of the rheological data.

Another problem with viscoelastic finite element simulations is that a compatibility condition for velocity, pressure and the extra-stress unknowns is necessary. It is recognized that with purely Newtonian problems, this compatibility condition, known as the Ladyzhenskaya-Babuska-Brezzi (LBB) condition [8], must be satisfied for all velocities and pressure components. Likewise, the addition of the weak form of the constitutive equations necessitates a compatibility condition on the interpolation functions of the triplet stress-velocity-pressure. It has been shown by Fortin and Pierre [9] that a stable mixed discretization of velocity, pressure and of the extra-stresses has to satisfy a generalized LBB condition.

1.6 Finite Element Methods for Solving Hyperbolic Equations

Several finite element methods exist for solving hyperbolic equations. The most widespread method to account for the convective term in the hyperbolic constitutive equations is the streamline-upwind/Petrov-Galerkin (SUPG) method developed by Brooks and Hughes [10], and first applied to viscoelastic flows by Marchal and Crochet [11]. They have shown that the SUPG method may produce oscillatory stress fields at steep stress boundary layers or near singularities. To circumvent this problem, they proposed to use the streamline-upwind (SU) formulation. Convergence up to very high values of the Weissenberg number was obtained for some benchmark problems such as the stick-slip problem and the 4-to-1 contraction, using this formulation. However, Crochet and Legat [12] showed that the SU method is only first-order accurate with respect to the extra-stresses.

An alternative to the SUPG or SU method is the discontinuous Galerkin (DG) or Lesaint-Raviart method. The extra-stress tensor is approximated discontinuously from one element to the next. In the context of viscoelastic fluid flow problems, this method was first introduced by Fortin and Fortin [13]. Both the SUPG and the DG methods have the formal advantage of proven convergence for linear first-order hyperbolic equations and for interpolation functions of all degree [14]. The interpolation functions are discontinuous across element boundaries for the DG method, whereas Lagrangian polynomials are used for the SUPG and the SU methods.

Researchers have pointed out several requirements for studying viscoelastic flow problems using finite element methods [14]. The formulation

has to be split into the resolution of the momentum and the continuity equations in order to calculate the velocity and pressure fields, and the extra-stress field using the hyperbolic constitutive equations. The momentum and sometimes the constitutive equations are reformulated in order to make explicit the elliptic character of the equations with respect to the velocity field. An appropriate discretization technique has then to be applied for solving the hyperbolic equations at moderate and high values of the Deborah number. These features were first implemented in the EEME (Explicitly Elliptic Momentum Equation) method, for the solution of the upper-convected Maxwell model, by King et al. [15], and were then generalized in the EVSS (Elastic-Viscous Split-Stress) method for constitutive models of the Oldroyd-B type by Rajagopalan et al. [16]. The EVSS method is based on a splitting of the extra-stress tensor into a viscous part and a viscoelastic part. Moreover, the rate-of-deformation tensor is introduced as an additional unknown.

The EVSS method, introduced by Chang et al. [17] and applied by Fortin et al. [18], is very popular today. According to Fortin et al. [18], this formulation enhances the convergence properties of numerical schemes. Brown et al. [19] have introduced least-squares interpolation of the velocity components in the EVSS-G formulation, and it was shown to enhance the temporal numerical stability of the finite element method. The EEME and EVSS formulations were important improvements over the previous methods, and stable and accurate calculations were possible at moderately high values of the Deborah number. However, there are levels of viscoelasticity that cannot be calculated with these methods, in almost every flow problems and for any given finite element meshes.

Since the numerical stability of these methods comes from the viscous term, if this term is dominant with respect to the viscoelastic stress contribution, the method performs better. Guénette and Fortin [20] have introduced a modification of the EVSS formulation. It consists of a discrete elastic viscous stress splitting (DEVSS) through the introduction of a stabilizing elliptic operator in the discrete version of the momentum equation. The DEVSS method is similar to the EVSS method but the computation of the objective derivative of the rate-of-strain tensor is avoided, and it is not restricted to a particular class of constitutive equations. It is also easier to impose boundary conditions. Liu et al. [21] have expanded the DEVSS method to develop the DEVSS-G formulation. The DEVSS-G method is based on the idea of a mixed formulation, which splits the viscous and viscoelastic components of the stresses. A continuous approximation, G, of the numerically discontinuous velocity gradient tensor, $\vec{\nabla}\vec{v}$, is introduced. In other words, a continuous interpolation of the velocity gradient is used. The numerical difference between G and $\vec{\nabla}\vec{v}$ is used to maintain the elliptic character of the momentum equation, leading to the satisfaction of the compatibility condition for velocity and the extra-stress. Hooper et al. [2] have used this method for modeling drop deformations.

1.7 Resolution of the Nonlinear Algebraic System of Equations

Newton's method is popular for solving the system of nonlinear algebraic equations coming from the discretization of partial differential equations with the finite element method. If the initial estimate is regular and close enough to the solution, it is known to converge quadratically [22].

However, the finite element discretization can lead to huge nonlinear systems of equations that require the computation of very large Jacobian matrices. The approximations of velocities, pressure and stresses have to be obtained at each node of a very fine mesh. As a result, Newton's method is not practical for multi-mode constitutive equations or for three-dimensional geometries. Fortin et al. [18] have used a Newton-Krylov method based on the generalized minimal residual (GMRES) algorithm in order to retain the good convergence properties of Newton's method, while avoiding the explicit construction of the large Jacobian matrices. They used the Lesaint-Raviart method [23] to discretize the constitutive equations, avoiding the construction of a large matrix for the computation of the stresses. Their method is interesting, especially for studying three-dimensional problems.

Béraudo et al. [22] proposed a finite element discretization which is a compromise between a fully coupled, and a decoupled method for the Stokes and the viscoelastic constitutive equations. It is based on Newton's method and on a discontinuous approximation of the components of the extra-stress tensor. This method allows the elimination of the stress variable at the element level by means of a static condensation technique, using the discontinuous interpolation of the stresses. Using this technique, a non-symmetric system with only the velocity degrees of freedom remaining, can be obtained. The advantage of this scheme is in the reduction of the storage requirements to that of the Stokes problem. This method can thus serve as an efficient algorithm for multi-mode models.

CHAPTER 2

EQUATIONS MODELING VISCOELASTIC MULTIFLUID FLOW PROBLEMS

In order to conduct the numerical modeling of viscoelastic multifluid flow problems, the following equations have to be considered:

the Stokes problem;

the constitutive equations;

the transport equation of the pseudo-concentration.

2.1 Stokes Problem

Numerical modeling of transient, incompressible, isothermal multifluid flow problems, of either Newtonian or viscoelastic fluids, requires the resolution of the Stokes problem for each fluid. In a two-dimensional geometry, $\Omega \subset R^2$ is considered as the whole computational domain with the boundary $\Gamma = \partial\Omega$. In this type of problem, mass conservation is expressed as

$$\frac{\partial \rho}{\partial t} + \vec{\nabla} \cdot (\rho \vec{u}) = 0, \qquad \text{in } \Omega. \qquad (2.1)$$

Assuming fluid incompressibility (ρ is constant), mass conservation is simplified as

$$\vec{\nabla} \cdot \vec{u} = 0, \qquad \text{in } \Omega. \qquad (2.2)$$

Conservation of momentum for this type of problem is expressed as

$$\rho \frac{D\vec{u}}{Dt} = \vec{\nabla} \cdot \bar{\bar{\sigma}} + \vec{f}, \qquad \text{in } \Omega, \qquad (2.3)$$

where:

ρ : fluid density;

$\vec{u}$: velocity field of the fluid;

$\frac{D\vec{u}}{Dt} = (\frac{\partial \vec{u}}{\partial t} + \vec{u} \cdot \vec{\nabla} \vec{u})$: substantial derivative;

$\bar{\bar{\sigma}}$: Cauchy stress tensor;

$\vec{f}$: external force, which includes gravity.

As a result, the momentum equations can be written as

$$\rho(\frac{\partial \vec{u}}{\partial t} + \vec{u} \cdot \vec{\nabla} \vec{u}) = \vec{\nabla} \cdot \bar{\bar{\sigma}} + \vec{f}, \tag{2.4}$$

so that

$$\bar{\bar{\sigma}} = \bar{\bar{\tau}} - p\bar{\bar{I}},$$

where:

$\bar{\bar{\tau}}$: extra-stress tensor;

p: hydrostatic pressure;

$\bar{\bar{I}}$: unit tensor.

Since most applications for polymers involve very small Reynolds numbers, the inertia term can be neglected. Consequently, the momentum equations (2.4) can be written as follows:

$$\rho(\frac{\partial \vec{u}}{\partial t}) = \vec{\nabla} \cdot \bar{\bar{\tau}} - \vec{\nabla} p + \vec{f}. \tag{2.5}$$

Accordingly, the system of Stokes equations is given by:

$$\begin{cases} \rho(\frac{\partial \vec{u}}{\partial t}) + \vec{\nabla} p = \vec{\nabla} \cdot \bar{\bar{\tau}} + \vec{f}; \\ \vec{\nabla} \cdot \vec{u} = 0. \end{cases} \tag{2.6}$$

The above system of equations has to be satisfied everywhere in the domain Ω. Appropriate boundary conditions of Dirichlet and Neumann types

complete the description of system (2.6). These boundary conditions are as follows:

$$\begin{cases} \vec{u} = \vec{u}_{D\vec{u}} & \text{on} \quad \Gamma_{D\vec{u}}; \\ \bar{\bar{\sigma}} \cdot \vec{n} = \vec{t}_{N\vec{u}} & \text{on} \quad \Gamma_{N\vec{u}}, \end{cases}$$

where $\vec{n}$ is the unit normal to the boundary Γ. $\Gamma_{D\vec{u}}$ and $\Gamma_{N\vec{u}}$ are the domains of the Dirichlet and the Neumann boundary conditions, which satisfy:

$$\begin{cases} \Gamma_{D\vec{u}} \cup \Gamma_{N\vec{u}} = \partial\Omega; \\ \Gamma_{D\vec{u}} \cap \Gamma_{N\vec{u}} = \varnothing. \end{cases}$$

2.2 Constitutive Equations

Viscoelastic fluids behave in a more complex manner than Newtonian fluids. The mathematical formulation of this physical behavior can be obtained by the so-called constitutive equations, which give the relationship between the extra-stress tensor and the velocity field. Choosing an appropriate model to simulate the viscoelastic behavior of the fluid is a critical step. However, it is generally accepted that no existing model is perfect and none of them can predict the exact behavior of a viscoelastic fluid.

In an Oldroyd-B framework, $\bar{\bar{\tau}}$ consists of two parts. One part is the solvent extra-stress component, and the other part is the viscoelastic extra-stress. We therefore have

$$\bar{\bar{\tau}} = \bar{\bar{\tau}}_s + \bar{\bar{\tau}}_v,$$

where:

$\bar{\bar{\tau}}_s$: solvent contribution of the extra-stress tensor;

$\bar{\bar{\tau}}_v$: viscoelastic contribution of the extra-stress tensor, which will be obtained through a constitutive equation.

The splitting expressed in the above expression is arbitrary and user-defined, and it can have a significant influence on the stability of the numerical scheme [24]. The viscous contribution is expressed by

$$\bar{\bar{\tau}}_s = 2\eta_s(\bar{\bar{\dot{\gamma}}})\bar{\bar{\dot{\gamma}}}(\vec{u}),$$

where:

$\eta_s(\bar{\bar{\dot{\gamma}}})$: solvent viscosity for a polymer solution.

Considering $\eta(\bar{\bar{\dot{\gamma}}}) = \eta_s(\bar{\bar{\dot{\gamma}}}) + \eta_v(\bar{\bar{\dot{\gamma}}})$, $\eta(\bar{\bar{\dot{\gamma}}})$ is the total viscosity of the polymer solution, and $\eta_v(\bar{\bar{\dot{\gamma}}})$ is the viscosity of the viscoelastic part. $\bar{\bar{\dot{\gamma}}}(\vec{u})$ is the rate-of-strain tensor, that is expressed as

$$\bar{\bar{\dot{\gamma}}}(\vec{u}) = \frac{1}{2}[\vec{\nabla}\vec{u} + (\vec{\nabla}\vec{u})^T],$$

with $(\vec{\nabla}\vec{u})_{ij} = \dfrac{\partial \vec{u}_i}{\partial x_j}$.

Therefore, in the case of a viscoelastic fluid flow problem (of an Oldroyd-B type), the system of equations (2.6) is incomplete without the specification of the extra-stress tensor. As a result, this system is rewritten as follows:

$$\begin{cases} \rho(\dfrac{\partial \vec{u}}{\partial t}) - \vec{\nabla}\cdot[2\eta_s(\bar{\bar{\dot{\gamma}}})\bar{\bar{\dot{\gamma}}}(\vec{u})] + \vec{\nabla}p = \vec{\nabla}\cdot\bar{\bar{\tau}}_v + \vec{f}; \\ \vec{\nabla}\cdot\vec{u} = 0; \\ H(\vec{u}, \vec{\nabla}\vec{u}, \bar{\bar{\tau}}_v) = 0, \end{cases} \qquad (2.7)$$

where $H(\vec{u},\vec{\nabla}\vec{u},\bar{\bar{\tau}}_v)=0$ represents the constitutive equations in terms of the viscoelastic part of the extra-stresses.

2.3 Rheological Behavior

Rheology is the study of the flow and deformation of materials. The focus of rheology is on the study of relations between stress and deformation in fluids. These relations are expressed in terms of constitutive equations, which mathematically relate the stress to the strain. Stress is a nonlinear function of the strain, or rate of strain. With generalized Newtonian fluids i.e. fluids for which the flow behavior is entirely described by their viscosity, different rheological models are available such as the Newtonian, the power law and the Carreau models.

2.3.1 Newtonian Model

In this model, $\eta=\eta_0$ where η_0 is a constant viscosity that depends only on temperature and pressure.

2.3.2 Power Law Model

The most popular type of generalized Newtonian fluid is the power law fluid that is defined as

$$\eta(\bar{\bar{\dot{\gamma}}})=\eta_0\bar{\bar{\dot{\gamma}}}^{n-1}, \qquad 0\le n\le 1,$$

where n is the power law index, whish is dimensionless.

2.3.3 Carreau Model

The Carreau model is also a function of the strain rate and is given by:

$$\eta(\bar{\bar{\dot{\gamma}}}) = \eta_0[1 + (\lambda\bar{\bar{\dot{\gamma}}})^2]^{\frac{n-1}{2}},$$

where n is the power law index which is dimensionless, λ is a time constant. η_0 is a viscosity defined in the limit of low shear rate, which is given by:

$$\eta_0 = \lim_{\dot{\gamma}\to 0}\eta(\bar{\bar{\dot{\gamma}}}).$$

2.4 Differential Viscoelastic Constitutive Equations

A mathematical model for viscoelastic fluid is given by $H(\vec{u},\vec{\nabla}\vec{u},\bar{\bar{\tau}}_v) = 0$. For the differential models, this relation is based on the Oldroyd law [25], which can be expressed as

$$A(\bar{\bar{\tau}}_v)\cdot\bar{\bar{\tau}}_v + \lambda\frac{\delta}{\delta t}\bar{\bar{\tau}}_v = 2\eta_v(\bar{\bar{\dot{\gamma}}})\bar{\bar{\dot{\gamma}}}(\vec{u}), \qquad (2.8)$$

where λ represents a characteristic relaxation time for the polymer system and $\eta_v(\bar{\bar{\dot{\gamma}}})$ is the viscoelastic part of the viscosity. $\frac{\delta}{\delta t}$ is a combination of the lower-convected derivative and the upper-convected derivative:

$$\frac{\delta}{\delta t} = a\frac{\delta^{(1)}}{\delta t} + (1-a)\frac{\delta_{(1)}}{\delta t}, \qquad 0 \le a \le 1,$$

with:

lower-convected derivative: $\dfrac{\delta^{(1)}}{\delta t}\bar{\bar{\tau}}_v = \dfrac{\partial\bar{\bar{\tau}}_v}{\partial t} + (\vec{u}\cdot\vec{\nabla})\bar{\bar{\tau}}_v + \vec{\nabla}\vec{u}^T\cdot\bar{\bar{\tau}}_v + \bar{\bar{\tau}}_v\cdot\vec{\nabla}\vec{u}$;

upper-convected derivative: $\dfrac{\delta_{(1)}}{\delta t}\bar{\bar{\tau}}_v = \dfrac{\partial\bar{\bar{\tau}}_v}{\partial t} + (\vec{u}\cdot\vec{\nabla})\bar{\bar{\tau}}_v - \vec{\nabla}\vec{u}\cdot\bar{\bar{\tau}}_v - \bar{\bar{\tau}}_v\cdot\vec{\nabla}\vec{u}^T$.

Obviously, equation (2.8) may not describe the exact behavior of all viscoelastic fluids. For example, it is well known that in order to describe the rheology of most viscoelastic fluids, a spectrum of relaxation times is necessary, even in the limit of small deformations. Such a spectrum may be described by a finite set of independent relaxation times, and a constitutive equation of the form of equation (2.8) can be used for each relaxation time. However, for the sake of simplicity, a single relaxation time with a constitutive equation that obeys equation (2.8) is considered in this work.

The presence of the two terms $A(\bar{\bar{\tau}}_v)$ and $(\vec{u}\cdot\vec{\nabla})\bar{\bar{\tau}}_v$ make the constitutive equations nonlinear. Therefore, $\bar{\bar{\tau}}_v$ cannot be expressed as a function of $\vec{u}$ and be carried out in the momentum equation to obtain the traditional Stokes equation.

2.4.1 Dimensionless Numbers

The dimensionless numbers that are used to describe viscoelastic fluid flows are defined as follows:

Reynolds number: $\mathrm{Re} = \rho\frac{UL}{\eta}$;

Weissenberg number: $We = \lambda\frac{U}{L}$;

Deborah number: $De = \lambda\dot{\gamma}_{wall}$,

where:

ρ : fluid density;

U : characteristic velocity of the flow;

L : characteristic length of the flow;

η: fluid viscosity;

λ : relaxation time of the fluid;

$\dot{\gamma}_{wall}$: shear rate at the solid wall of the domain

2.4.2 Examples of Differential Models

The choice of the operator $A(\bar{\bar{\tau}}_v)$ in the constitutive equation contributes to the simplification of the model described in [25]. Actually, by choosing $A(\bar{\bar{\tau}}_v) = \bar{\bar{I}}$ and $\eta_s(\bar{\bar{\dot{\gamma}}}) = 0$, a Maxwell model is obtained, or to be more specific:

upper-convected Maxwell model with $a = 0$;

corotational Maxwell model with $a = \frac{1}{2}$;

lower-convected Maxwell model with $a = 1$.

An Oldroyd model with three parameters is obtained when $A(\bar{\bar{\tau}}_v) = \bar{\bar{I}}$ and $\eta_s(\bar{\bar{\dot{\gamma}}}) \neq 0$. In particular, by choosing $a = 0$, the Oldroyd-B model will be obtained, which leads to one of the simplest set of nonlinear, time-dependent differential constitutive equations [24], which is given by

$$\bar{\bar{\tau}}_v + \lambda[\frac{\partial \bar{\bar{\tau}}_v}{\partial t} + (\vec{u}\cdot\vec{\nabla})\bar{\bar{\tau}}_v - \vec{\nabla}\vec{u}\cdot\bar{\bar{\tau}}_v - \bar{\bar{\tau}}_v\cdot\vec{\nabla}\vec{u}^T] = 2\eta_v(\bar{\bar{\dot{\gamma}}})\bar{\bar{\dot{\gamma}}}(\vec{u}). \qquad (2.9)$$

Another model which is more complex, but more realistic, is known as the Phan-Thien and Tanner (PTT) model. In this model, $A(\bar{\bar{\tau}}_v)$ is expressed as

$$A(\bar{\bar{\tau}}_v) = [1 + \frac{\varepsilon\lambda}{\eta_v(\bar{\bar{\dot{\gamma}}})} Trace(\bar{\bar{\tau}}_v)]\bar{\bar{I}} .$$

The constitutive equations for the PTT model are then given by

$$[1+\frac{\varepsilon\lambda}{\eta_v(\bar{\bar{\dot{\gamma}}})}Trace(\bar{\bar{\tau}}_v)]\bar{\bar{\tau}}_v+\lambda[\frac{\partial\bar{\bar{\tau}}_v}{\partial t}+(\vec{u}\cdot\vec{\nabla})\bar{\bar{\tau}}_v-\vec{\nabla}\vec{u}\cdot\bar{\bar{\tau}}_v-\bar{\bar{\tau}}_v\cdot\vec{\nabla}\vec{u}^T]=2\eta_v(\bar{\bar{\dot{\gamma}}})\bar{\bar{\dot{\gamma}}}(\vec{u}),$$

where:

η_v : viscoelastic viscosity;

λ : relaxation time of the fluid;

ε : dimensionless material parameter.

In some traditional constitutive equations used to model polymer melts, such as the PTT model, the rheology is controlled by the macroscopic parameters and functions. Rheometric experiments usually give appropriate values for these parameters that are not related to the microstructure. In other words, any direct link between the values of these parameters and the molecular structure is not available. A new category of constitutive equations was introduced by McLeish and Larson [26], which are based on a tube theory model for a branched polymer ('pom-pom') molecule. This class of constitutive equations provides a direct link between the molecular topology and the flow properties of the melt. The pom-pom constitutive equations are based on the dynamics of a melt of identical molecules with a very simple branching structure, which is called a 'pom-pom' molecule. A pom-pom molecule consists of two identical q-armed stars connected by a 'backbone' section.

The pom-pom constitutive equations are related to the molecular structure, and its fundamental parameters are all directly related to features of the idealized polymer molecule. McLeish and Larson's study of the flow behavior of their model [26] is limited to either simple shear or pure

extension. Although they have shown that the results from these two simple flows are promising. The main purpose of studying pom-pom model is to determine how changes to the molecular geometry affect the flow pattern.

Although the Maxwell and the Oldroyd-B models are not very realistic (except in the case of very small deformation rates), they have been used in many numerical studies. This work is based on the Oldroyd-B model. However, more complex models such as the PTT model can be easily applied within the framework of this study.

2.5 Multifluid Flows and the Conditions at the Interface

When two nonmiscible fluids are in contact, the region at the interface of the fluids is called a free surface. A free surface can be a region that separates two materials with the same phase, but with different properties. In this research, the fluid-fluid interface is investigated. Let us consider the free surface flow problem illustrated in figure 2.1. The region in Ω occupied by the first fluid is denoted Ω_1 and the second fluid occupies the region Ω_2, while the interface separating the two fluids is denoted by Σ. The unit normal to the interface is denoted $\vec{n}_\Sigma$. Since the fluids under study are immiscible, $\Omega_1 \cap \Omega_2 = \varnothing$. The computational domain can therefore be defined as $\Omega_1 \cup \Omega_2 = \Omega$.

Appropriate conditions at the interface Σ are the continuity of normal and tangential velocities, and the force balance at the interface.

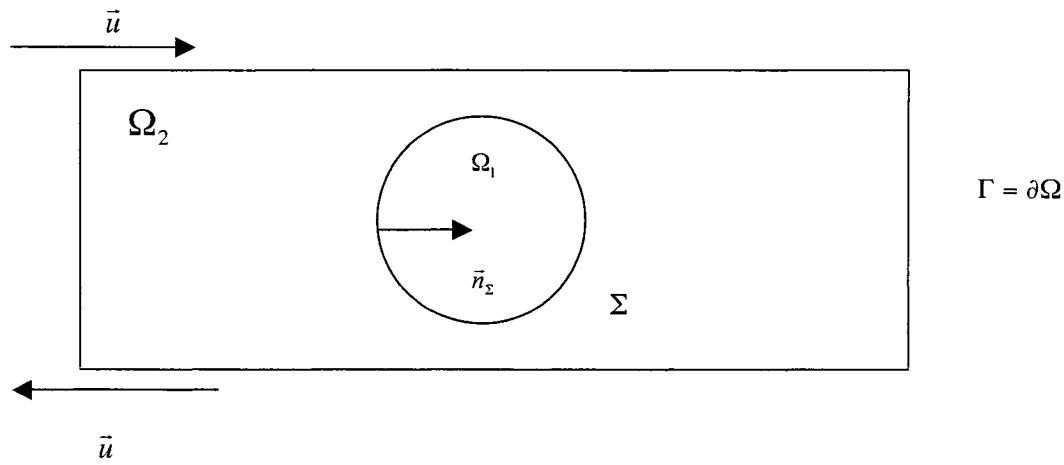

Figure 2.1 Free surface flow problem

2.5.1 Immiscibility and the Pseudo-Concentration

One of the conditions at the interface Σ is the continuity of normal velocities [27], which is given by

$$\vec{u}_1 \cdot \vec{n}_\Sigma = \vec{u}_2 \cdot \vec{n}_\Sigma = \vec{u}_\Sigma \cdot \vec{n}_\Sigma, \tag{2.10}$$

where:

$\vec{u}_1$: velocity of fluid 1;

$\vec{u}_2$: velocity of fluid 2;

$\vec{u}_\Sigma$: velocity of the interface Σ.

Since we are dealing with the flow of immiscible fluids, the kinematic condition at the interface (2.10) can be written as

$$\vec{u}_\Sigma \cdot \vec{n}_\Sigma = 0, \tag{2.11}$$

which is known as the immiscibility condition, and is only defined on the interface Σ. Since the location of the free surface is *a priori* unknown, the imposition of this condition is not an easy matter. Eulerian surface capturing

techniques are used to simplify this process. Using this approach, the zero thickness interface has been replaced by a transition zone through the use of a marker variable, the pseudo-concentration of fluids 1 and 2 in Ω [28], defined as:

$$F(\vec{x}) = \begin{cases} 1 & if \quad \vec{x} \in \Omega_1; \\ 0 & if \quad \vec{x} \in \Omega_2. \end{cases} \tag{2.12}$$

It is possible to identify the region where the free surface is located by locating the region for which isovalues of $F(\vec{x})$ are equal to $1/2$. It can be shown that condition (2.11) is equivalent, in a distributional sense, to the stationary transport equation of the pseudo-concentration [29], which is given by

$$\vec{u} \cdot \vec{\nabla} F(\vec{x}) = 0, \qquad \forall \vec{x} \in \Omega.$$

In the case of transient problems, where we have $F(\vec{x},t)$ we can compute

$$\frac{d}{dt}F = \frac{\partial F}{\partial x} \cdot \frac{dx}{dt} + \frac{\partial F}{\partial y} \cdot \frac{dy}{dt} + \frac{\partial F}{\partial t} \cdot \frac{dt}{dt} = \frac{\partial F}{\partial t} + \vec{u} \cdot \vec{\nabla} F.$$

In a unit volume area, ΔV, let's suppose that

$$\frac{d}{dt}\int_{\Delta V} F dV = 0.$$

According to the Reynolds transport theorem, we can write

$$\frac{d}{dt}\int_{\Delta V} F dV = \int_{\Delta V} (\frac{\partial F}{\partial t} + \vec{u} \cdot \vec{\nabla} F) dV,$$

therefore

$$\int_{\Delta V} (\frac{\partial F}{\partial t} + \vec{u} \cdot \vec{\nabla} F) dV = 0.$$

Since ΔV is an arbitrary volume, the above equation must apply to all possible volumes in the flow. The only way for the integral over ΔV to be identically zero is if

$$\frac{\partial F}{\partial t} + \vec{u} \cdot \vec{\nabla} F = 0.$$

This is the transport equation of the pseudo-concentration for transient problems. The solution of this hyperbolic equation in Ω will determine the regions occupied by each fluid and, as a result, the position of the interface. This solution requires an appropriate boundary condition at the inflow, which is given by

$$\Gamma^{-} = \{ \vec{x} \in \partial\Omega \mid \vec{u} \cdot \vec{n} < 0 \}.$$

The pseudo-concentration function is also used to evaluate the physical parameters for each fluid. As an example, the viscosity on the whole domain Ω is obtained by the following expression:

$$\eta(F) = \eta_2 + (\eta_1 - \eta_2)F.$$

Consequently, the description of the viscoelastic multifluid flow problem that obeys the Oldroyd-B model in each phase is given by:

$$\begin{cases} \rho(\dfrac{\partial \vec{u}}{\partial t}) - \vec{\nabla} \cdot [2\eta_s(\bar{\bar{\dot{\gamma}}})\bar{\bar{\dot{\gamma}}}(\vec{u})] + \vec{\nabla} p = \vec{\nabla} \cdot \bar{\bar{\tau}}_v + \vec{f}; \\ \vec{\nabla} \cdot \vec{u} = 0; \\ \dfrac{\partial F}{\partial t} + \vec{u} \cdot \vec{\nabla} F = 0; \\ \bar{\bar{\tau}}_v + \lambda[\dfrac{\partial \bar{\bar{\tau}}_v}{\partial t} + (\vec{u} \cdot \vec{\nabla})\bar{\bar{\tau}}_v - \vec{\nabla}\vec{u} \cdot \bar{\bar{\tau}}_v - \bar{\bar{\tau}}_v \cdot \vec{\nabla}\vec{u}^T] = 2\eta_v(\bar{\bar{\dot{\gamma}}})\bar{\bar{\dot{\gamma}}}(\vec{u}). \end{cases} \qquad (2.13)$$

Since the transport equation of the pseudo-concentration and the constitutive equations are hyperbolic, and the conservation equations are elliptic, an appropriate discretization method must be subsequently chosen according to the mathematical nature of each equation. The unknowns of this system are the two velocity components (u,v), the pressure component (p), the pseudo-concentration (F) and the three extra-stress components $(\tau_{11},\tau_{12},\tau_{22})$ for two-dimensional flows.

2.5.2 Force Balance Condition at the Interface

The dynamics of two immiscible fluids often exhibit a behavior characterized by an elastic membrane which seems to be present at the interface. This behavior is caused by the intermolecular attraction of similar molecules. This is known as interfacial tension. The influence of interfacial tension is included in our model through the force balance condition at the interface, that is given by

$$(\bar{\bar{\sigma}}_2 - \bar{\bar{\sigma}}_1)\cdot \vec{n}_\Sigma = \alpha\kappa\vec{n}_\Sigma \,, \tag{2.14}$$

where $\bar{\bar{\sigma}}_1$ and $\bar{\bar{\sigma}}_2$ are the Cauchy stress tensor of fluids 1 and 2, $\alpha > 0$ is the interfacial tension coefficient between fluids 1 and 2, and κ is the local curvature of the interface, which is expressed by

$$\kappa = (\frac{1}{R_1} + \frac{1}{R_2}),$$

where R_1 and R_2 are the local radii of curvature of the interface.

Interfacial tension influences the topology of the interface and also creates a jump in pressure across the interface, which is known as the capillary

pressure. The force responsible for the interfacial tension is the capillary force, which has a normal direction to the free surface. In the case of two immiscible fluids, where a drop of an arbitrary shape is immersed in another fluid at rest, the capillary force between the two fluids generates a flow that causes the drop to reach a topology that minimizes energy, which is a circle in two-dimensions. According to Laplace's law, there is a connection between the interfacial tension coefficient and the jump in pressure. This relationship is given by

$$p_1 - p_2 = \alpha\kappa .$$

This study is limited to constant interfacial tension coefficients.

2.6 Numerical Model for Interfacial Tension

Lagrangian methods make it easier to numerically model multifluid flow problems with interfacial tension, since the imposition of the force balance condition (2.14) is straightforward [27].

The imposition of the force balance condition (2.14), and consequently the modeling of the interfacial tension, is not an easy task using an Eulerian approach since the position of the interface is not explicitly known. In order to model interfacial tension in an Eulerian framework, several formulations are available, and all of them are based on the idea behind the Continuum Surface Force (CSF) technique. This work draws on the CSF model of Brackbill et al. [29].

As illustrated in figure 2.2, the surface capillary force $\vec{f}_s = \alpha\kappa\vec{n}_\Sigma\vec{\delta}_\Sigma$, defined on a unit surface area ΔS, is approximated by a *volumic* capillary force $\vec{f}_v = \alpha\kappa(F)\vec{\nabla}F$, defined in the region of transition of F, noted ΔV, which satisfies

$$\lim_{h\to 0}\int_{\Delta v}\vec{f}_v dV = \int_{\Delta s}\vec{f}_s dS.$$

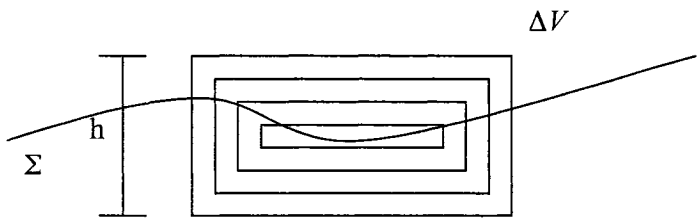

Figure 2.2 The CSF model

The Dirac delta function $\vec{\delta}_\Sigma$, defined on the interface Σ, is approximated numerically in the region of transition of F using $\left\|\vec{\nabla}F\right\|$, and the local curvature is approximated using the expression

$$\kappa = -\vec{\nabla}\cdot\vec{n}_\Sigma \approx -\vec{\nabla}\cdot\left(\frac{\vec{\nabla}F}{\left\|\vec{\nabla}F\right\|}\right). \qquad (2.15)$$

The *volumic* capillary force $\vec{f}_v$ is included in the Stokes equations to yield

$$\rho\left(\frac{\partial\vec{u}}{\partial t}\right) = \vec{\nabla}\cdot\bar{\bar{\sigma}} + \vec{f}_v.$$

The description of the viscoelastic multifluid flow problem with interfacial tension, using the Oldroyd-B model, is thus given by:

$$\begin{cases} \rho(\dfrac{\partial \vec{u}}{\partial t}) - \vec{\nabla} \cdot [2\eta_s(\dot{\bar{\gamma}})\dot{\bar{\gamma}}(\vec{u})] + \vec{\nabla} p = \vec{\nabla} \cdot \bar{\bar{\tau}}_v + \vec{f}_v; \\ \vec{\nabla} \cdot \vec{u} = 0; \\ \dfrac{\partial F}{\partial t} + \vec{u} \cdot \vec{\nabla} F = 0; \\ \bar{\bar{\tau}}_v + \lambda[\dfrac{\partial \bar{\bar{\tau}}_v}{\partial t} + (\vec{u} \cdot \vec{\nabla})\bar{\bar{\tau}}_v - \vec{\nabla}\vec{u} \cdot \bar{\bar{\tau}}_v - \bar{\bar{\tau}}_v \cdot \vec{\nabla}\vec{u}^T] = 2\eta_v(\dot{\bar{\gamma}})\dot{\bar{\gamma}}(\vec{u}), \end{cases} \tag{2.16}$$

which has to be solved for each fluid.

CHAPTER 3

FINITE ELEMENT DISCRETIZATIONS

Since the nature of the equations of system (2.16) used to model viscoelastic multifluid flow problems are various (elliptic or hyperbolic), different discretization methods have to be considered. This chapter is devoted to describing the standard Galerkin method, stabilized techniques such as the streamline-upwind (SU) method and the streamline-upwind/Petrov-Galerkin (SUPG) method, and the discontinuous Galerkin (DG) method.

3.1 Functional Spaces

Consider V, Q, W and Φ the functional spaces associated with velocity, pressure, pseudo-concentration and the viscoelastic stresses, respectively. These spaces are defined as follows:

$$V = H^1(\Omega)^n ;$$

$$Q = L^2(\Omega);$$

$$W = W(\Omega);$$

$$\Phi = L^2(\Omega)^{n\times n}.$$

Let us define the functional spaces, which are used in this work. The space of the square integrable functions, with its scalar product, is given by:

$$L^2(\Omega) = \{v : \Omega \rightarrow R \mid \int_{\Omega} v^2 d\Omega < \infty\};$$

$$(u,v)_{0,\Omega} = \int_{\Omega} uv \; d\Omega.$$

In general, the space of n-dimensional square integrable functions, with its scalar product, is defined as

$$L^2(\Omega)^n = \{\vec{v} : \Omega \rightarrow R^n \mid \int_\Omega \vec{v} \cdot \vec{v}\ d\Omega < \infty\};$$

$$(\vec{u},\vec{v})_{0,\Omega} = \int_\Omega \vec{u} \cdot \vec{v}\ d\Omega.$$

The Sobolev space $H^1(\Omega)$ is given by:

$$H^1(\Omega) = \{v \in L^2(\Omega) \mid \frac{\partial v}{\partial x_i} \in L^2(\Omega), i = 1,2,...,n\}.$$

The n-dimensional space version of $H^1(\Omega)$ is written as

$$H^1(\Omega)^n = \{\vec{v} \in L^2(\Omega)^n \mid \frac{\partial \vec{v}}{\partial \vec{x}_i} \in L^2(\Omega)^n, i = 1,2,...,n\}.$$

$H^1_{D\vec{u}}(\Omega)^n$ is derived from $H^1(\Omega)$ and is defined as

$$H^1_{D\vec{u}}(\Omega)^n = \{\vec{v} \in H^1(\Omega)^n \mid \vec{v} = 0 \text{ on } \Gamma_{D\vec{u}}\}.$$

This space is required for studying the variational formulation of the conservation of momentum equations.

The solution of the transport equation of the pseudo-concentration leads to the definition of the following space:

$$W(\Omega) = \{w \in L^2(\Omega) \mid \vec{u} \cdot \nabla w \in L^2(\Omega) \text{ and } w|_{\Gamma^-} \in L^2_{\vec{u}}(\Gamma^-)\},$$

where

$$L^2_{\vec{u}}(\Gamma) = \{w \mid \int_\Gamma |\vec{u} \cdot \vec{n}| w^2 d\Gamma < \infty\}.$$

For studying the variational formulation of the transport equation of the pseudo-concentration, the following space is used:

$$W_{\Gamma^-}(\Omega) = \{w \in W(\Omega) \mid w = 0 \text{ on } \Gamma^-\}.$$

In the viscoelastic case, the viscoelastic stresses will be in the space

$$\Phi = \{\bar{\bar{\sigma}} \in L^2(\Omega)^{n\times n} \mid \sigma_{ij} = \sigma_{ji} \;;\; i,j = 1,2,...,n\}.$$

3.2 The Galerkin Method and the Stokes Problem

The finite element method, based on the Galerkin formulation, has proven to be an effective approach for solving elliptic partial differential equations, such as the Stokes problem. Let us consider Ω_h, the discretization of Ω that consists of K elements so that $\Omega = \bigcup_K K$. Let us also define the discrete functional spaces used to discretize the velocity and the pressure, $V_h \subset V$ and $Q_h \subset Q$. The dependent variables can then be approximated using elements of these discrete spaces. For example, the discrete velocity $\vec{u}_h$ is expressed as

$$\vec{u}_h = \sum_{i=1}^{n} \vec{u}_i \varphi_i(\vec{x}), \tag{3.1}$$

where $\vec{u}_i$ is the value of the velocity on the i^{th} node of an element of Ω_h and $\varphi_i(\vec{x})$ is an interpolation function, which is one of the n functions forming the base of the space V_h. Let us consider $\vec{v}_h \in V_h$ and $q_h \in Q_h$ as the finite element test function. This is known as the Galerkin method. The discrete variational formulation of the Stokes problem is written as follows:

Find $\vec{u}_h \in V_h$ and $p_h \in Q_h$ so that:

$$\begin{cases} \int_{\Omega} (\rho \frac{\partial \vec{u}_h}{\partial t} \cdot \vec{v}_h) d\vec{x} + \int_{\Omega} [(2\eta_s(\bar{\bar{\dot{\gamma}}})\bar{\bar{\dot{\gamma}}}(\vec{u}_h) + \bar{\bar{\tau}}_h) : \vec{\nabla}\vec{v}_h] d\vec{x} \\ \qquad -\int_{\Omega} (p_h \vec{\nabla} \cdot \vec{v}_h) d\vec{x} - \int_{\Omega} \vec{f}_v \vec{v}_h = 0, \qquad \forall \vec{v}_h \in V_h; \\ \int_{\Omega} (q_h \vec{\nabla} \cdot \vec{u}_h) d\vec{x} = 0, \qquad \forall q_h \in Q_h. \end{cases} \tag{3.2}$$

By replacing the discrete approximations of the dependent variables and the discrete test functions in the variational formulations of the Stokes problem, a system of matrix equations will be obtained:

$$\begin{cases} A \cdot \vec{U} + B^T \cdot \vec{P} = \vec{G}; \\ B \cdot \vec{U} = \vec{0}, \end{cases} \tag{3.3}$$

where A is the viscous term matrix and B is the divergence matrix. The vector $\vec{U}$ contains the degrees of freedom in velocity and $\vec{P}$ contains the degrees of freedom in pressure. $\vec{G}$ is related to body force.

The spaces V_h and Q_h cannot be chosen independently. They have to be chosen in such a way that the Ladyzhenskaya-Babuska-Brezzi (LBB) condition is satisfied [8]. This condition ensures the existence and the uniqueness of the solution $(\vec{u}_h, p_h)$ of the discrete problem, and that the discrete solution converges to $(\vec{u}, p)$. In this work, we are going to use the Crouzeix-Raviart element, also known as the $P_2^+ - P_1$ element combination. This combination, illustrated in figure 3.1, consists of a quadratic

approximation of velocity, plus a "bubble" function associated with the central node, and a piecewise discontinuous linear approximation of the pressure. This element is second-order accurate ($O(h^2)$) and it satisfies the LBB condition.

(a) Velocity interpolation $(\vec{u})$ (b) Pressure interpolation (p)

Figure 3.1 Crouzeix-Raviart element combination

3.2.1 Time Integration Schemes for the Stokes Problem

An accurate discretization of the velocity field of the fluids is important for an accurate advection $(\vec{u}\cdot\vec{\nabla}F)$ of the pseudo-concentration function. Consequently, the choice of an appropriate time integration scheme, to discretize the transient term of the equations, is very important to help conserve mass for each fluid. In this research, for the transient term of the Stokes equation, $\frac{\partial \vec{u}}{\partial t}$, the second order accurate $(O(\Delta t)^2)$, A-stable, backward differentiation formula (BDF2), also known as the Gear scheme, is used.

A time integration strategy, which includes an adaptive scheme for the transient term of the Navier-Stokes equations, is proposed in [30]. With this strategy, larger time steps are used during the transient phase of the flow, while smaller time steps are used when approaching steady-state.

3.3 Stabilization Techniques

As mentioned previously, the mathematical nature of the studied equations is various. The convection term produces the hyperbolic character of the system, whereas the viscous term gives an elliptic nature to the equations. For example, the conservation of momentum equations are given by

$$\rho(\frac{\partial \vec{u}}{\partial t} + \vec{u} \cdot \vec{\nabla}\vec{u}) = \vec{\nabla} \cdot \bar{\bar{\sigma}} + \vec{f}, \tag{3.4}$$

where $\vec{u} \cdot \vec{\nabla}\vec{u}$ is known as the convective term and $\vec{\nabla} \cdot \bar{\bar{\sigma}}$ is the viscous term. Therefore, these equations are either more elliptic or hyperbolic, depending on the order of magnitude of these two terms. In the case of polymers, inertia can be neglected ($\vec{u} \cdot \vec{\nabla}\vec{u} \approx 0$). These equations therefore have an elliptic nature.

The transport equation of the pseudo-concentration is purely hyperbolic,

$$\frac{\partial F}{\partial t} + (\vec{u} \cdot \vec{\nabla})F = 0. \tag{3.5}$$

The Galerkin method cannot be used for this purely hyperbolic equation. As a result, the Galerkin FEM, which suffers from oscillations in this case, can no longer give reliable results. In order to use the Galerkin method, some authors add a small diffusive term to (3.5) to yield the convection dominant equation

$$\frac{\partial F}{\partial t} + (\vec{u} \cdot \vec{\nabla})F = \beta \vec{\nabla}^2 F, \tag{3.6}$$

where β is a small constant. Since this artificial diffusion term is added to the equation, it produces diffusion in all directions. This is the weak point of this approach. Moreover, the transport equation is completely changed. We do not

discretize the right equation. The discrete solution that is obtained by the Galerkin method cannot be accurate, especially when the boundary condition contains an abrupt variation. As a result, numerical nonphysical oscillations occur. It is therefore necessary to use a special discretization method to solve this kind of problem.

Another way of tackling this problem consists in using an upstream discretization, using a backward difference, which is known as an upwinding technique. This approach was adapted to the finite element method by modifying the test functions in order to add this upwinding property to the FEM. In this method, a larger weight is given to the discretization upstream, resulting in a discretization of the Petrov-Galerkin type. Even though this approach makes it possible to eliminate the numerical oscillations, in practice, problems of excessive diffusion will be observed.

Another technique, introduced by Raithby [31] into the context of the finite differences, considers a diffusion term that acts only in the direction of the flow. This approach makes it possible to solve the equations with dominant convection, without causing problems of excessive diffusion. Hughes and Brooks [32] adapted this strategy to the finite element method in a technique known as the streamline-upwind (SU) method. The SU method consists in a modified test function of the convective term. The problem with this approach is that the method is not consistent, i.e. that the pointwise truncation error vanishes as the grid size goes to zero. Even if this method is not consistent, it is still popular and seems to be effective for modeling viscoelastic flows.

Obviously, it is important to have a stable finite element method which is consistent. In order to satisfy this property, the modified test function of the SU method must be applied to all the terms of the weak form of the convection-diffusion equation. In practice, the weak form of the Galerkin method plus the residual of the equation of convection-diffusion multiplied by the modified test function is used. This method is known as the streamline-upwind/Petrov-Galerkin (SUPG) technique. This method is the most widespread technique to account for purely hyperbolic equations.

3.3.1 Discretization of the Transport Equation of the Pseudo-Concentration

Numerical simulations involving the transport of the pseudo-concentration usually produces nonphysical oscillations or numerical diffusion. The finite element discretization of the transport equation, the time integration scheme and the structure of the mesh are the most important factors leading to these numerical difficulties. In this research, the SUPG method is used to discretize the transport equation of the pseudo-concentration using a six-node quadratic element, as illustrated in figure 3.2.

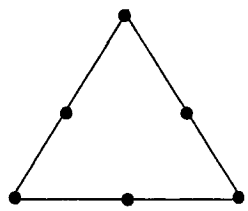

Figure 3.2 Pseudo-concentration element

Since continuous interpolation functions are used, the pseudo-concentration function has a region of transition that can be smooth. Moreover, using continuous interpolation functions simplifies the calculation of the various components entering the modeling of surface tension such as normals to the free surfaces and the curvature. Consequently, this method is used for this project.

Let us define the discrete functional space used to discretize the pseudo-concentration, $W_h \subset W$. Consider $w_h \in W_h$ as the finite element test function. The SUPG formulation for the transport equation is written as:

Find $F_h \in W_h$ so that:

$$\int_{\Omega} (\frac{\partial F_h}{\partial t} + \vec{u}_h \cdot \vec{\nabla} F_h) w_h d\Omega + \sum_k \int_k (\frac{\partial F_h}{\partial t} + \vec{u}_h \cdot \vec{\nabla} F_h)(\beta \vec{u}_h \cdot \vec{\nabla} w_h) dk = 0,$$

$$\forall w_h \in W_h, \quad (3.7)$$

where β is a stabilization parameter which is given by $\frac{h}{2}\|\vec{u}\|$, and h is the local mesh size.

By replacing the discrete approximation of the pseudo-concentration and the discrete test function in the variational formulation (3.7), system (3.3) can now be written as:

$$\begin{cases} A \cdot \vec{U} + B^T \cdot \vec{P} = \vec{G}; \\ B \cdot \vec{U} = \vec{0}; \\ C(\vec{U}) \cdot \vec{F} = \vec{0}, \end{cases}$$

where C is the convection matrix. $\vec{F}$ contains the degrees of freedom of the pseudo-concentration. It is important to note that all of these equations are linked together, through $\vec{U}$ and $\vec{F}$. Since $\vec{F}$ contains jumps, this will contribute to the non-linearity of the system [27]. An appropriate strategy to solve this nonlinear system of equations is therefore necessary.

3.3.2 Time Integration Schemes for the Transport Equation

The choice of an accurate time integration scheme to discretize the transient term of the transport equation, $\frac{\partial F}{\partial t}$, is important since it directly influences mass conservation [30]. The trapezoid rule (TR), the backward differentiation formulae (BDF) and the implicit midpoint rule (IMR) are three popular implicit, second order accurate time integration schemes. The performance of the TR, BDF and IMR schemes, with respect to mass conservation, has been studied [30] and the IMR scheme gives impressive results with respect to mass conservation. This scheme is A-stable and introduces hardly any artificial numerical oscillations. On the other hand, the IMR scheme introduces little undesirable damping in comparison with other A-stable schemes, which makes it interesting with respect to the advection equation. Consequently, in this work, the IMR scheme is used to discretize the transient term of the transport equation of the pseudo-concentration and is expressed as follows:

1 - given F^n, solve the following equation using the SUPG method:

$$\frac{F^{n+\frac{1}{2}} - F^n}{(\frac{\Delta t}{2})} + \vec{u}^{n+\frac{1}{2}} \cdot \vec{\nabla} F^{n+\frac{1}{2}} = 0;$$

2 - update the pseudo-concentration using,

$$F^{n+1} = 2F^{n+\frac{1}{2}} - F^{n}$$

3 - $t_{n+1} = t_n + \Delta t$, and go to step 1.

3.4 The Discontinuous Galerkin Method

The discontinuous Galerkin method is used for discretizing purely hyperbolic equations. Let us consider the two-dimensional domain Ω, shown in figure 3.3, and the following problem:

$$\begin{cases} \vec{u}\cdot\vec{\nabla}T + \alpha T = \vec{f}, & \text{on} \quad \Omega; \\ T = g, & \text{on} \quad \Gamma^{-}, \end{cases} \tag{3.8}$$

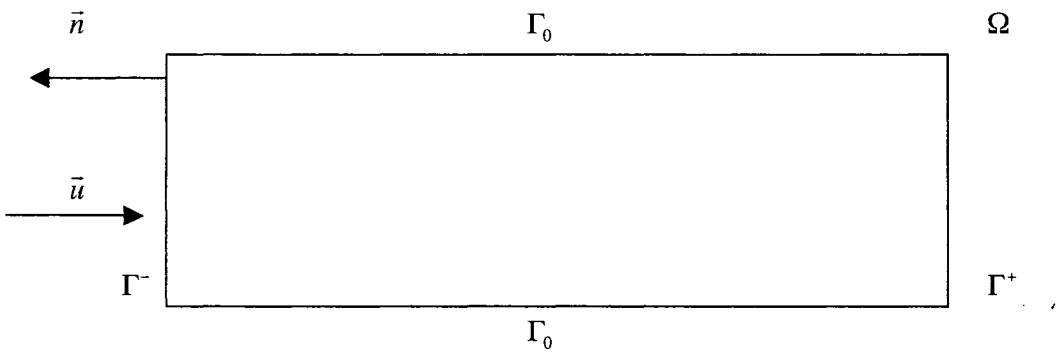

Figure 3.3 Domain and its boundaries

where Γ is the boundary of Ω and $\vec{n}$ denotes the outward normal to Γ. Then, $\Gamma^{-} = \{x \in \Gamma; \vec{u}\cdot\vec{n} < 0\}$ is the inlet and $\Gamma^{+} = \{x \in \Gamma; \vec{u}\cdot\vec{n} > 0\}$ is the outlet of the domain. Γ_0 are the solid walls where $\vec{u} = 0$. T is approximated using T_h so that $\{T_h|_K \in P_m(K)\}$, where $P_m(K)$ are piecewise polynomials of degree m

defined on each element K. The discretization is therefore discontinuous between elements. This implies that the problem can be solved element by element. A major advantage of this method is that no global matrix needs to be assembled, which leads to a minimal use of memory. Let's denote the discrete functional space used to discretize T, $\Psi_h \subset \Psi$. If we consider figure 3.4, the jump of T_h on the border B between elements K_1 and K_2, is defined as

$$[T_h](\vec{x}) \equiv \lim_{h \to 0^-} T_h(\vec{x} + h\vec{u}) - \lim_{h \to 0^+} T_h(\vec{x} + h\vec{u}) \equiv T_h^-(\vec{x}) - T_h^+(\vec{x}), \quad \forall \vec{x} \in \mathrm{B}.$$

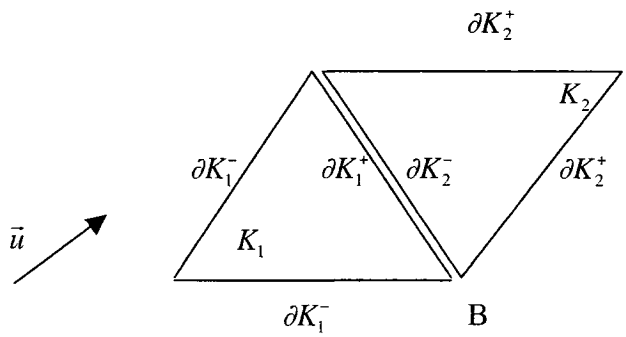

Figure 3.4 Two elements with their boundaries

The weak form of equation (3.8) is obtained by multiplying the test function, $\vec{v}$ to the equation and integrating over Ω. If T_h is a continuous approximation, the following relation is obtained:

$$\int_\Omega (\vec{u}_h \cdot \vec{\nabla}) T_h \vec{v}_h d\vec{x} + \int_\Omega \alpha T_h \vec{v}_h d\vec{x} = \int_\Omega \vec{f}_h \vec{v}_h d\vec{x}, \qquad \forall \vec{v}_h \in \Psi_h. \qquad (3.9)$$

Now suppose that ∂K_2^- is the inflow of element K_2. Then $\vec{u} \cdot \vec{n} < 0$ on ∂K_2^-. ∂K_1^+ represents the outflow boundary of element K_1, and therefore $\vec{u} \cdot \vec{n} > 0$ on

that boundary. If K_2 is the current element and since a discontinuous approximation of T is used, therefore $T^+_{K_1}$ and $T^-_{K_2}$ are two approximations of T on ∂K_1^+ and ∂K_2^-.

We have

$$T_h = T^-_{K_2} \qquad \text{on} \qquad \partial K_2^-;$$

$$T_h = T^+_{K_1} \qquad \text{on} \qquad \partial K_1^+;$$

$$[T_h] = T^-_{K_2} - T^+_{K_1} \qquad \text{on} \qquad \text{B}.$$

Since:

$$\int_{K_2} (\vec{u}_h \cdot \vec{\nabla}) T_h \vec{v}_h d\vec{x} = \int_{K_2} (\vec{u}_h \cdot \vec{\nabla}) T_h \vec{v}_h d\vec{x} + \int_{\partial K_2^-} (\vec{u}_h \cdot \vec{n}) [T_h] \vec{v}_h ds,$$

as a result:

$$\int_{K_2} (\vec{u}_h \cdot \vec{\nabla}) T_h \vec{v}_h d\vec{x} + \int_{\partial K_2^-} (\vec{u}_h \cdot \vec{n}) [T_h] \vec{v}_h ds + \int_{K_2} \alpha T_h \vec{v}_h d\vec{x} = \int_{K_2} \vec{f}_h \vec{v}_h d\vec{x},$$

$$\forall \vec{v}_h \in \Psi_h. \qquad (3.10)$$

If $T^-_{K_2}$ is known, then (3.10) can be solved on element K_2. It is important to note that this assumption enforces a particular ordering of the elements to ensure that $T^-_{K_2}$ is always known when solving (3.10) on a particular element. For flows with no recirculation, Lesaint and Raviart [23] have shown that this ordering always exists.

3.4.1 Discretization of the Constitutive Equations

Therefore the discussion on the discretization of the transport equation of the pseudo-concentration (cf. section 3.3.1) also apply here. In this research, the discontinuous Galerkin method is used to discretize the constitutive equation of the Oldroyd-B type. Since discontinuous approximations of the stresses are used, we have more degrees of freedom per geometric nodes, and therefore more flexibility from this type of discretization.The extra-stress tensor is discretized using a quadratic (6-nodes) approximation, as illustrated in figure 3.5.

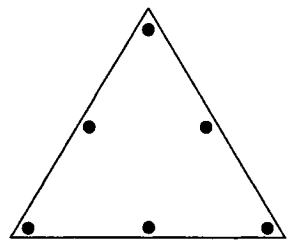

Figure 3.5 Extra-stress element

Baranger and Sandri [33] have shown that second-order accuracy can be achieved with this triangular quadratic approximation. Let us consider the finite dimensional approximation space Φ_h of Φ. The choice of the basis functions must be done in such a way that V_h, Q_h and Φ_h satisfy a compatibility condition between velocity, pressure and the stresses. Fortin and Pierre [9] have shown that with this discretization, a compatibility condition, similar to the LBB condition, is satisfied on the stress-velocity-pressure triplet. Considering $\bar{\bar{\varphi}}_h \in \Phi_h$ as the test functions, we multiply the constitutive equation (2.9) by these test functions to yield:

Find $\bar{\bar{\tau}}_{vh} \in \Phi_h$ so that:

$$\int_{\Omega} (\{\bar{\bar{\tau}}_{vh} + \lambda\left[\frac{\partial \bar{\bar{\tau}}_{vh}}{\partial t} + (\vec{u}_h \cdot \vec{\nabla})\bar{\bar{\tau}}_{vh} - \vec{\nabla}\vec{u}_h \cdot \bar{\bar{\tau}}_{vh} - \bar{\bar{\tau}}_{vh} \cdot \vec{\nabla}\vec{u}_h^{\,T}\right] - 2\eta_v \bar{\bar{\dot{\gamma}}}(\vec{u}_h)\} : \bar{\bar{\varphi}}_h) d\vec{x} = 0,$$

$$\forall \bar{\bar{\varphi}}_h \in \Phi_h. \qquad (3.11)$$

The extra-stress tensor is then approximated by piecewise discontinuous polynomials on each element. These approximations are quadratic on each element and discontinuous at the element interfaces. We then define:

$$\bar{\bar{\tau}}_{vh} = \bar{\bar{\tau}}_{vh\,K_2}^{-} \qquad \text{on} \qquad \partial K_2^{-};$$

$$\bar{\bar{\tau}}_{vh} = \bar{\bar{\tau}}_{vh\,K_1}^{+} \qquad \text{on} \qquad \partial K_1^{+};$$

$$[\bar{\bar{\tau}}_{vh}] = \bar{\bar{\tau}}_{vh\,K_2}^{-} - \bar{\bar{\tau}}_{vh\,K_1}^{+} \qquad \text{on} \qquad \text{B},$$

and using

$$\int_{K_2} (\vec{u}_h \cdot \vec{\nabla}\bar{\bar{\tau}}_{vh}) : \bar{\bar{\varphi}}_h d\vec{x} = \int_{K_2} (\vec{u}_h \cdot \vec{\nabla}\bar{\bar{\tau}}_{vh}) : \bar{\bar{\varphi}}_h d\vec{x} + \int_{\partial K_2^-} \vec{u}_h \cdot \vec{n}[\bar{\bar{\tau}}_{vh}] : \bar{\bar{\varphi}}_h ds, \qquad (3.12)$$

we obtain

$$\int_{K_2} (\{\bar{\bar{\tau}}_{vh} + \lambda\left[\frac{\partial \bar{\bar{\tau}}_{vh}}{\partial t} + (\vec{u}_h \cdot \vec{\nabla})\bar{\bar{\tau}}_{vh} - \vec{\nabla}\vec{u}_h \cdot \bar{\bar{\tau}}_{vh} - \bar{\bar{\tau}}_{vh} \cdot \vec{\nabla}\vec{u}_h^{\,T}\right]$$

$$-2\eta_v \bar{\bar{\dot{\gamma}}}(\vec{u}_h)\} : \bar{\bar{\varphi}}_h) d\vec{x} + \int_{\partial K_2^-} (\vec{u} \cdot \vec{n})[\bar{\bar{\tau}}_{vh}] : \bar{\bar{\varphi}}_h ds = 0, \qquad \forall \bar{\bar{\varphi}}_h \in \Phi_h.$$

(3.13)

Considering that $\vec{u}$ and $\bar{\bar{\tau}}_{vh\,K_2}^{-}$ are known for a given element K_2, then $\bar{\bar{\tau}}_{vh}$ can be computed on this element through a linear system with 18 equations and 18 unknowns, which are the components of the extra-stress tensor resulting from (3.13).

3.4.2 Time Integration Schemes for the Constitutive Equations

Since our study mainly focuses on transient problems, it is very important to choose a proper time integration scheme to discretize the transient term of the constitutive equations, $\frac{\partial \bar{\bar{\tau}}}{\partial t}$. From the same reasons we choose the IMR scheme for the transport equation of the pseudo-concentration, we choose the same scheme for the transport equation of the viscoelastic stresses.

CHAPTER 4

DISCRETE SYSTEMS OF EQUATIONS

The numerical modeling of viscoelastic multifluid flow problems is expensive. For example, in two-dimensional geometries, two velocity components, the pressure, the pseudo-concentration and three components of the symmetric extra-stress tensor have to be discretized. With three-dimensional problems, where the extra-stress tensor has six components, the situation is more complicated. Therefore, it is important to choose an appropriate discretization method of the variables in order to minimize the size of the global discrete system. The choice of an appropriate discretization for each equation is important, but not sufficient, to guarantee the success of the numerical simulation of a viscoelastic multifluid flow problem.

In this chapter, a transient viscoelastic multifluid flow problem with interfacial tension, using the Oldroyd-B model, is considered. Inertia and gravity are neglected. In the following subsections, three different formulations are presented in order to solve this problem.

4.1 First Mixed Formulation

Considering V, Q, W and Φ as the functional spaces associated with velocity, pressure, pseudo-concentration and the stresses, the basic mixed formulation is given by:

Find $(\vec{u}, p, F, \bar{\bar{\tau}}_v) \in V \times Q \times W \times \Phi$ so that:

$$\begin{cases} \rho(\dfrac{\partial \vec{u}}{\partial t}) - \vec{\nabla} \cdot [2\eta_s(\bar{\bar{\dot{\gamma}}})\bar{\bar{\dot{\gamma}}}(\vec{u})] + \vec{\nabla} p = \vec{\nabla} \cdot \bar{\bar{\tau}}_v + \vec{f}_v, & \text{in } \Omega; \\ \vec{\nabla} \cdot \vec{u} = 0, & \text{in } \Omega; \\ \dfrac{\partial F}{\partial t} + \vec{u} \cdot \vec{\nabla} F = 0, & \text{in } \Omega; \\ \bar{\bar{\tau}}_v + \lambda[\dfrac{\partial \bar{\bar{\tau}}_v}{\partial t} + (\vec{u} \cdot \vec{\nabla})\bar{\bar{\tau}}_v - \vec{\nabla}\vec{u} \cdot \bar{\bar{\tau}}_v - \bar{\bar{\tau}}_v \cdot \vec{\nabla}\vec{u}^T] = 2\eta_v \bar{\bar{\dot{\gamma}}}(\vec{u}), & \text{in } \Omega. \end{cases} \quad (4.1)$$

The Galerkin variational formulation associated with system (4.1) is obtained by multiplying these equations by $\vec{v} \in V$, $q \in Q$, $w \in W$ and $\bar{\bar{\varphi}} \in \Phi$ ($\vec{v}$, q, w and $\bar{\bar{\varphi}}$ are the test functions related to the spaces V, Q, W and Φ respectively) and integrating by parts. Consequently, the basic mixed finite element formulation can be expressed as:

Find $(\vec{u}, p, F, \bar{\bar{\tau}}_v) \in V \times Q \times W \times \Phi$ so that:

$$\begin{cases} \displaystyle\int_\Omega (\rho \frac{\partial \vec{u}}{\partial t}) \cdot \vec{v} d\vec{x} + \int_\Omega [(2\eta_s(\bar{\bar{\dot{\gamma}}})\bar{\bar{\dot{\gamma}}}(\vec{u}) + \bar{\bar{\tau}}_v) : \vec{\nabla}\vec{v}] d\vec{x} \\ \qquad\qquad - \displaystyle\int_\Omega (p\vec{\nabla} \cdot \vec{v}) d\vec{x} - \int_\Omega \vec{f}_v \vec{v} d\vec{x} = 0, \quad \forall \vec{v} \in V; \\ \displaystyle\int_\Omega (q\vec{\nabla} \cdot \vec{u}) d\vec{x} = 0, & \forall q \in Q; \\ \displaystyle\int_\Omega (\frac{\partial F}{\partial t} \cdot w) d\vec{x} + \int_\Omega [(\vec{u} \cdot \vec{\nabla} F) \cdot w] d\vec{x} = 0, & \forall w \in W; \\ \displaystyle\int_\Omega (\{\bar{\bar{\tau}}_v + \lambda\left[\frac{\partial \bar{\bar{\tau}}_v}{\partial t} + (\vec{u} \cdot \vec{\nabla})\bar{\bar{\tau}}_v - \vec{\nabla}\vec{u} \cdot \bar{\bar{\tau}}_v - \bar{\bar{\tau}}_v \cdot \vec{\nabla}\vec{u}^T\right] \\ \qquad\qquad - 2\eta_v \bar{\bar{\dot{\gamma}}}(\vec{u})\} : \bar{\bar{\varphi}}) d\vec{x} = 0, & \forall \bar{\bar{\varphi}} \in \Phi. \end{cases} \quad (4.2)$$

The discretization of the equations of system (4.2) results in a nonlinear algebraic system of equations of the form:

$$\vec{E}(\vec{X}) = \vec{0}\ , \tag{4.3}$$

where $\vec{X}$ is the vector of the degrees of freedom of the unknown variables $(u, v, p, F, \tau_{11}, \tau_{22}, \tau_{12})$. Techniques for the treatment of this nonlinear problem are explained in the following subsections. The advantages and disadvantages of each of these techniques are also discussed.

4.1.1 The Coupled Approach

The global nonlinear system of algebraic equations $\vec{E}(\vec{X}) = \vec{0}$ can be solved iteratively using Newton's method:

1 - $\vec{X}_0$ is an initial estimate of the solution;

2 - solve $J(\vec{X}_n)\vec{\delta X} = -\vec{E}(\vec{X}_n)$ for $n = 0,1,2,...$; (4.4)

3 - update the solution, $\vec{X}_{n+1} = \vec{X}_n + \vec{\delta X}$;

4 - if $\left\|\vec{E}(\vec{X}_{n+1})\right\| \le \varepsilon_1$ and $\left\|\vec{\delta X}\right\| \le \varepsilon_2$ stop, if not return to step 2.

$J(\vec{X}_n)$ is the Jacobian matrix of $\vec{E}(\vec{X}_n)$ at the nth iteration. The resulting linear system of equations can be solved using an LU factorization. This leads to a fully coupled approach in which all the equations are solved simultaneously.

4.1.2 The Decoupled Approach

One way to reduce the memory requirements of the coupled approach is to solve the conservation equations and the transport equation of the

pseudo-concentration, and the constitutive equations independently. The global system (4.2) is then split into two subsystems. A first system of equations, which contains the degrees of freedom in $\vec{u}$, p and F, is solved independently of a second system of equations which contains the degrees of freedom of the viscoelastic stresses. Coupling between these two subsystems is done iteratively by means of the Picard scheme (the fixed-point iterative method).

By using this uncoupled approach, system (4.1) is divided into the two following subsystems:

Find $(\vec{u}, p, F) \in V \times Q \times W$ so that:

$$\begin{cases} \rho(\dfrac{\partial \vec{u}}{\partial t}) - \vec{\nabla} \cdot [2\eta_s(\dot{\bar{\bar{\gamma}}})\bar{\bar{\gamma}}(\vec{u})] + \vec{\nabla} p = \vec{\nabla} \cdot \bar{\bar{\tau}}_v + \vec{f}_v, & \text{in } \Omega; \\ \vec{\nabla} \cdot \vec{u} = 0, & \text{in } \Omega; \\ \dfrac{\partial F}{\partial t} + \vec{u} \cdot \vec{\nabla} F = 0, & \text{in } \Omega. \end{cases} \qquad (4.5)$$

Find $\bar{\bar{\tau}}_v \in \Phi$ so that:

$$\bar{\bar{\tau}}_v + \lambda[\frac{\partial \bar{\bar{\tau}}_v}{\partial t} + (\vec{u} \cdot \vec{\nabla})\bar{\bar{\tau}}_v - \vec{\nabla}\vec{u} \cdot \bar{\bar{\tau}}_v - \bar{\bar{\tau}}_v \cdot \vec{\nabla}\vec{u}^T] = 2\eta_v \bar{\bar{\gamma}}(\vec{u}), \quad \text{in } \Omega. \qquad (4.6)$$

The system of equations (4.5) consists of the Stokes equations and of the transport equation of the pseudo-concentration, solved in a coupled manner. Solving these equations in a coupled way makes convergence much faster when compared to an uncoupled approach. Equations (4.6) are the

constitutive equations, which obey the Oldroyd-B model. The term $\vec{\nabla} \cdot \bar{\bar{\tau}}_v$ in the Stokes problem ensures the coupling between subsystems (4.5) and (4.6).

4.1.2.1 The Fixed-Point Iterative Method

For a viscoelastic multifluid flow problem, the fixed-point method, also known as the Picard's iteration scheme, is used as follows:

1 - initialize $\vec{u}^{(0)}, p^{(0)}$, $F^{(0)}$ and $\bar{\bar{\tau}}^{(0)}$ on Ω_h at $t = t_0$;

2 - evaluate the different physical parameters, such as viscosity, by means of the expression

$$\eta^{(n)}(F^{(n-1)}) = \eta_2 + (\eta_1 - \eta_2)F^{(n-1)};$$

3 - solve the conservation of mass and momentum equations by means of the Galerkin method to obtain $\vec{u}^{(n)}$ and $p^{(n)}$, and solve the transport equation of the pseudo-concentration by means of the SUPG method to obtain $F^{(n)}$;

4 - solve the constitutive equations by means of the DG method to obtain $\tau^{(n)}$;

5 - update the velocity field, the pressure and the pseudo-concentration by solving the conservation of mass and momentum equations, and by solving the transport equation of the pseudo-concentration, using the extra-stresses computed in step 4;

6 - check the stopping criteria for the velocity, the pressure, the pseudo-concentration and the stresses. If it is satisfied, the iterative procedure stops. If not, it continues to step 4.

7 - $t_{n+1} = t_n + \Delta t$, and go to step 2 in order to evaluate the various physical parameters with the assistance of the new pseudo-concentration.

4.1.2.2 The Generalized Minimal Residual (GMRES) Method

Saad and Schultz [34] introduced the generalized minimal residual (GMRES) method for the resolution of non-symmetric linear systems. A Newton-GMRES method is an implementation of Newton's method in which GMRES is used to iteratively solve the linear system at each Newton step. One advantage of this method is that it allows the resolution of large nonlinear systems of equations without computing large Jacobian matrices. Fortin and Fortin [35] applied this method to viscoelastic flow problem.

4.1.3 Uzawa's Algorithm

The finite element discretization of the conservation of mass and momentum equations yields an algebraic system of equations of the form (cf. section 3.2):

$$\begin{cases} A \cdot \vec{U} + B^T \cdot \vec{P} = \vec{G}; \\ B \cdot \vec{U} = \vec{0}. \end{cases} \tag{4.7}$$

In order to reduce the number of degrees of freedom, the Stokes solver is based on Uzawa's algorithm. According to Fortin and Glowinski [36], the resolution of system (4.7) is equivalent to solving the saddle point problem

$$L(\vec{V},\vec{Q}) = \frac{1}{2}(A\vec{V},\vec{V})_{0,\Omega} + (B\vec{V},\vec{Q})_{0,\Omega} + (\vec{G},\vec{V})_{0,\Omega}, \tag{4.8}$$

and the related augmented Lagrangian saddle point problem is given by

$$L_r(\vec{V},\vec{Q}) = L(\vec{V},\vec{Q}) + \frac{r}{2}\left\|B\vec{V}\right\|^2, \tag{4.9}$$

where $\left\|B\vec{V}\right\|^2 = (B\vec{V}, B\vec{V})_{0,\Omega}$. In order to solve the saddle point problem (4.9), Uzawa's algorithm can be used as follows [37]:

1 - $\vec{U}^0$ and $\vec{P}^0$ are given;

2 - compute $\vec{\delta U}$ by solving:

$$(A + rB^T B)\vec{\delta U} = (A + rB^T B)\vec{U}^n - B^T P^n + \vec{G};$$

3 - update $\vec{U}^n$ and $\vec{P}^n$:

$$\vec{U}^{n+1} = \vec{U}^n - \vec{\delta U};$$

$$\vec{P}^{n+1} = \vec{P}^n - \vec{\delta P}, \qquad \text{where} \qquad \vec{\delta P} = r\nabla \cdot \vec{U}^{n+1};$$

4 - stop if $\left\|B\vec{U}^n\right\| \leq \varepsilon$, else return to step 2.

In practice, r is chosen to be large ($r \approx 10^8$). Usually, this algorithm converges in 2 or 3 iterations. The linear system, in step 2, can be solved using an LU factorization.

The Stokes solver is based on this algorithm, and a condensation technique is used, which allows the elimination of two degrees of freedom in pressure and of two degrees of freedom in velocity associated with the barycentre of each element. Consequently, 4×(number of elements) equations can be removed from the Stokes problem without losing accuracy. This technique, with Uzawa's algorithm, reduce the required storage space and therefore the computing time necessary to solve the Stokes problem.

4.2 Second Mixed Formulation (Brown et al.)

One of the difficulties with the systems of equations (4.5) and (4.6) is related to the momentum and the continuity equations. These equations are not well posed if the extra-stress tensor $\bar{\bar{\tau}}_v$ is kept fixed. Therefore, a fixed-point iterative method cannot be used for solving this system, even at low Weissenberg numbers [20]. It is therefore necessary to use another mixed formulation in order to overcome this difficulty. Consequently, the following change of variable, proposed by Brown et al. [19], has been considered:

$$\bar{\bar{S}} = \bar{\bar{\tau}}_v - 2\eta_v \bar{\bar{\dot{\gamma}}}(\vec{u}). \tag{4.10}$$

Fortin and Zine [38] observed that this change of variable enhances the convergence properties of the numerical scheme. As a result, systems (4.5) and (4.6) can now be rewritten, considering $\eta = \eta_s + \eta_v$, as:

Find $(\vec{u}, p, F) \in V \times Q \times W$ so that:

$$\begin{cases} \rho(\dfrac{\partial \vec{u}}{\partial t}) - \vec{\nabla} \cdot [2(\eta_s + \eta_v)(\bar{\bar{\dot{\gamma}}})\bar{\bar{\dot{\gamma}}}(\vec{u})] + \vec{\nabla} p = \vec{\nabla} \cdot \bar{\bar{S}} + \vec{f}_v, & \text{in } \Omega; \\ \vec{\nabla} \cdot \vec{u} = 0, & \text{in } \Omega; \\ \dfrac{\partial F}{\partial t} + \vec{u} \cdot \vec{\nabla} F = 0, & \text{in } \Omega. \end{cases} \tag{4.11}$$

Find $\bar{\bar{S}} \in \Phi$ so that:

$$\bar{\bar{S}} + \lambda[\frac{\partial \bar{\bar{S}}}{\partial t} + (\vec{u} \cdot \vec{\nabla})\bar{\bar{S}} - \vec{\nabla}\vec{u} \cdot \bar{\bar{S}} - \bar{\bar{S}} \cdot \vec{\nabla}\vec{u}^T] =$$

$$-2\eta_v \lambda[\frac{\partial \bar{\bar{\dot{\gamma}}}(\vec{u})}{\partial t} + (\vec{u} \cdot \vec{\nabla})\bar{\bar{\dot{\gamma}}}(\vec{u}) - \vec{\nabla}\vec{u} \cdot \bar{\bar{\dot{\gamma}}}(\vec{u}) - \bar{\bar{\dot{\gamma}}}(\vec{u}) \cdot \vec{\nabla}\vec{u}^T], \text{ in } \Omega. \tag{4.12}$$

For this $(\vec{u},p,F,\bar{\bar{S}})$ formulation, the ellipticity of the Stokes problem is recovered, since an elliptic contribution in the weak form of the momentum equations is added [20]. But there are new terms appearing in the constitutive equations such as the convected derivative of the rate-of-strain tensor, $(\vec{u}\cdot\vec{\nabla})\bar{\bar{\dot{\gamma}}}(\vec{u})$. Since this term involves second order derivatives of the velocity, it requires special attention. To circumvent this difficulty, Fortin and Zine [38] have performed an integration by parts. This method leads to the computation of a boundary integral at the geometry outlet.

The Galerkin variational formulation associated with the systems of equations (4.11) and (4.12) is given by:

Find $(\vec{u},p,F)\in V\times Q\times W$ so that:

$$\begin{cases} \int_\Omega (\rho\dfrac{\partial\vec{u}}{\partial t}\cdot\vec{v})d\vec{x}+\int_\Omega[(2\eta(\bar{\bar{\dot{\gamma}}})\bar{\bar{\dot{\gamma}}}(\vec{u})+\bar{\bar{S}}):\vec{\nabla}\vec{v}]d\vec{x} \\ \qquad -\int_\Omega(p\vec{\nabla}\cdot\vec{v})d\vec{x}-\int_\Omega\vec{f}_v\vec{v}=0, & \forall\vec{v}\in V; \\ \int_\Omega(q\vec{\nabla}\cdot\vec{u})d\vec{x}=0, & \forall q\in Q; \\ \int_\Omega(\dfrac{\partial F}{\partial t}\cdot w)d\vec{x}+\int_\Omega[(\vec{u}\cdot\vec{\nabla}F)\cdot w]d\vec{x}=0 & \forall w\in W. \end{cases} \qquad (4.13)$$

Find $\bar{\bar{S}}\in\Phi$ so that:

$$\int_\Omega(\{\bar{\bar{S}}+\lambda[\frac{\partial\bar{\bar{S}}}{\partial t}+(\vec{u}\cdot\vec{\nabla})\bar{\bar{S}}-\vec{\nabla}\vec{u}\cdot\bar{\bar{S}}-\bar{\bar{S}}\cdot\vec{\nabla}\vec{u}^T]\}:\bar{\bar{\varphi}})d\vec{x}=$$

$$\int_\Omega(\{-2\eta_v\lambda[\frac{\partial\bar{\bar{\dot{\gamma}}}(\vec{u})}{\partial t}+(\vec{u}\cdot\vec{\nabla})\bar{\bar{\dot{\gamma}}}(\vec{u})-\vec{\nabla}\vec{u}\cdot\bar{\bar{\dot{\gamma}}}(\vec{u})-\bar{\bar{\dot{\gamma}}}(\vec{u})\cdot\vec{\nabla}\vec{u}^T]\}:\bar{\bar{\varphi}})d\vec{x},$$

$$\forall\bar{\bar{\varphi}}\in\Phi. \qquad (4.14)$$

The DG method associated with equation (4.14) is given by:

Find $\bar{\bar{S}}_h \in \Phi_h$ so that:

$$\int_k (\left\{ \bar{\bar{S}}_h + \lambda \left[\frac{\partial \bar{\bar{S}}_h}{\partial t} + (\vec{u}_h \cdot \vec{\nabla}) \bar{\bar{S}}_h - \vec{\nabla}\vec{u}_h \cdot \bar{\bar{S}}_h - \bar{\bar{S}}_h \cdot \vec{\nabla}\vec{u}_h^{\,T} \right] \right\} : \bar{\bar{\varphi}}_h) d\vec{x}$$

$$+ \lambda \int_{\partial k^-} (\vec{u}_h \cdot \vec{n}_k)[\bar{\bar{S}}_h] : \bar{\bar{\varphi}}_h ds =$$

$$2\eta_v \lambda \int_k [\vec{\nabla}\vec{u}_h \cdot \dot{\bar{\bar{\gamma}}}(\vec{u}_h) + \dot{\bar{\bar{\gamma}}}(\vec{u}_h) \cdot \vec{\nabla}\vec{u}_h^{\,T}] : \bar{\bar{\varphi}}_h d\vec{x} - 2\eta_v \lambda \int_k (\vec{u}_h \cdot \vec{\nabla}) \dot{\bar{\bar{\gamma}}}(\vec{u}_h) : \bar{\bar{\varphi}}_h d\vec{x}$$

$$-2\eta_v \lambda \int_k (\frac{\partial \dot{\bar{\bar{\gamma}}}(\vec{u}_h)}{\partial t}) : \bar{\bar{\varphi}}_h d\vec{x}, \quad \forall \bar{\bar{\varphi}}_h \in \Phi_h, \quad (4.15)$$

where

$$-2\eta_v \lambda \int_k (\vec{u}_h \cdot \vec{\nabla}) \dot{\bar{\bar{\gamma}}}(\vec{u}_h) : \bar{\bar{\varphi}}_h d\vec{x}$$

can be written as

$$-2\eta_v \lambda \int_k (\vec{u}_h \cdot \vec{\nabla}) \dot{\bar{\bar{\gamma}}}(\vec{u}_h) : \bar{\bar{\varphi}}_h d\vec{x} - 2\eta_v \lambda \int_{\partial k^-} (\vec{u}_h \cdot \vec{n}_k)[\dot{\bar{\bar{\gamma}}}(\vec{u}_h)] : \bar{\bar{\varphi}}_h ds. \quad (4.16)$$

This mixed formulation is restricted to the Oldroyd-B type constitutive equations. Since we have a change of variable into the constitutive equations as a result, we also have a change with the boundary conditions.

4.3 Mixed Formulation of Guénette and Fortin

Guénette and Fortin [20] have introduced a stabilizing elliptic operator in the discrete version of the momentum equation. As a result, the derivative of the rate-of-strain tensor is avoided and the method is not restricted to a

particular class of constitutive equations. The following change of variable is used:

$$\bar{\bar{S}} = \bar{\bar{\tau}}_v - 2\alpha\, d, \tag{4.17}$$

where α is a positive parameter. The following mixed formulation is then obtained:

Find $(\vec{u}, p, F, \bar{\bar{\tau}}_v, d) \in V \times Q \times W \times \Phi$ so that:

$$\begin{cases} \rho(\dfrac{\partial \vec{u}}{\partial t}) - \vec{\nabla} \cdot [2\eta_s(\bar{\bar{\dot{\gamma}}})\bar{\bar{\dot{\gamma}}}(\vec{u})] - \vec{\nabla} \cdot [2\alpha \bar{\bar{\dot{\gamma}}}(\vec{u})] + \vec{\nabla} p = \vec{\nabla} \cdot \bar{\bar{\tau}}_v - \nabla \cdot (2\alpha\, d) + \vec{f}_v; \\ \vec{\nabla} \cdot \vec{u} = 0; \\ \dfrac{\partial F}{\partial t} + \vec{u} \cdot \vec{\nabla} F = 0; \\ \bar{\bar{\tau}}_v + \lambda[\dfrac{\partial \bar{\bar{\tau}}_v}{\partial t} + (\vec{u} \cdot \vec{\nabla})\bar{\bar{\tau}}_v - \vec{\nabla}\vec{u} \cdot \bar{\bar{\tau}}_v - \bar{\bar{\tau}}_v \cdot \vec{\nabla}\vec{u}^T] = 2\eta_v \bar{\bar{\dot{\gamma}}}(\vec{u}); \\ d = \bar{\bar{\dot{\gamma}}}(\vec{u}). \end{cases} \tag{4.18}$$

In the discrete momentum equation, an elliptic operator is introduced, which is $2\alpha\vec{\nabla} \cdot d$, where d is a discrete approximation of the rate-of-strain tensor $\bar{\bar{\dot{\gamma}}}(\vec{u})$. This elliptic operator vanishes with the analytical solution [24]. The effectiveness of the Brown et al. and Guénette and Fortin mixed formulations' is related to the added elliptic term into the momentum equation, which helps to solve the Stokes problem using the Galerkin method. The Guénette and Fortin mixed formulation results in a scheme that is more stable since there is an additional elliptic term in the momentum equation and also it does not make it necessary to make a change of a variable into the constitutive equations and therefore with the boundary conditions.

4.4 Advantages and Disadvantages of the Iterative Methods

The most important advantage of the coupled approach is that convergence is faster, when compared with the decoupled approach. Newton's method yields quadratic convergence when the initial estimate is carefully chosen (sufficiently near to the exact solution). However, the major disadvantage of this approach is that it requires the computation of very large Jacobian matrices at each iteration. In the case of a two-dimensional viscoelastic multifluid flow problem, a large number of equations have to be solved, which significantly increases the memory capacity required. As a result, three-dimensional problems and multi-mode models become more difficult to study [24].

The main advantage of the decoupled approach is the breakup of the global system into the solution of two smaller problems. Each problem can then be discretized, taking its specific mathematical nature into account. However, the main disadvantage of this approach lies in the iterative procedure. Picard-type schemes are often slow to converge and the attainable Weissenberg number is usually lower than with a coupled solver [24]. By using a preconditioned Generalized Minimal Residual (GMRES) iterative solver to enforce coupling, the attainable Weissenberg number increases and the number of iterations required to reach convergence is reduced [18,35].

In this work, we chose to solve the Stokes equations using Uzawa's algorithm. The Stokes and the transport of the pseudo-concentration are solved together using a coupled approach, which is based on Newton's method. As a result, the convergence is faster than with the uncoupled

approach. The constitutive equations are solved separately from the Stokes equations and the transport equation of the pseudo-concentration in a decoupled way, using a fixed-point iterative method. This reduces the size of the overall problem. The second mixed formulation is used to ensure the compatibility between the Stokes problem and the constitutive equations.

CHAPTER 5

TREATMENT OF THE NUMERICAL OSCILLATIONS AND DIFFUSION

The accurate simulation of multifluid flows is a challenging task. One of the key purposes of these simulations is to accurately determine the position of the interface, which is a priori unknown. Over the past few decades, many methods have been developed to follow a sharp interface as accurately as possible, such as the volume-of-fluid (VOF) method, the level-set method and the pseudo-concentration method. The common point of all these techniques is the color function F that identifies the regions of the domain occupied by each fluid. If we consider the pseudo-concentration technique, the following equation describes the evolution with time of the regions occupied by each fluid:

$$\frac{\partial}{\partial t}F + (\vec{u}\cdot\vec{\nabla})F = 0. \qquad (5.1)$$

It is well known that the transport equation of the pseudo-concentration is hyperbolic and, as a result, nonphysical oscillations may appear in the discrete solution of (5.1). In order to avoid these oscillations, the jump of this function can be redefined as a sharp but regular transition region. This approach is even justified from a physical point of view since it is known that a small region of mixture between two immiscible fluids exists [27]. The solution of equation (5.1) can be difficult to determine. In the finite-element method framework, upwinding techniques, such as the streamline-upwind/Petrov-Galerkin (SUPG) method, can be used to improve the Galerkin formulation. But even this technique cannot eliminate all of the non-physical oscillations. One way

to improve this method is to use mesh refinement techniques. But this does not guarantee the complete elimination of the undesirable oscillations. Consequently, a specific algorithm must be used in order to eliminate these oscillations.

5.1 Local Least-squares Free Surface Updating

These numerical difficulties can be controlled using the free surface updating strategy proposed by Dufour and Malidi [39]. This approach is based on least-squares problems defined on patches of elements. This allows us to locally reinitialize F, without having a region of transition that is too sharp, in order to avoid numerical oscillations. Each patch is formed by all the elements connected to a vertex of the mesh (cf. figure 5.1).

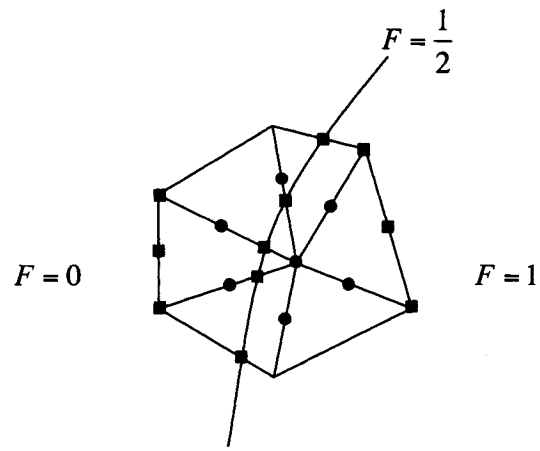

Figure 5.1 Patch of quadratic elements for the free surface update

The pseudo-concentration is updated at the interior nodes (•) of the patch using the value of F at the sampling points (■) and at the interior nodes. The first sampling points are chosen to be the intersection of the

interface with the edges of the elements of the patch, in order to minimize the displacement of the free surface in the update process. Since the updated region of transition must be in the finite element space, the reinitialized pseudo-concentration in the patch of elements is expressed as

$$F_h^{updated}(\vec{x}) = \sum_{j=1}^{d} a_j \varphi_j(\vec{x}),$$

where $d = 6$ and the φ_j are the quadratic finite element interpolation functions. The coefficients $\vec{a} = (a_1, a_2, ...a_d)$ are computed by solving the least-squares problems

$$\Theta(\vec{a}) = \frac{1}{2} \sum_{i=1}^{k} \{F_h(\vec{x}_i) - \sum_{j=1}^{d} a_j \varphi_j(\vec{x}_i)\}^2,$$

on each patch, where F_h is the finite element discretization of the pseudo-concentration and the $\vec{x}_i$ are the k sampling points and interior nodes of the patch.

The proposed methodology helps conserve mass locally, since the free surface is updated on patches of elements. This strategy results in a smooth region of transition of constant width, which helps to accurately model interfacial physics.

5.2 Adding a Non-linear Absorption Term

In order to eliminate overshoots and undershoots when solving a convection dominant problem using finite element method Layton and Polman [40] have proposed a technique which involves adding a nonlinear absorption term of the form $A(F)$ to the standard Galerkin finite element

method. This technique can be applied to the Galerkin finite element method or to a stabilized formulation for solving the transport equation. The nonlinear absorption term is defined [40] as

$$A(F) = \rho^{-1}[\min\{F - F_{\min}, 0\} + \max\{F - F_{\max}, 0\}] \ , \qquad (5.2)$$

where ρ is a very small parameter of the order of h^2, and h is the maximum triangle diameter. We know, from the definition of the pseudo-concentration function, that $F_{\min} = 0 \le F \le 1 = F_{\max}$. The nonlinear term (5.2) is then rewritten as

$$A(F) = \rho^{-1}[\min\{F, 0\} + \max\{F - 1, 0\}] \ . \qquad (5.3)$$

By adding this term to the finite element formulation, overshoots and undershoots are considerably reduced, but small oscillations still remain.

As a test problem, we will consider a Newtonian drop in a Newtonian matrix, submitted to a shear flow. This implies that the relaxation times are $\lambda_d = 0$ and $\lambda_m = 0$. The viscosity ratio is set to $\frac{\eta_d}{\eta_m} = 1$, where $\eta_d = \eta_{d_s} + \eta_{d_v}$ and $\eta_m = \eta_{m_s} + \eta_{m_v}$ so that $\eta_{m_s} = \eta_{d_s} = \frac{1}{9}$ (solvent viscosities of matrix and drop) and $\eta_{m_v} = \eta_{d_v} = \frac{8}{9}$ (viscoelastic viscosities of matrix and drop). The shear rate is set to 0,3. Figure 5.2 shows the mesh used, which consists of 13414 elements and 27165 nodes. The shape of the drop is shown after 100 time steps with $\Delta t = 0{,}02$. Figure 5.3 shows the pseudo-concentration of the drop with no updating, while figure 5.4 illustrates the pseudo-concentration of the drop using Layton and Polman's correction, which shows the elimination of the overshoots and undershoots. But this technique cannot remove all the numerical oscillations, and diffusion problems remain.

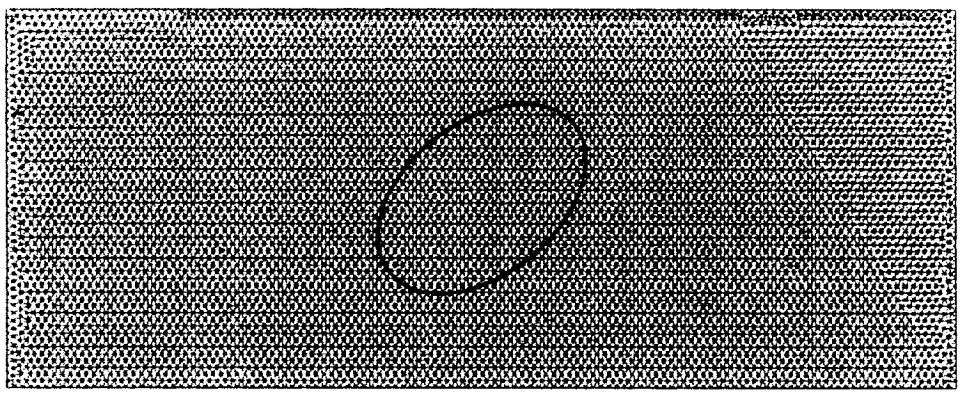

Figure 5.2 Mesh and the shape of the drop after 100 time steps

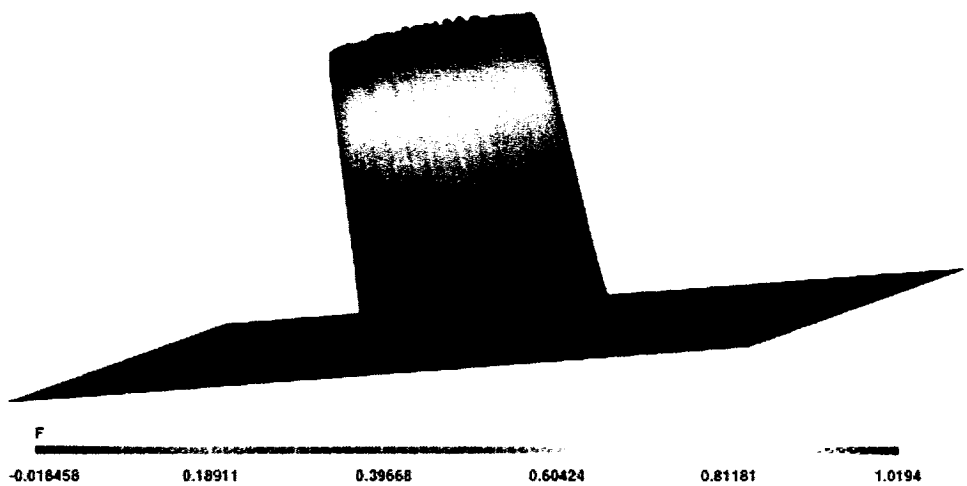

Figure 5.3 Pseudo-concentration with no correction after 100 time steps

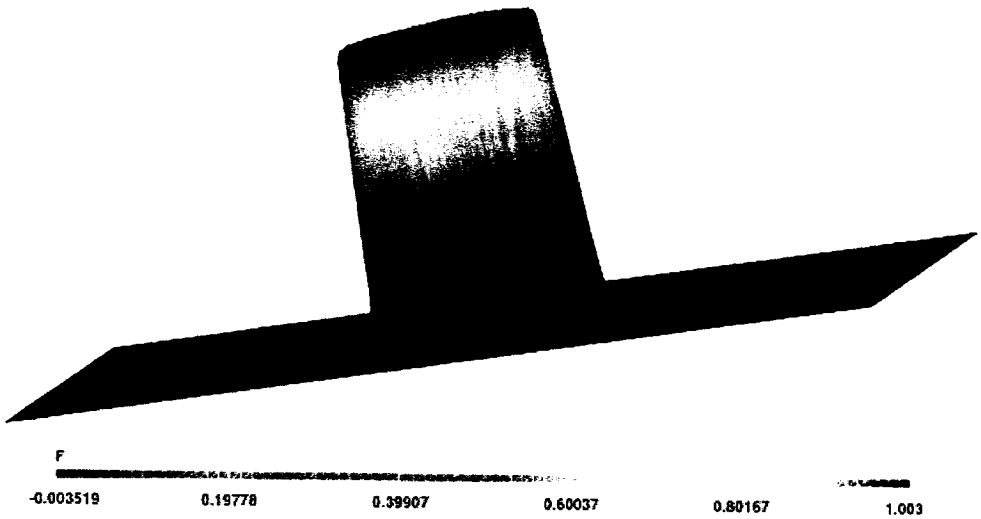

Figure 5.4 Pseudo-concentration using the nonlinear absorption term of Layton and Polman [40], after 100 time steps

5.3 The Filtering Technique

Devals et al. [41] have proposed a technique to filter out oscillations through a change of variable that can be used for both steady and transient problems. This change of variable is used to sharpen the region of transition of the marker variable by eliminating the numerical oscillations that may result from the solution of the advection equation (5.1). The goal of this approach is to find a continuous positive step function that varies between zero and one. One possibility for this function is given by

$$F = \frac{1}{1+\exp(-2G)}, \quad \text{for} \quad F \in [-1,1] \text{ and } G \in]-\infty,+\infty[. \tag{5.4}$$

By replacing (5.4) into (5.1), the following expression is obtained:

$$\frac{-2\exp(-2G)}{(1+\exp(-2G))^2}\left(\frac{\partial G}{\partial t} + \vec{u}.\vec{\nabla}G\right) = 0 \ . \tag{5.5}$$

It is obvious that the first term on the left-hand side is non-zero. Consequently,

$$\frac{\partial G}{\partial t} + \vec{u}.\vec{\nabla}G = 0 \ . \tag{5.6}$$

In practice, a scaling factor G_0 is necessary for a better behavior of the filtering strategy. Therefore, a better control of the oscillations will occur. The following expression is considered:

$$G = G_0 g, \qquad g \in [-1,1]. \tag{5.7}$$

Substituting equation (5.7) into (5.6) gives

$$\frac{\partial g}{\partial t} + \vec{u} \cdot \vec{\nabla} g = 0. \tag{5.8}$$

To obtain a function ranging from 0 to 1, the following transformation is needed:

$$g = 2f - 1, \qquad f \in [0,1]. \tag{5.9}$$

Equation (5.8) then becomes

$$\frac{\partial f}{\partial t} + \vec{u} \cdot \vec{\nabla} f = 0, \tag{5.10}$$

which is identical to (5.1). This equation provides a solution for f using the SUPG method, and after applying transformations (5.9), (5.7) and (5.4), F is obtained. In this work, the choice of $G_0 = 6$ seems to give good results. This choice yields $F \in [\varepsilon, 1-\varepsilon]$ with $\varepsilon = 1.3955 \times 10^{-6}$. By choosing a larger value of G_0, a smaller value of ε could be obtained. This technique was applied in both stationary and transient verification problems [41]. In the transient case, the two-dimensional Zalesak's problem, which is commonly used to test the quality of advection methods, was studied. It was shown that this technique can reduce the amount of diffusion resulting from the use of the SUPG method, and all of the numerical oscillations were removed. This technique

can be implemented in existing finite element codes at low cost. Devals et al. [41] also believe that the performance of the filtering technique could get close to what is obtained with accurate but expensive volume-tracking methods, by combining it with mesh adaptivity strategies.

By using this technique, we obtain a very sharp region of transition. Figure 5.5 illustrates the mesh used, which consists of 13414 elements, and the shape of the drop after 100 time steps, after using the filtering technique. Figure 5.6 shows the pseudo-concentration of the drop at the same time.

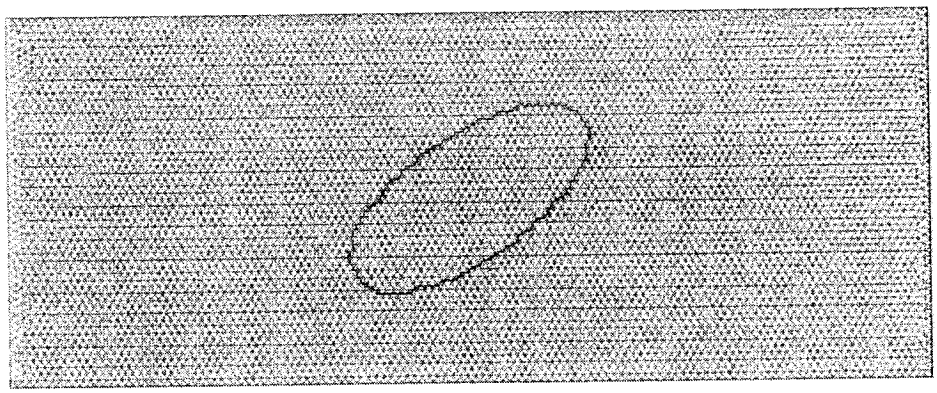

Figure 5.5 Mesh and the shape of the drop after 100 time steps, using the filtering technique

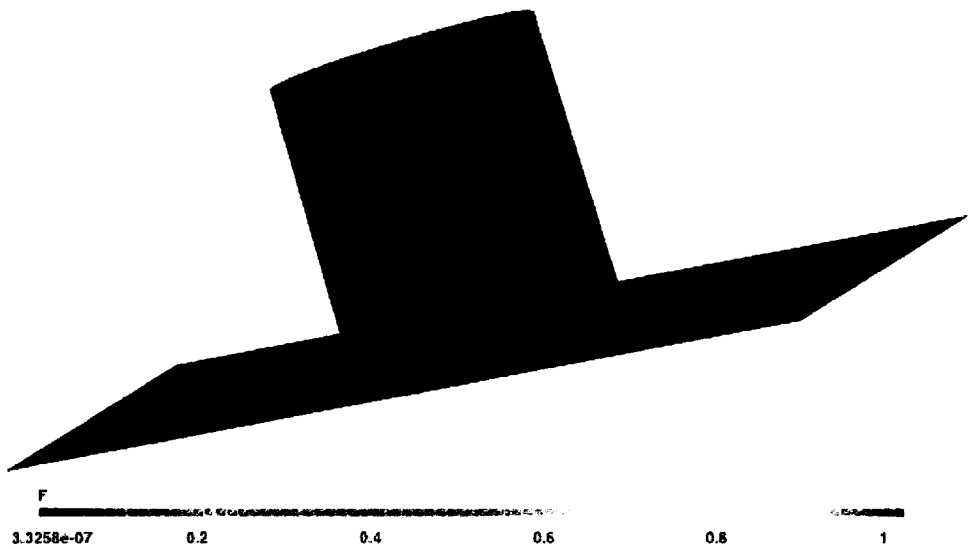

Figure 5.6 Pseudo-concentration after 100 time steps, using the filtering technique

We can see that all the numerical oscillations are completely removed. But at the same time, the pseudo-concentration of the drop becomes too sharp for interfacial tension modeling, since the shape of the drop is not smooth (cf. figure 5.5). In order to accurately compute the derivatives of the pseudo-concentration, we need a sharp but smooth region of transition of F. As a result, we decided to convolve this sharp function with a smooth kernel function.

5.4 Kernel-Based Smoothing Techniques

When solving the transport equation of the pseudo-concentration function,

$$\frac{\partial}{\partial t}F + (\vec{u}\cdot\vec{\nabla})F = 0,$$

we need a sharp but smooth region of transition of F in order to accurately determine the position of the free surface. Moreover, since it is difficult to accurately compute first and second order spatial derivatives of the color function with a very sharp transition region, convergence is difficult to achieve when modeling interfacial tension. These derivatives are required in order to accurately approximate free surface related quantities such as the unit normal to the interface, that is approximated using

$$\vec{n} = \frac{\vec{\nabla} F}{\left\| \vec{\nabla} F \right\|}, \tag{5.11}$$

and the local curvature, that is expressed as

$$\kappa = -\vec{\nabla} \cdot \vec{n}. \tag{5.12}$$

The transition of F has to be sharp, but smooth enough to allow the accurate computation of first and second order derivatives. In the original CSF model [42], the color function F is first convolved with a kernel K to yield a mollified function $\tilde{F}$. Interface normals are then computed using

$$\vec{n} = \frac{\vec{\nabla} \tilde{F}}{\left\| \vec{\nabla} \tilde{F} \right\|}.$$

The local curvature is then obtained using (5.12). Williams et al. [42] have shown that convolution methods can also be applied to surface force distributions, which is a major improvement over the original CSF model.

5.4.1 Convolution Product Smoothing

Consider $F(\vec{x})$ as a discontinuous pseudo-concentration function, which could result from the filtering technique described in section 5.3. The

convolution of $F(\vec{x})$ with the kernel K at the point $\vec{x}$, noted $K * F$, is given by

$$\tilde{F}(\vec{x}) = K * F(\vec{x}) = \int_{\Omega} F(\vec{x}')K(\vec{x}' - \vec{x})d\vec{x}' \,, \tag{5.13}$$

where $F(\vec{x})$ is the discontinuous function and $\tilde{F}(\vec{x})$ is the smoothed function. It should be noted that if $K \in C^k$ then $\tilde{F}(\vec{x}) = K * F(\vec{x}) \in C^k$.

There are a number of possibilities for the approximation of the convolution integral (5.13). According to Williams et al. [42], one way to approximate the convolution integral is by using a simple midpoint rule:

$$K * F(\vec{x}) = \int_{\Omega} F(\vec{x}')K(\vec{x}' - \vec{x})d\vec{x}' \approx \sum_{i} (\vec{x}_i' - \vec{x})F(\vec{x}_i')\Delta\vec{x}_i', \tag{5.14}$$

where $\vec{x}_i'$ are the set of discrete sampling points around the point $\vec{x}$.

The support of the kernel is denoted by Ω_l, which is the portion of the domain over which the kernel is nonzero. For a function with circular support, ε is the radius of the support. Since the kernel is a function of $\vec{x}$ and ε, then the correct notation for the kernel is $K(\vec{x},\varepsilon)$ and must satisfy the following properties:

1 - have a compact support;

2 - be monotically decreasing with respect to $|\vec{x}|$;

3 - be smooth for $k \geq 1$;

4 - have the normality property, $\int_{\Omega} K(\vec{x},\varepsilon)d\vec{x} = 1$;

5 - approach the Dirac delta function in the limit $|\Omega_l| \to 0$.

As $|\Omega_i| \to 0$, which means as $\varepsilon \to 0$, kernel derivatives have a tendency to become singular. As a result, resolving discontinuities and extrema in the kernel and its derivatives may require more discrete points within the radius of the support of the kernel. Consequently, for any given kernel, it is important to find a relation between the value of ε and the number of discrete points. Moreover, it is very important to note that there is also a relationship between the radius of the support of the kernel and the mesh. As a result, an estimation of the influence of the mesh, and of interface orientation on accuracy and convergence, is required, and should be investigated in the future.

In order to use convolutions in the continuum surface force model, it is important to choose a kernel that can satisfy all the required properties that have been mentioned above. In recent years, different kernels have been studied such as Gaussians, smooth polynomials, cosine curves, etc. The eighth-degree kernel K_8 satisfies all these properties [42]. It is given by:

$$K_8(r,\varepsilon) = \begin{cases} A[1-(\frac{r}{\varepsilon})^2]^4 & if \quad r < \varepsilon; \\ 0 & if \quad r \geq \varepsilon, \end{cases} \tag{5.15}$$

where A is a normalization constant that satisfies $\int_{\Omega} K_8(r,\varepsilon)dr = 1$. This kernel is easy to implement and it generates accurate results for an acceptable ratio of support radius to mesh spacing.

Our strategy was to use the filtering technique to remove all the numerical oscillations and diffusion. A very sharp region of transition for the pseudo-concentration function is then obtained. Then, an eighth-degree kernel

is used to smooth the region of transition of the pseudo-concentration in order to accurately compute the derivatives of the pseudo-concentration function. Figure 5.7 shows the mesh used, which consists of 5235 elements, and the shape of the drop after 100 time steps with $\Delta t = 0{,}02$. Figure 5.8 shows the pseudo-concentration without any correction, whereas figure 5.9 shows the pseudo-concentration of the drop after 100 time steps, where the filtering technique and convolution with the eighth-degree kernel are used every 10 time steps.

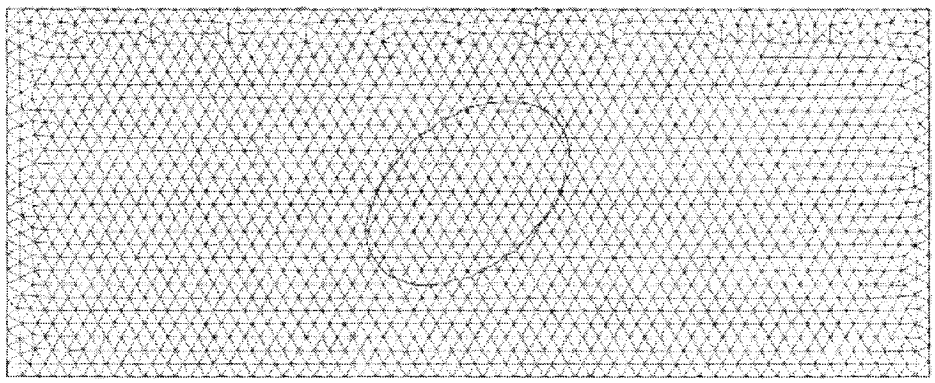

Figure 5.7 Mesh and the shape of the drop after 100 time steps

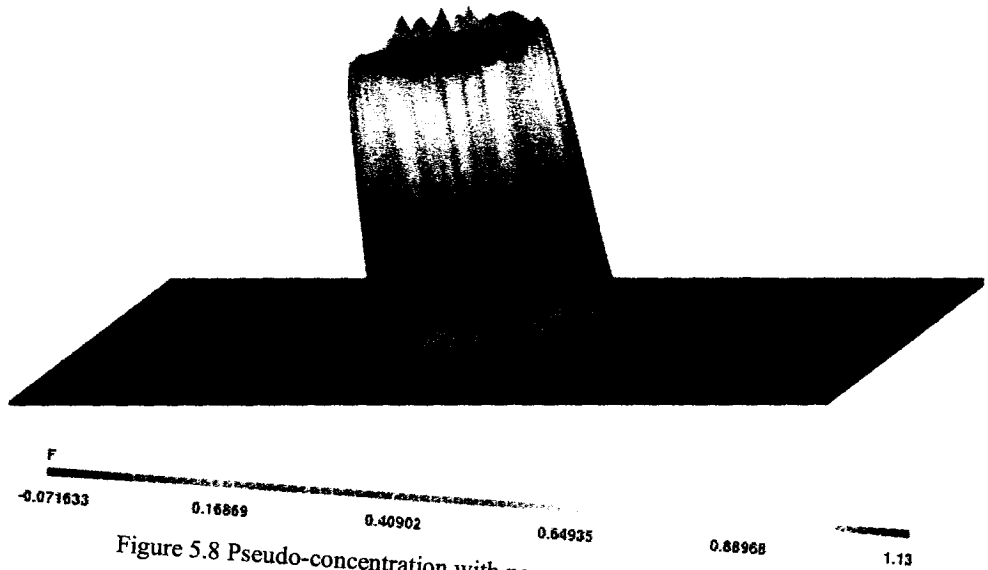

Figure 5.8 Pseudo-concentration with no correction after 100 time steps

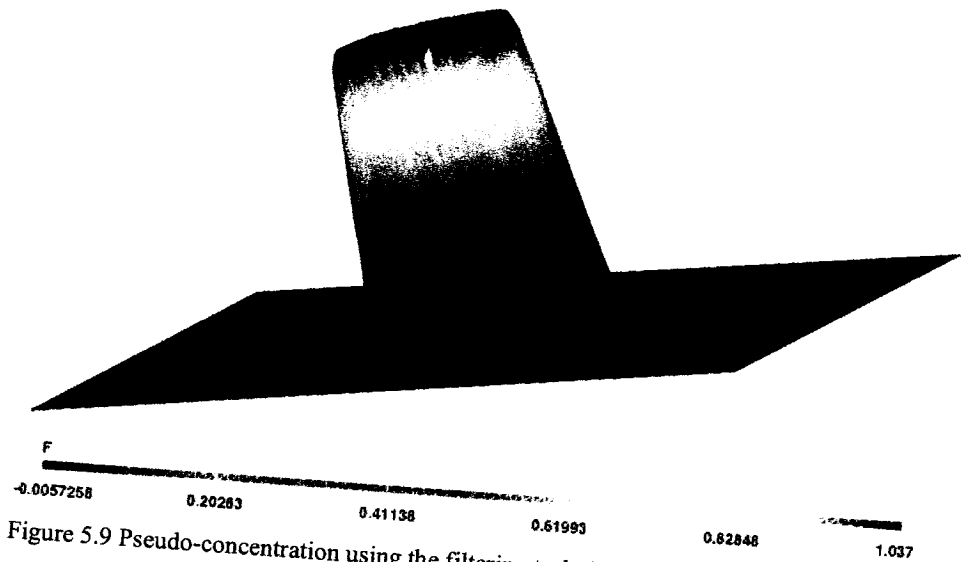

Figure 5.9 Pseudo-concentration using the filtering technique and the convolution with the eighth-degree kernel, after 100 time steps

As it was explained earlier, there is a relationship between the radius of the support of the kernel and the size of the mesh, and also the shape and orientation of the interface. If we change the size of the mesh, or the shape of the interface (drop in our case), we have to change the radius of the support of the kernel in order to get acceptable results. Therefore, in order to understand these relationships, more work needs to be done.

CHAPTER 6

VERIFICATION OF THE NUMERICAL MODEL

The verification of the numerical modeling of transient viscoelastic multifluid flow problems are presented in this chapter. Results are shown for two different verification problems. The first problem is the Poiseuille flow, which is used for the verification of our transient schemes, applied to the flow of a viscoelastic fluid. The second problem is the transport of a drop in a Poiseuille flow, which consists of a viscoelastic drop immersed in a matrix that can be either Newtonian or viscoelastic.

The numerical results are obtained using the standard Galerkin method for discretizing the Stokes problem, using Uzawa's algorithm for enforcing the incompressibility constraint, the SUPG method for the transport equation of the pseudo-concentration and the DG method for the constitutive equations. For approximating the transient term in Stokes problem, the BDF2 scheme is used, and the IMR is used for the transport equation of the pseudo-concentration and the constitutive equations. The fluids under study are Oldroyd-B fluids. Even though the Guénette-Fortin formulation is more popular in the literature, for time limitation reasons, we used the second mixed formulation of Brown et al. [19] (cf. chapter 5 for details). Interfacial tension is modeled using the CSF model. Free surface updating is performed using the local least-squares updating technique.

6.1 The Poiseuille Flow Verification Problem

A parabolic velocity profile is imposed at the inlet of a rectangular channel. Let H be the height and L be the length of the channel. The geometry is illustrated in figure 6.1. The length of the channel is $L = 20$ and the height is $H = 2$. The analytical solution of the Stokes problem is therefore given by:

$$\begin{cases} \vec{u} = (\frac{4y}{H^2}(H - y), 0); \\ p = \frac{-4x}{H^2} + c, \end{cases}$$

where c is a constant. We define the Deborah number for transient flows as

$$De = \lambda \dot{\gamma}_{wall},$$

where $\dot{\gamma}_{wall}$ is the shear rate at the solid walls of the domain. The modeling of viscoelastic Poiseuille flow problems can exhibit instabilities at the outlet of the channel. This is caused by our limited knowledge of the boundary conditions to impose at the outlet. We therefore use a longer channel to reduce the drawbacks of using the wrong boundary conditions.

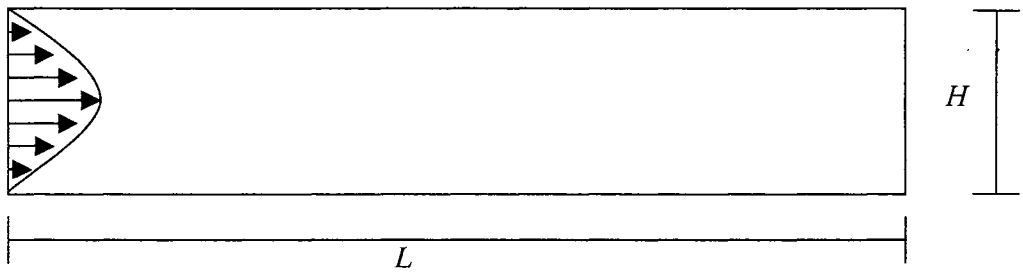

Figure 6.1 Geometry for the Poiseuille flow

The boundary conditions for the Stokes problem, on the left-hand side of the channel, are given by:

$$\begin{cases} u = 2y - y^2; \\ v = 0. \end{cases}$$

The boundary conditions for the extra-stresses, in Brown et al. mixed formulation, on the left-hand side of the channel are given by:

$$\begin{cases} \tau_{11} = 2\eta_v \lambda(4 + 4y^2 - 8y) + 2\eta_v \dfrac{\partial u}{\partial x}; \\ \tau_{22} = 0 + 2\eta_v \dfrac{\partial v}{\partial y}; \\ \tau_{12} = \eta_v(2 - 2y) - \eta_v(\dfrac{\partial u}{\partial y} + \dfrac{\partial v}{\partial x}). \end{cases}$$

At the top and bottom of the channel, we have:

$$\begin{cases} u = 0; \\ v = 0, \end{cases}$$

and finally at the right-hand side of the channel, we have:

$$\begin{cases} u = (\vec{\bar{\sigma}} \cdot \vec{n})_x = 0; \\ v = 0. \end{cases}$$

The initial conditions for the extra-stresses are the same as the analytical solution:

$$\begin{cases} \tau_{11} = 2\eta_v \lambda(4 + 4y^2 - 8y); \\ \tau_{22} = 0; \\ \tau_{12} = \eta_v(2 - 2y). \end{cases} \qquad (6.1)$$

The results for the Poiseuille flow problem are shown for stationary and transient viscoelastic fluid flow problems with the free boundary conditions at the outlet. The stationary problem allows us to verify our

discretization strategy. The transient problem allows us to verify our time integration schemes by comparing the results with the ones obtained for the steady-state problem. The unstructured mesh used for these simulations consists of 18884 triangular elements and 38399 nodes. Figure 6.2 shows the components of velocity in a stationary viscoelastic Poiseuille flow simulation with $\lambda = 0{,}1$ and $\eta_v = \frac{8}{9}$, whereas figure 6.3 shows the same components for the transient problem with $\Delta t = 0{,}02$ after 100 time steps.

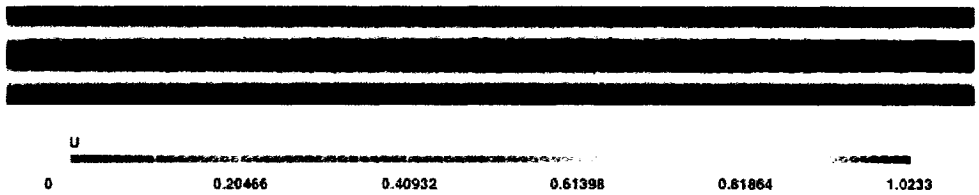

(a) x component of velocity, u

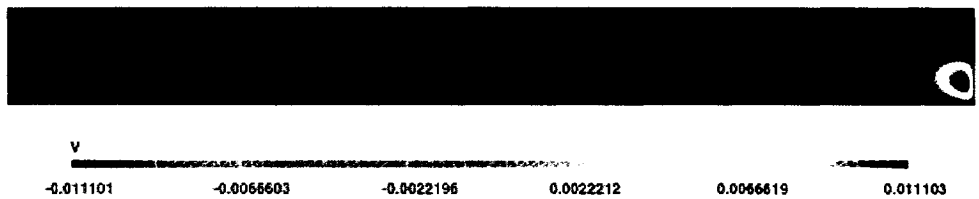

(b) y component of velocity, v

Figure 6.2 Stationary viscoelastic Poiseuille flow problem $(\lambda = 0{,}1)$

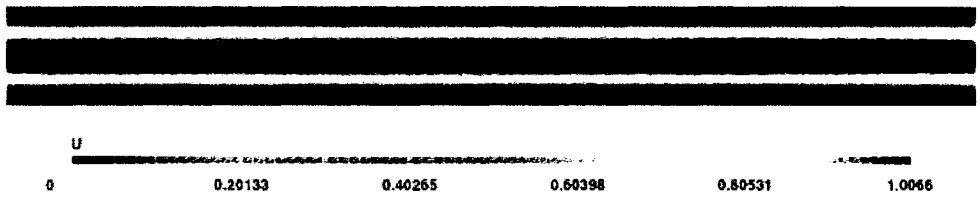

(a) x component of velocity, u

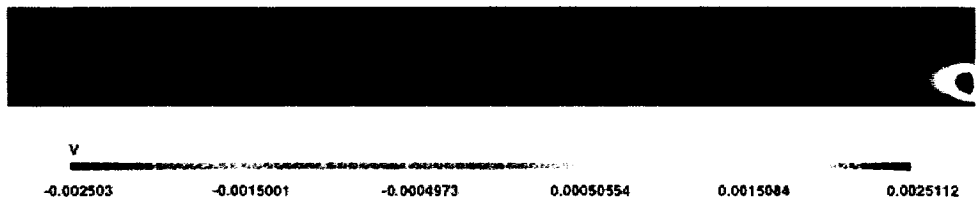

(b) y component of velocity, v

Figure 6.3 Transient viscoelastic Poiseuille flow problem after 100 time steps $(\lambda = 0,1)$

As it can be observed, the velocity components of the stationary and transient viscoelastic flow simulations are identical. These results agree with the analytical solution. In our case, the analytical solution for the velocity components is given by:

$$\begin{cases} u = y(2-y); \\ v = 0. \end{cases}$$

It is shown in figures 6.2(a) and 6.3(a) that the x component of velocity is a function of y^2, which agrees with the analytical solution. Figures 6.2(b) and 6.3(b) illustrate that the y component of velocity is always equal to zero, which is in accordance with the analytical solution. But there are instabilities at the outlet, since the free boundary conditions are used. In order to avoid these instabilities, we can use a longer channel or impose the inlet boundary conditions at the outlet of the geometry.

Figure 6.4 illustrates the components of the extra-stress tensor for the stationary viscoelastic Poiseuille flow simulation, and figure 6.5 shows the same components for the transient simulation with $\Delta t = 0{,}02$, after 100 time steps.

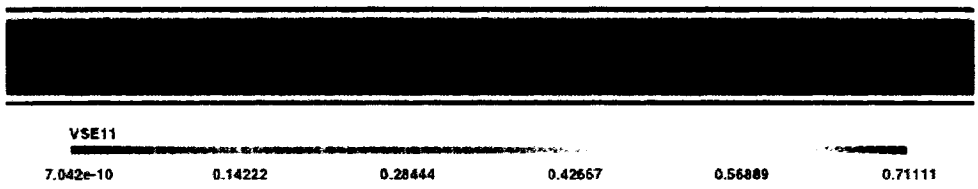

(a) τ_{11} component

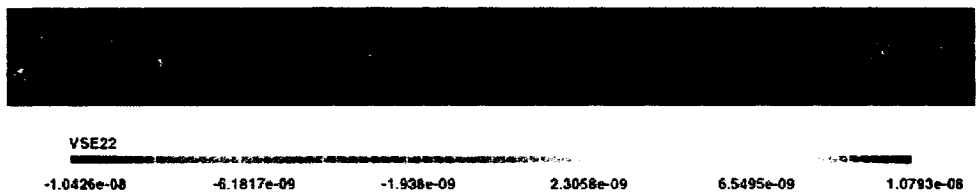

(b) τ_{22} component

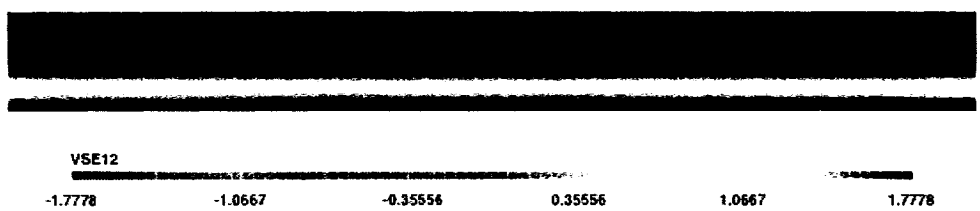

(c) τ_{12} component

Figure 6.4 Extra-stress components for the stationary viscoelastic Poiseuille flow problem

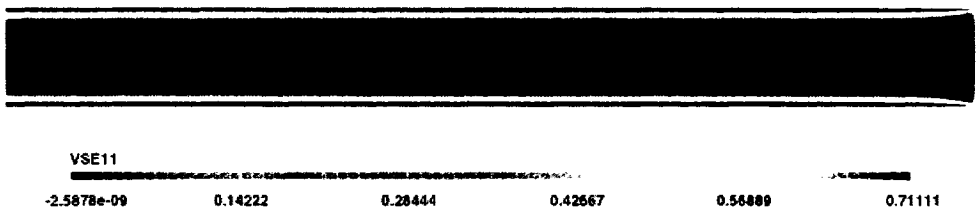

(a) τ_{11} component

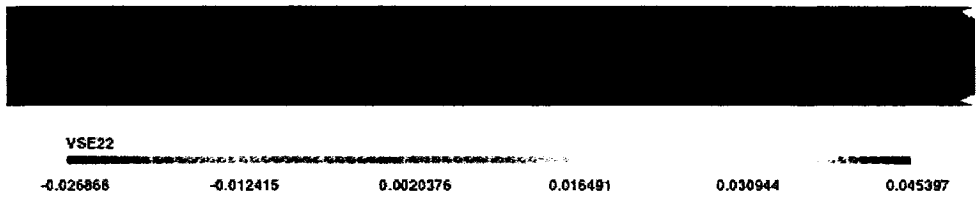

(b) τ_{22} component

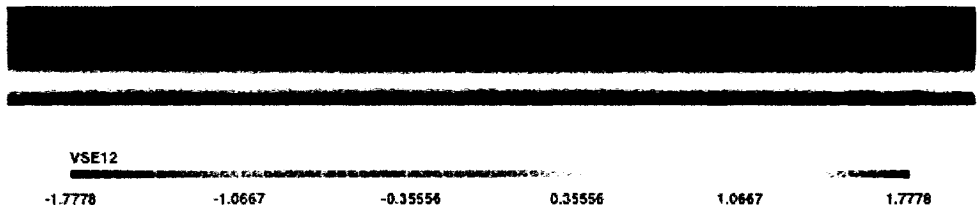

(c) τ_{12} component

Figure 6.5 Extra-stress components for the transient viscoelastic Poiseuille flow problem, after 100 time steps

As it can be observed, the extra-stress components for the stationary and transient viscoelastic flow simulations are identical. These results agree with the analytical solution (6.1).

It can be seen, from figures 6.4(a) and 6.5(a), that the τ_{11} component seems to agree with the τ_{11} expression of equation 6.1. This component has

maximum values at the top and bottom of the geometry where y is equal to 2 and 0 respectively, and it has minimum values at the centerline of the geometry, where y is equal to 1. Figures 6.4(b) and 6.5(b) illustrate the τ_{22} component, which is equal to 0, which is in accordance with the analytical solution. Figures 6.4(c) and 6.5(c) show the τ_{12} component that is a linear function of y. This component has a maximum at the bottom of the geometry where y is equal to 0, and it is minimum at the top of the geometry where y is equal to 2, which is in accordance with the analytic solution as well. Some instabilities at the outlet of the channel is observed because of the free boundary conditions at the outlet.

6.2 Drop Advection Problem

A "two-dimensional drop", of radius r_d, is submitted to a parabolic velocity profile that is imposed at the inlet of a rectangular channel. This is known to be a challenging problem for free surface capturing techniques, since the marker variable is subject to numerical oscillations or diffusion. The geometry is illustrated in figure 6.6. The length of the channel is 20 and the height of the channel is 2.

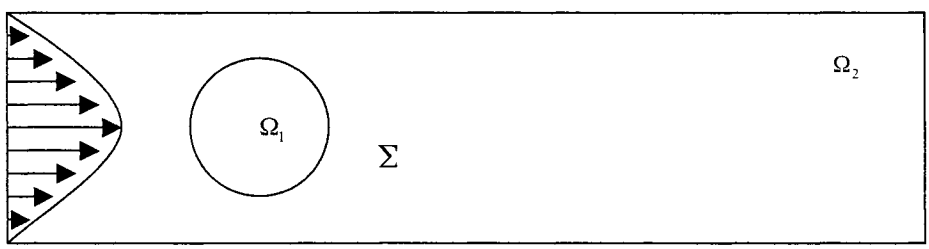

Figure 6.6 Geometry for the transport of a drop in a Poiseuille flow

The boundary conditions for the Stokes problem, on the left-hand side of the channel, are given by:

$$\begin{cases} u = 2y - y^2; \\ v = 0. \end{cases}$$

The boundary conditions for the extra-stresses, in Brown et al. mixed formulation, on the left-hand side of the channel are given by:

$$\begin{cases} \tau_{11} = 2\eta_v \lambda(4 + 4y^2 - 8y) + 2\eta_v \dfrac{\partial u}{\partial x}; \\ \tau_{22} = 0 + 2\eta_v \dfrac{\partial v}{\partial y}; \\ \tau_{12} = \eta_v(2 - 2y) - \eta_v(\dfrac{\partial u}{\partial y} + \dfrac{\partial v}{\partial x}). \end{cases}$$

At the top and at the bottom of the channel, we have:

$$\begin{cases} u = 0; \\ v = 0, \end{cases}$$

and finally at the right-hand side of the channel, we have:

$$\begin{cases} u = (\vec{\bar{\sigma}} \cdot \vec{n})_x = 0; \\ v = 0. \end{cases}$$

The initial condition for the stresses is the same as the analytical solution of the Poiseuille flow (6.1). The initial condition for the pseudo-concentration is given by:

$$F(\vec{x}) = \begin{cases} 1 & if \quad \vec{x} \in \Omega_1; \\ 0 & if \quad \vec{x} \in \Omega_2. \end{cases}$$

Since we are using the SUPG method for solving the transport equation of the pseudo-concentration, it is necessary to impose a free boundary condition for F over $\partial\Omega$.

The results for the transport of the drop are shown for a viscoelastic drop ($\lambda_d = 0{,}1$) immersed in a Newtonian fluid. This problem allows us to verify the advection of the viscoelastic drop, and of the extra-stress components in a transient flow. The unstructured mesh used for this simulation consists of 18884 triangular elements and 38399 nodes. Figure 6.7 shows the initial shape of the drop, which is a circle of radius $r_d = 0{,}5$.

Figure 6.7 Initial shape of the drop

Figure 6.8 illustrates the initial pseudo-concentration function (a) and the pseudo-concentration function after 25 (b), 50 (c), 75 (d) and 100 (e) time steps, with $\Delta t = 0{,}02$.

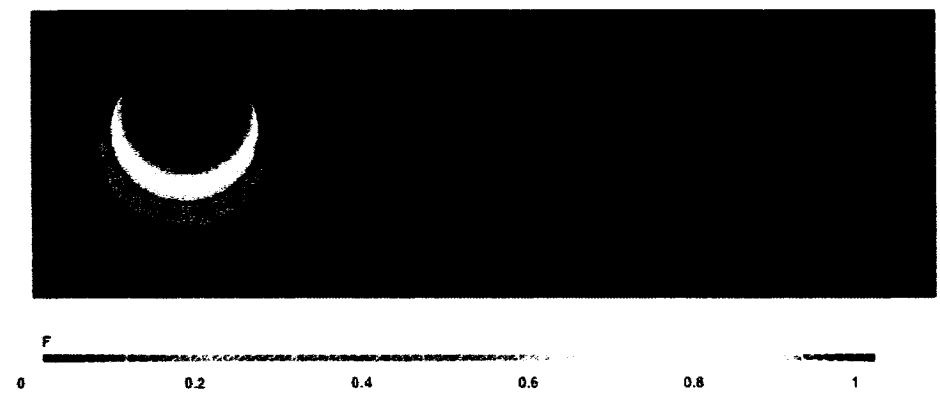

(a) Initial pseudo-concentration

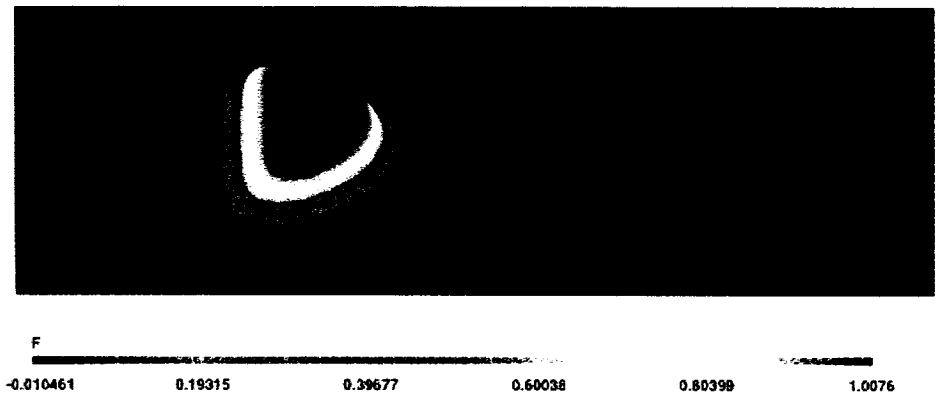

(b) Pseudo-concentration after 25 time steps

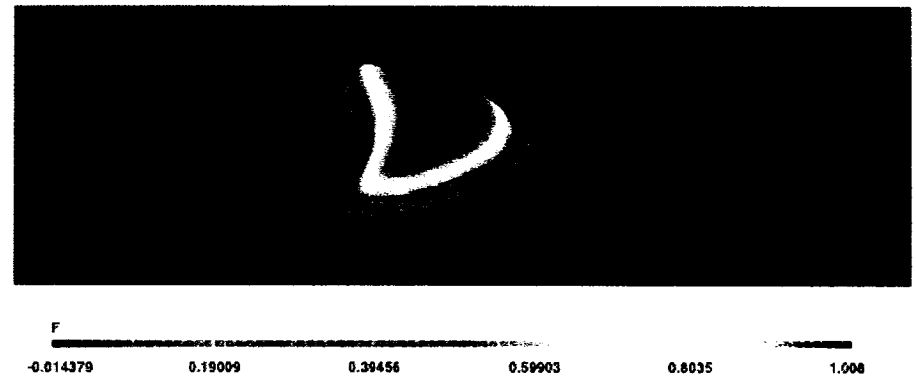

(c) Pseudo-concentration after 50 time steps

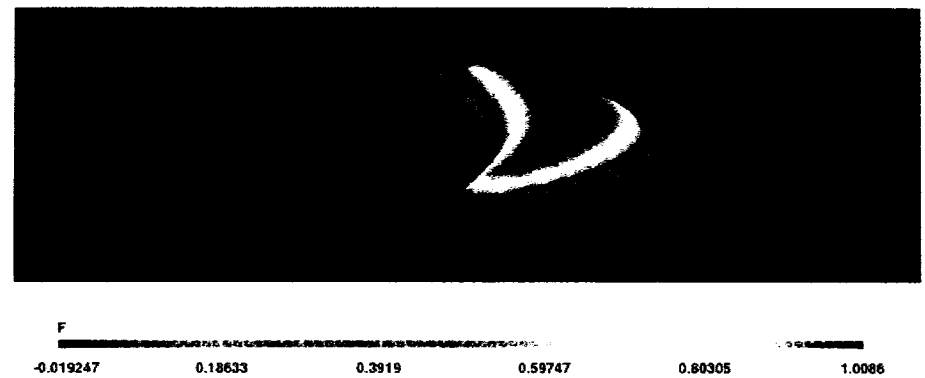

(d) Pseudo-concentration after 75 time steps

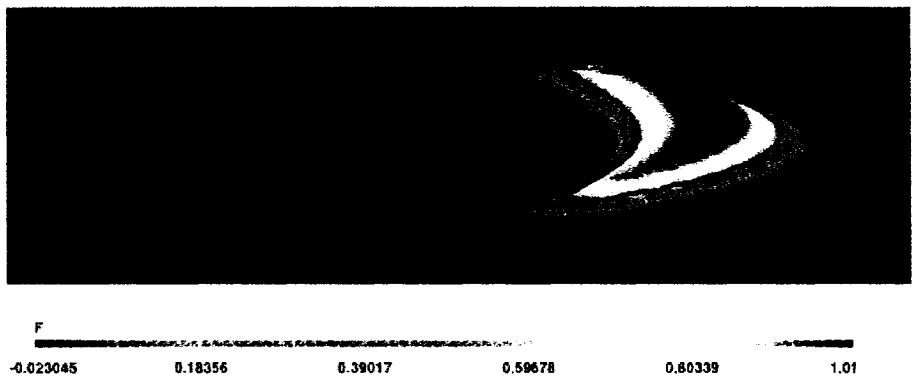

(e) Pseudo-concentration after 100 time steps

Figure 6.8 Transport of the pseudo-concentration function of a viscoelastic drop in a Newtonian matrix

As it is shown in figure 6.8, the pseudo-concentration function is transported by the velocity field. The deformation of the pseudo-concentration is caused by the Poiseuille velocity profile. Note that no free surface updating technique was used for this problem, in order to focus the study on the advection of the various quantities.

Figure 6.9 shows the τ_{11}, τ_{22} and τ_{12} components of the extra-stress tensor, after 100 time steps, with $\Delta t = 0{,}02$.

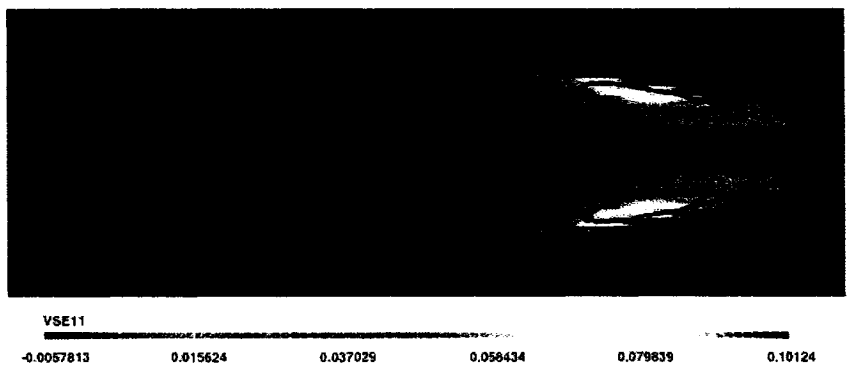

(a) τ_{11} component

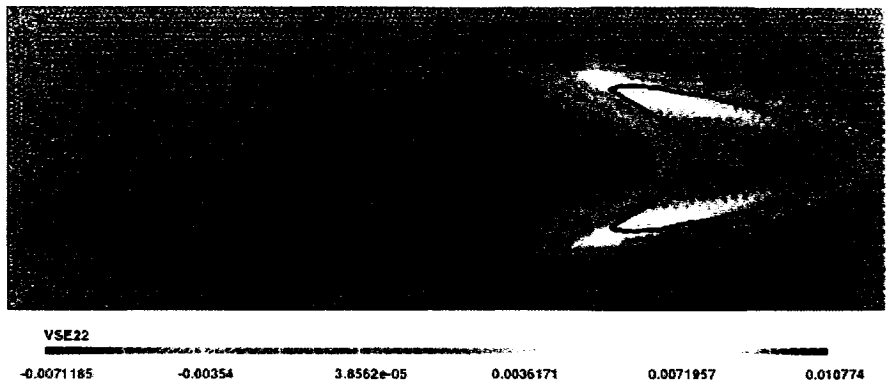

(b) τ_{22} component

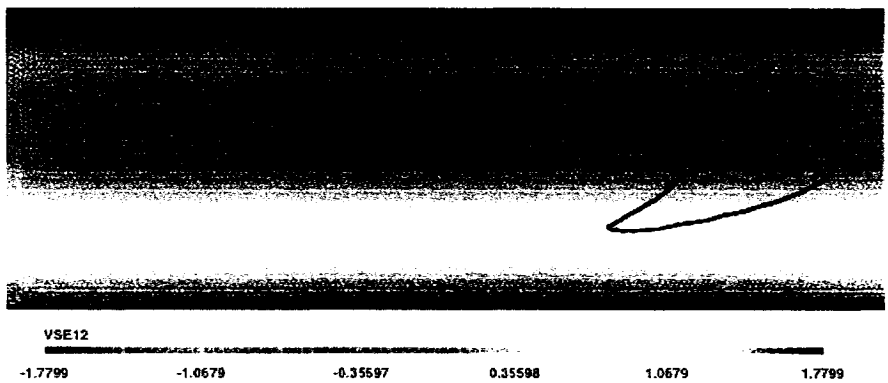

c) τ_{12} component

Figure 6.9 Extra-stress components for the transport of a viscoelastic drop in a Newtonian matrix after 100 time steps.

The results illustrated in figure 6.9 are in accordance with the analytical solution for the extra-stress tensor (cf. equation 6.1). Figure 6.9(a) shows the τ_{11} component, which is equal to 0 for the Newtonian matrix ($\lambda = 0$). This component, inside of the drop, is equal to 0 in the middle of the channel. When y has its maximum and minimum values, the τ_{11} component is maximum, which agrees with the analytical solution. Figure 6.9(b) shows that the τ_{22} component is almost 0 everywhere, for the matrix and the drop. Figure

6.9(c) illustrates that the τ_{12} component is maximum at the bottom, and minimum at the top of the domain and it is equal to zero when $y = 1$, which agrees with the fact that this component is a linear function of y.

CHAPTER 7

VALIDATION OF THE NUMERICAL MODEL

The validation of the numerical modeling of transient viscoelastic multifluid flow problems are presented in this chapter. Results are shown for two different validation problems. The first problem is the deformation of a single viscoelastic drop immersed in a Newtonian fluid in a shear flow. The second problem consists in the study of coalescence of multiple Newtonian drops immersed in a viscoelastic matrix.

7.1 Single Viscoelastic Drop Submitted to a Shear Flow

An initially circular drop of radius r_d is placed at the center of a rectangular geometry and submitted to a shear flow by moving the top and the bottom walls in opposite directions. By studying this problem, we want to see the influence of the capillary number and elasticity on the deformation of the drop. The geometry is illustrated in figure 7.1. Constant velocities are imposed at the top and at the bottom plates, in such a way that the shear rate is constant during the entire computation. The size of the domain is 1 by 1 non-dimensional length units.

The boundary conditions for the Stokes problem on the left, right, top and bottom of the domain are given by:

$$\begin{cases} u = \dfrac{v_{Max} \cdot y}{2}; \\ v = 0. \end{cases}$$

The boundary conditions for the extra-stresses, in Brown et al. mixed formulation, on the left, right, top and bottom of the domain are given by:

$$\begin{cases} \tau_{11} = 2\eta_v \lambda (\frac{v_{Max}}{2})^2 + 2\eta_v \frac{\partial u}{\partial x}; \\ \tau_{22} = 0 + 2\eta_v \frac{\partial v}{\partial y}; \\ \tau_{12} = \eta_v (\frac{v_{Max}}{2}) - \eta_v (\frac{\partial u}{\partial y} + \frac{\partial v}{\partial x}). \end{cases}$$

The initial conditions for the extra-stresses are given by the analytical solution:

$$\begin{cases} \tau_{11} = 2\eta_v \lambda (\frac{\partial u}{\partial y})^2 = 2\eta_v \lambda (\frac{v_{Max}}{2})^2; \\ \tau_{22} = 0; \\ \tau_{12} = \eta_v (\frac{\partial u}{\partial y}) = \eta_v (\frac{v_{Max}}{2}). \end{cases} \quad (7.1)$$

The initial condition for the pseudo-concentration is given by:

$$F(\vec{x}) = \begin{cases} 1 & if \quad \vec{x} \in \Omega_1; \\ 0 & if \quad \vec{x} \in \Omega_2. \end{cases}$$

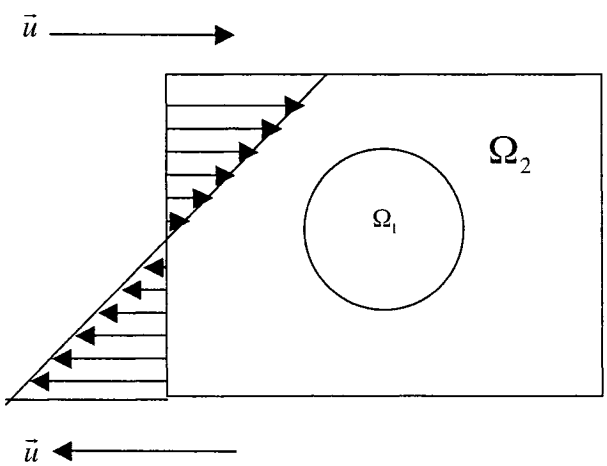

Figure 7.1 Drop in a shear flow: Geometry

7.1.1 Literature Review on the Numerical Modeling of the Deformation of a Single Drop in a Shear Flow

Drop deformation problems have received considerable attention. Taylor [43] provided an analytical solution about the deformation of a drop that is first-order accurate. He described the deformation of a Newtonian drop in another Newtonian fluid, in a shear flow. This theory was later refined and extended to viscous drops surrounded by a viscoelastic fluid, or to the deformation of viscoelastic particles. These studies are limited to small deformations. Sheth et al. [44] considered the deformation of liquid drops submitted to a simple shear flow at finite Reynolds numbers, which implies that the Navier-Stokes equations have been considered. They have shown that inertia effects amplify the deformation and lead to breakups.

It is well known that the balance between viscous and elastic forces inside and outside the drop, and interfacial tension, determine the drop shape. In steady shear flows, it is generally accepted that the viscoelastic drop phase inhibits deformation. When the surrounding fluid is viscoelastic, there are contradicting conclusions in the literature. Yue et al. [46] used numerical simulations and performed a detailed analysis of the underlying physics to clear up the confusion in the literature. They have used a diffuse-interface model for two-phase flows, which deals with the interfacial dynamics and non-Newtonian rheology in a unified framework. The diffuse-interface method is based on the energy formulation, which permits easy incorporation of complex rheology. They have shown that a viscoelastic drop deforms less than a Newtonian drop. When the matrix is viscoelastic, however, the drop deformation is small when the Deborah number is small, but it increases with

the Deborah number. When the drop is viscoelatic and the matrix is Newtonian, the deformation of the drop decreases with an increasing Deborah number.

Drop deformation is characterized by dimensionless numbers. In a two-fluid morphology, the deformation of a single drop immersed in another fluid is controlled by the capillary number, which is defined by:

$$Ca = \frac{\eta_m \cdot \dot{\gamma} \cdot r_d}{\alpha},$$

where η_m is the viscosity of the surrounding fluid, $\dot{\gamma}$ is the shear rate, r_d is the droplet radius, and α is the interfacial tension coefficient. The capillary number expresses the ratio between the viscous force, which tries to deform and break the drop, and the capillary force, which attempts to keep it spherical. Basically, two phenomena may occur. Since interfacial tension tends to resist drop deformation, high interfacial tensions, and therefore a low capillary number, lead to small deformations. In other situations, the interfacial tension may be small which results in a high capillary number. Consequently, when the capillary number becomes large, this leads to large drop deformations and to break-ups. Other common non-dimensional numbers are the viscosity ratio, $s = \frac{\eta_d}{\eta_m}$, and the Deborah number.

7.1.2 A Single Viscoelastic Drop in a Newtonian Fluid

The influence of the capillary number on the deformation of a single viscoelastic drop ($\lambda_d = 0{,}1$) is investigated in this validation problem. An initial circular drop with a radius of $r_d = 0{,}2$ is placed at the center of a

rectangular geometry with dimensions 1 by 1 non-dimensional units. The two fluids have the same viscosities. As a result, the viscosity ratio $\frac{\eta_d}{\eta_m}$ is equal to 1. The shear rate is set to 1. Various capillary numbers lead to different drop deformations. Two different capillary numbers are considered: $Ca = 10$ and $Ca = 0{,}5$. Figure 7.2 shows the mesh, which consists of 13732 elements and 27773 nodes, and the initial shape of the drop.

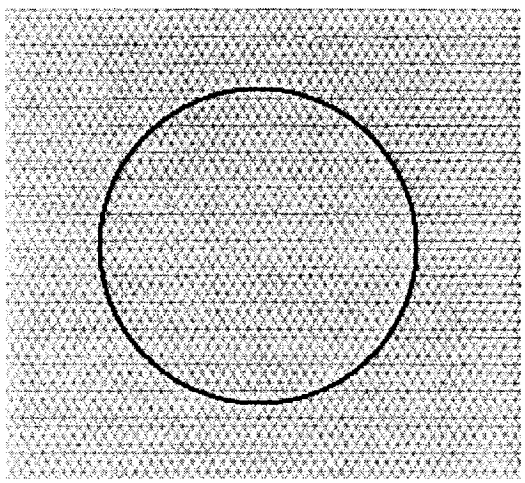

Figure 7.2 Mesh and the initial shape of the drop

Figure 7.3 shows the deformation of the drop after 30 time steps, where the capillary number is set to 10. Figure 7.4 shows the deformation of the same initial drop with $Ca = 0{,}5$.

As it is expected, by decreasing the capillary number, the interfacial tension coefficient increases, which leads to less deformation. Similar results were obtained by Yue et al. [46].

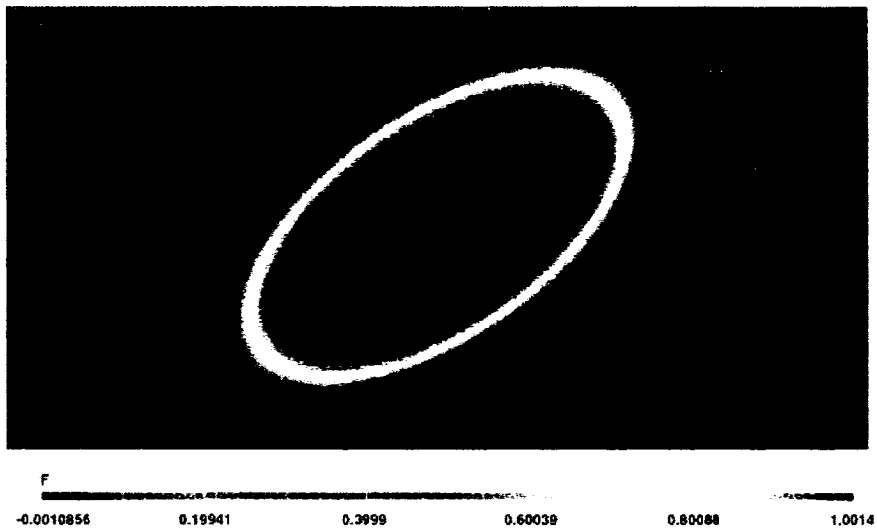

Figure 7.3 Deformation of a single viscoelastic drop in a Newtonian matrix $(Ca = 10)$, after 30 time steps

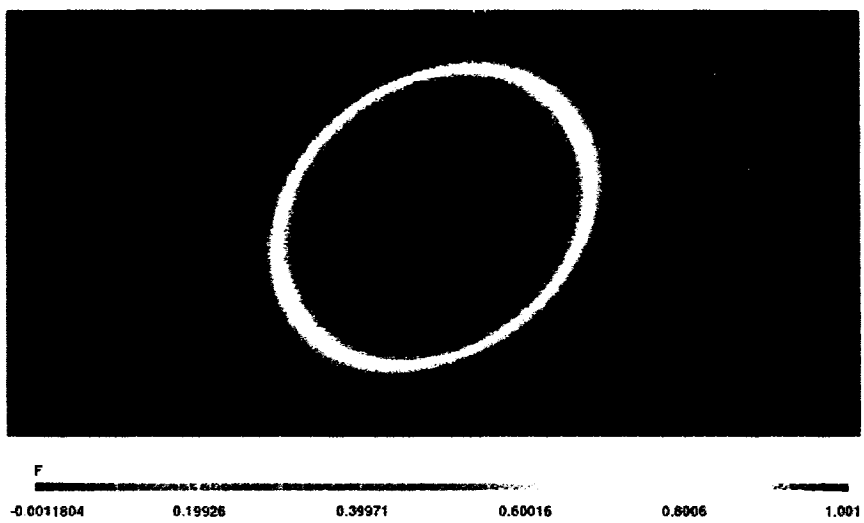

Figure 7.4 Deformation of a single viscoelastic drop in a Newtonian matrix $(Ca = 0{,}5)$, after 30 time steps

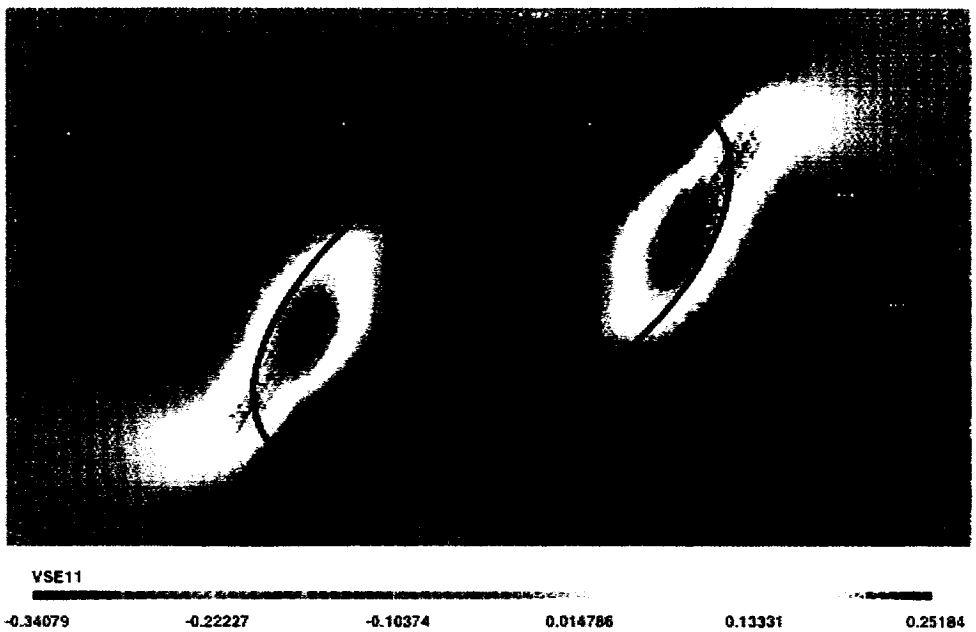

(a) τ_{11} component

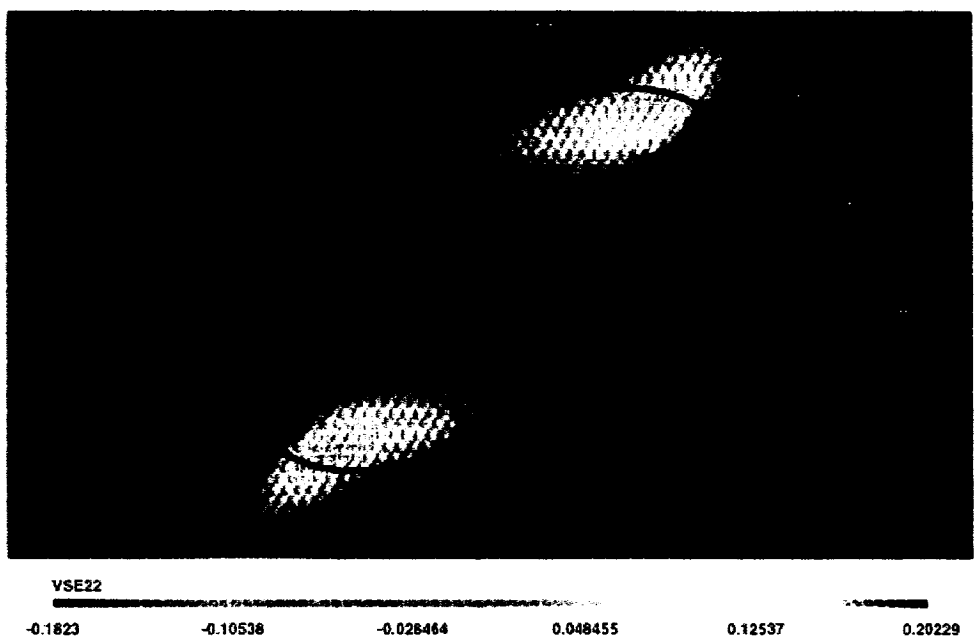

(b) τ_{22} component

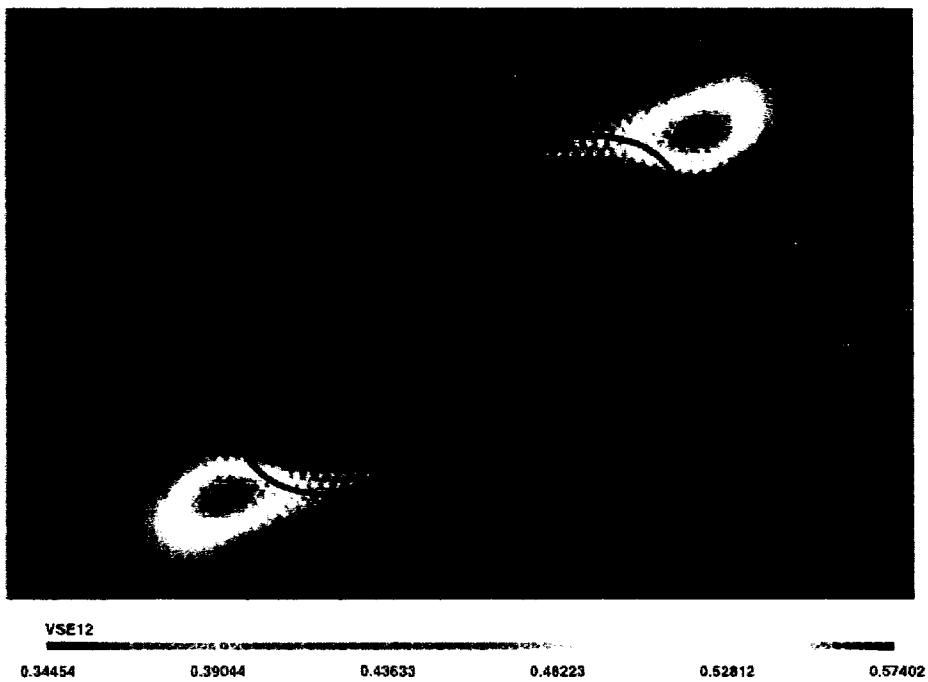

(c) τ_{12} component

Figure 7.5 Extra-stress components of a single viscoelastic drop in a Newtonian matrix with $Ca = 10$ and $\lambda_d = 0{,}1$

Figure 7.5 shows the extra-stress components when $Ca = 10$, with the relaxation time of the viscoelastic drop set to 0,1. Figure 7.6 illustrates the same components for $Ca = 10$ and $\lambda_d = 10$.

It is shown in figure 7.5(a) and 7.6(a) that the τ_{11} component varies considerably when we change λ_d from 0,1 to 10. These results agree with the analytical solution (7.1) as well. Figures 7.5(b) and 7.6(b) show that the τ_{22} component is almost zero. It can be observed in figures 7.5(c) and 7.6(c) that the τ_{12} component is almost the same since λ_d does not have influence this component, which is obvious from the analytical solution (7.1).

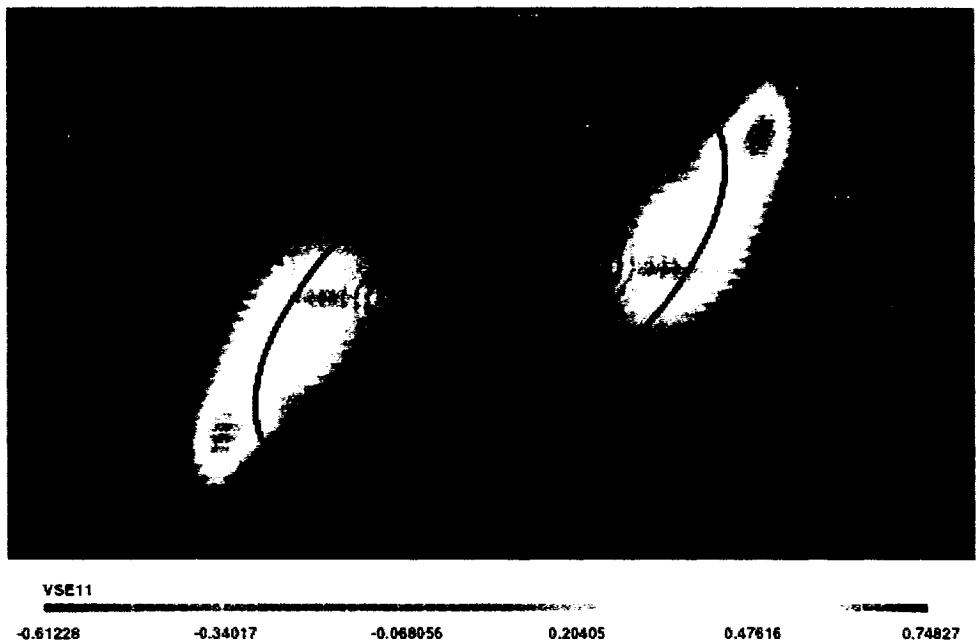

(a) τ_{11} component

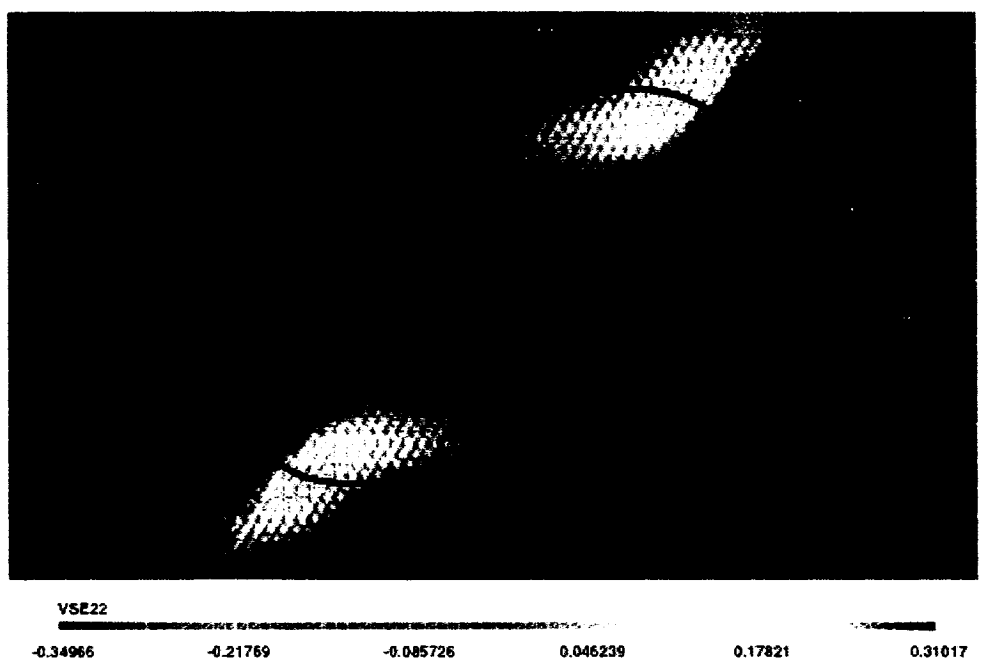

(b) τ_{22} component

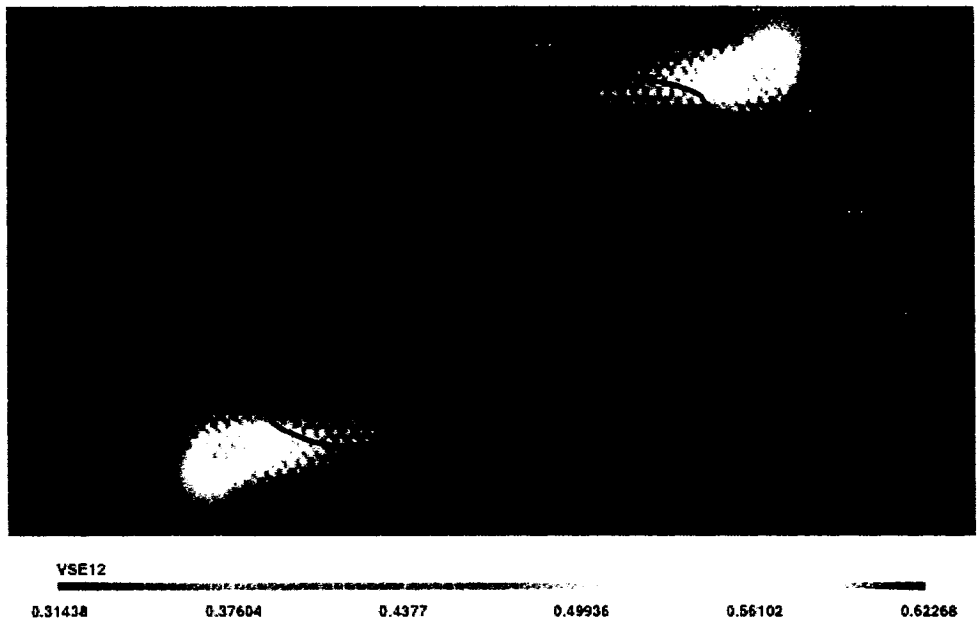

(c) τ_{12} component

Figure 7.6 Extra-stress components of a single viscoelastic drop in a Newtonian matrix with $Ca = 10$ and $\lambda_d = 10$

7.2 Coalescence of a Large Number of Drops in a Shear Flow

Drops dynamics influence the morphology of two-fluid flows such as blends. On the other hand, the rheology component has a significant effect on drops dynamics. An important example is the influence of viscoelasticity on drops deformation in polymer blends [45].

Coalescence is a process in which two or more particles collide and physically merge into one particle. Coalescence in a shear flow can occur in two ways. Collisions between neighboring droplets, due to different relative velocities, or through a head-to-tail interaction, which appears when the

droplets are elongated by a shear flow. We expect that low shear rates coalescence will be dominated by collisions between neighboring droplets on different flow path lines. As the shear rate is increased, the width of the deformed droplets decreases and coalescence can occur by head-to-tail collisions. Coalescence in shear flows is characterized by the applied strain, the viscosity ratio, the concentration of the dispersed phase and interfacial tension. Coalescence can be observed after a shorter period of time for highly concentrated blends.

7.2.1 50/50 Concentration Blend

Coalescence is investigated with a 50/50 blend and a capillary number equal to 1000. Note that for technical reasons, the 50/50 blend is located at the center of the computational domain. The blend consists of Newtonian drops $(\lambda_d = 0)$, immersed in a viscoelastic matrix $(\lambda_m = 0,1)$. The shear rate $\dot{\gamma}$ is equal to 2. The viscosity ratio $s = \frac{\eta_d}{\eta_m}$ is set to 1. The time-step size is equal to 0,02. Figure 7.7 shows the mesh and the initial shapes and distribution of the drops. The mesh consists of 15422 elements in a 3 by 2 non-dimensional length unit domain. In this problem, we use the updating technique explained in section 5.1, which seems to perform better for this problem.

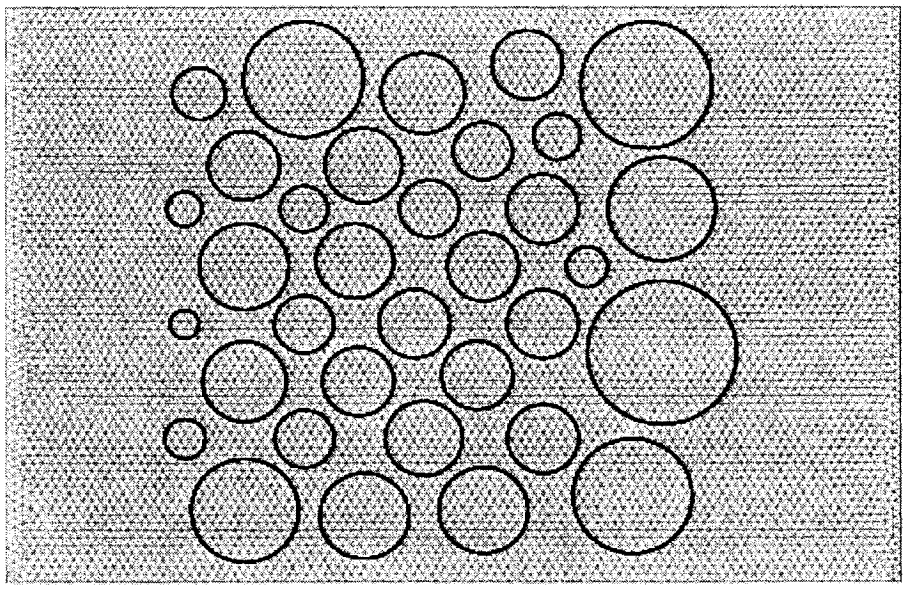

Figure 7.7 Mesh and the initial shape of the drops (50/50 concentration)

We can see that all the particles have an initial circular shape and their radii varies between 0,05 and 0,25. Figure 7.8 illustrates the initial pseudo-concentration associated with this problem.

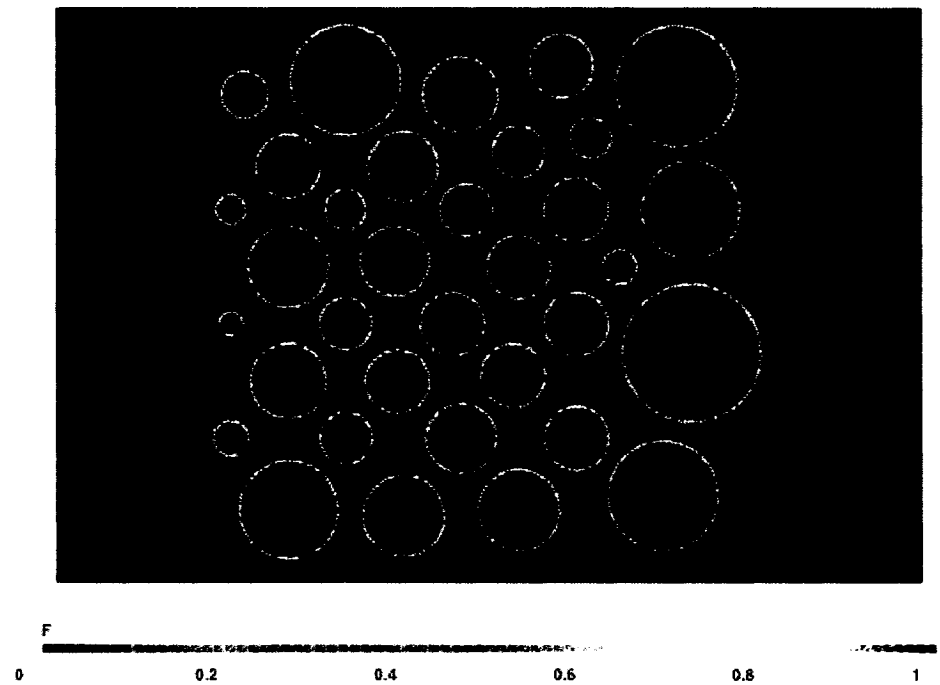

Figure 7.8 Initial pseudo-concentration for the 50/50 concentration problem

Figure 7.9 shows the deformation of the dispersed phase at various time steps. After 10 time steps, the particles change their shape from a circle to an ellipse due to the shear flow. The drops, in different path lines, start to get closer together (cf. 7.9(a)). Figure 7.9(b) shows that some particles start to collide after 20 time steps. Figures 7.9(c) and (d) illustrate that more particles collide and produce larger particles after 30 and 40 time steps. Finally, in the last figure (cf. 7.9(e)), most of the particles collided to produce a co-continuous phase instead of the initial dispersed phase.

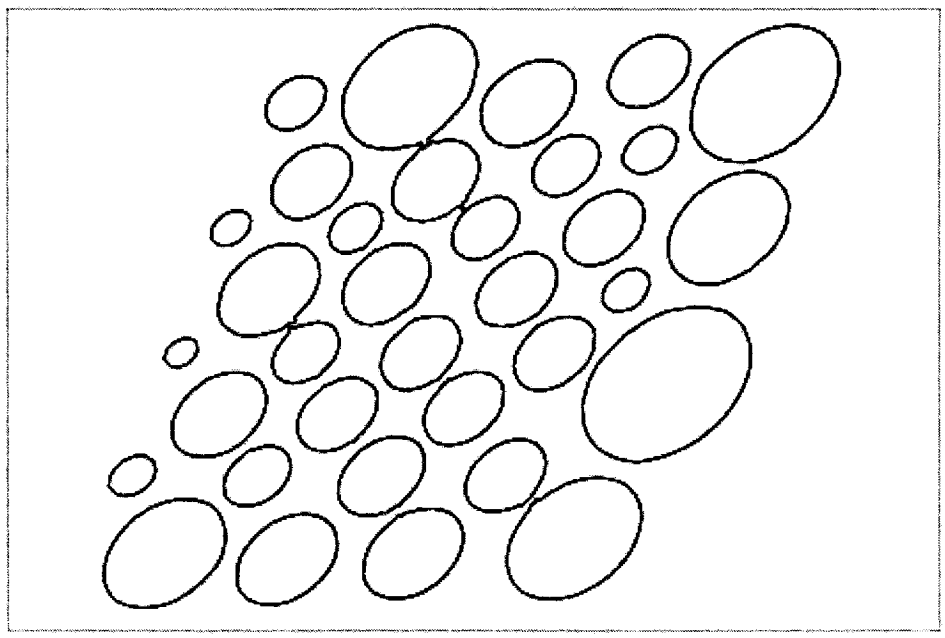

(a) After 10 time steps

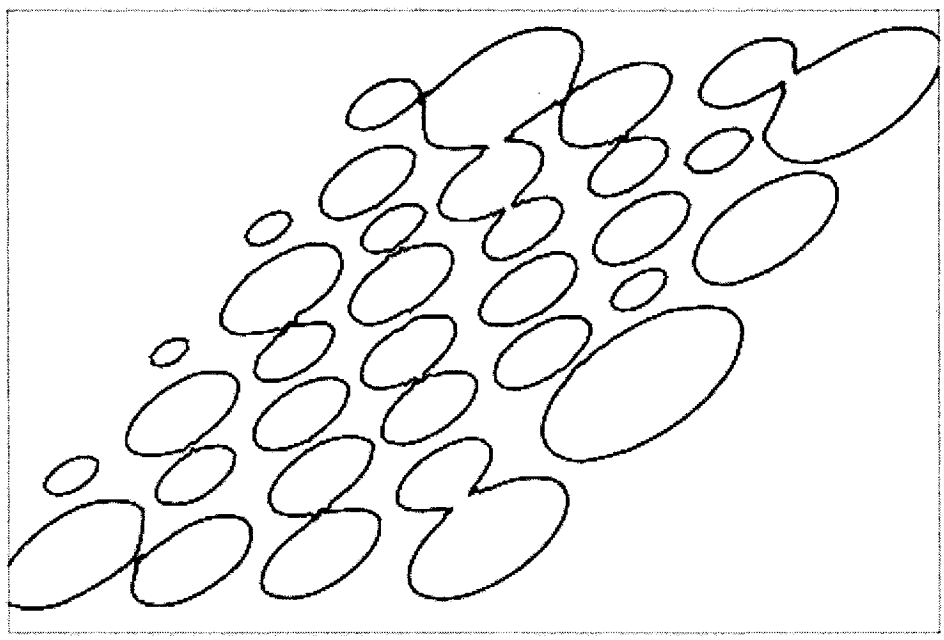

(b) After 20 time steps

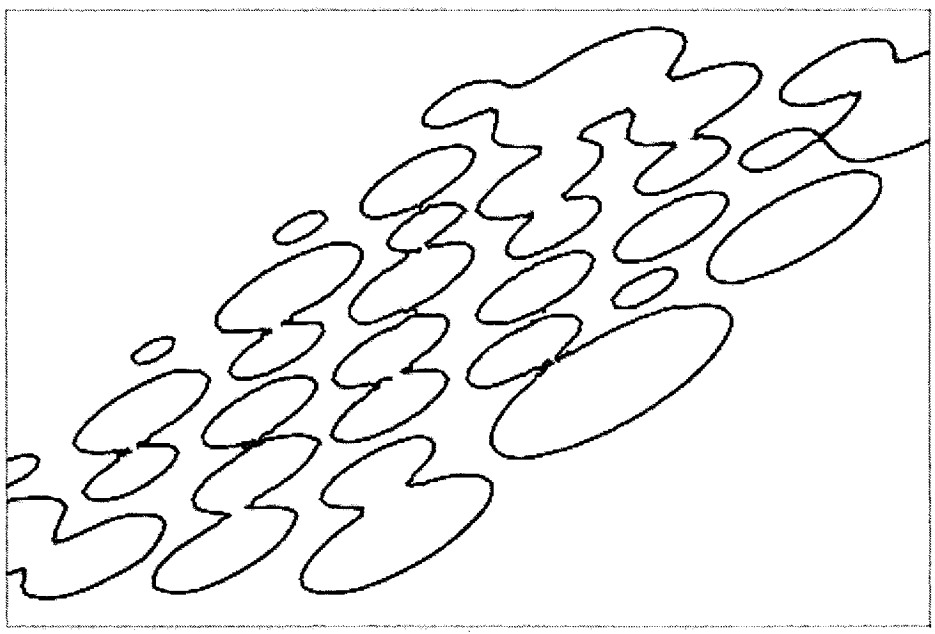

(c) After 30 time steps

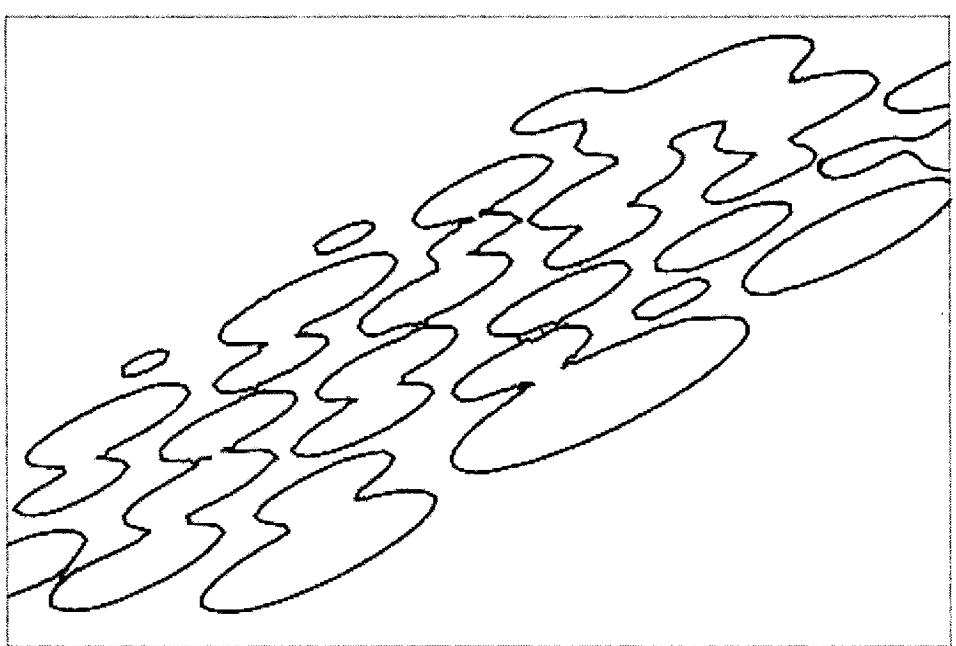

(d) After 40 time steps

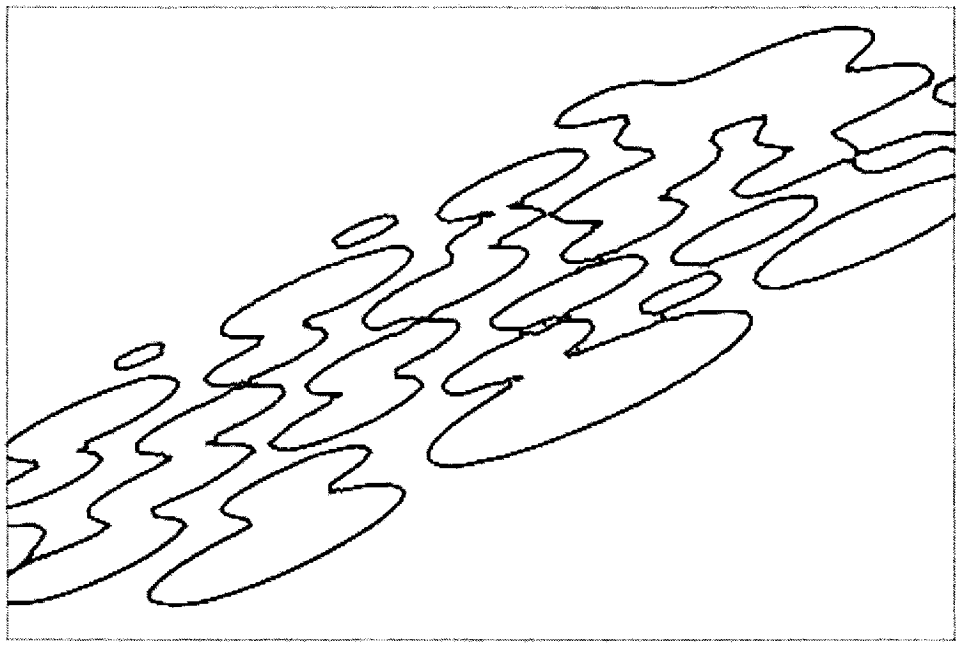

(e) After 45 time steps

Figure 7.9 Deformation of the Newtonian drops in a viscoelastic matrix (50/50 blend), at different time steps

7.2.2 25/75 Concentration Blend

Coalescence is investigated with a 25/75 blend, located at the center of the computational domain, for a capillary number of 1000. The blend consists of 25% of Newtonian drops ($\lambda_d = 0$), immersed in a viscoelastic matrix ($\lambda_m = 0{,}1$). The shear rate $\dot{\gamma}$ is equal to 2. The viscosity ratio $s = \frac{\eta_d}{\eta_m}$ is set to 1. The time-step size is equal to 0,02.

Figure 7.10 shows the mesh and the initial shape of the drops. The mesh consists of 15422 elements in a 3 by 2 non-dimensional length units domain.

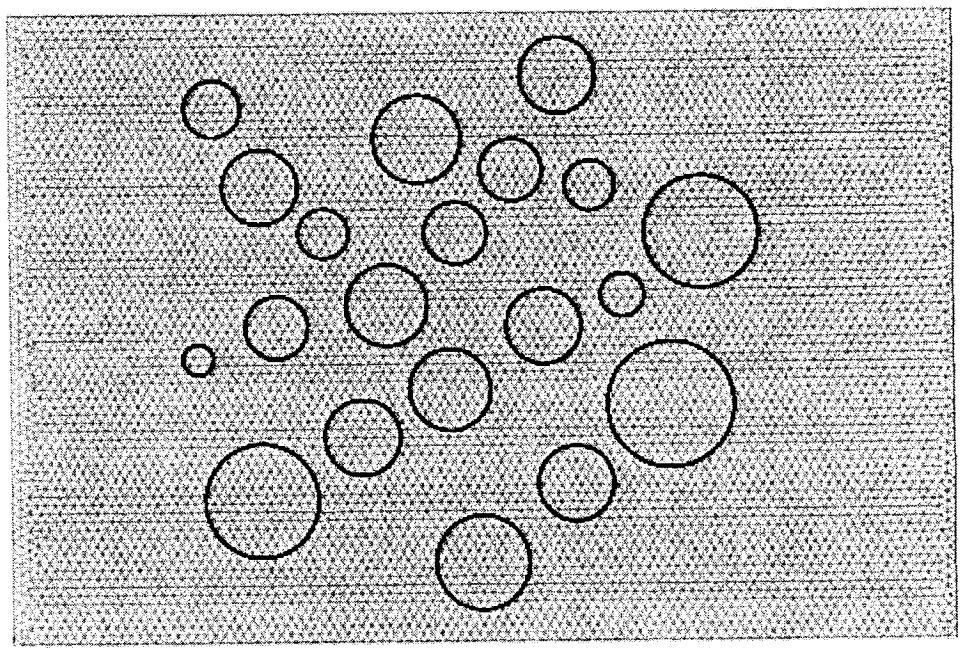

Figure 7.10 Mesh and the initial shape of the drops (25/75 concentration)

We can see that all the particles have an initial circular shape and that their radii varies between 0,05 and 0,20. Figure 7.11 illustrates the initial pseudo-concentration function used to represent the initial state of the problem.

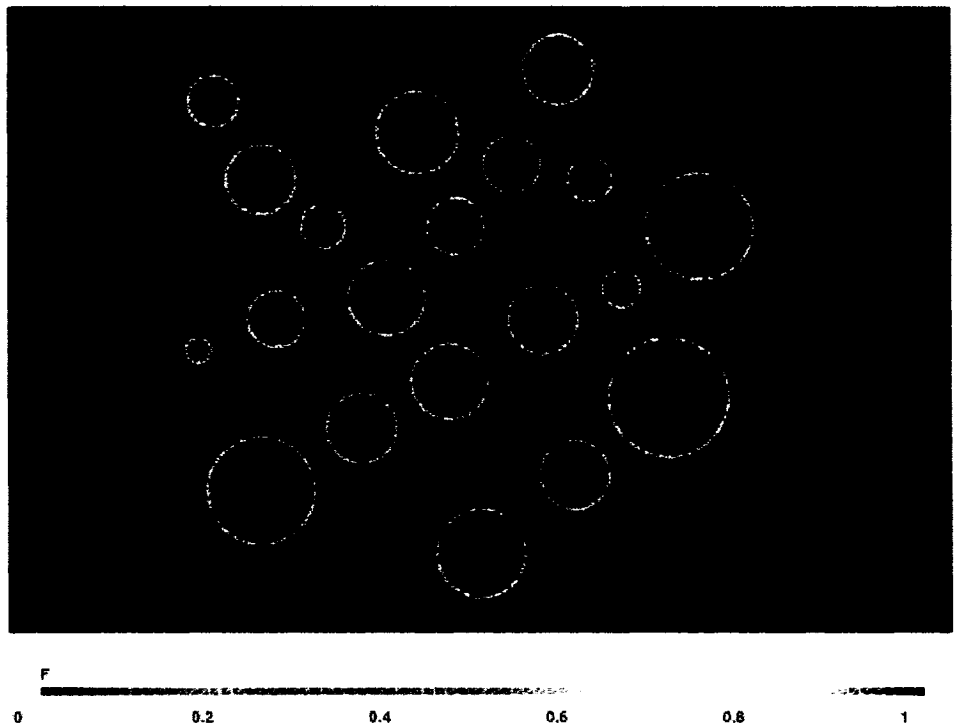

Figure 7.11 Initial pseudo-concentration for the 25/75 concentration problem

Figure 7.12 shows the deformation of the dispersed phase at various time steps. Since the concentration of the dispersed phase is less than for the previous problem, it takes longer for the drops to get closer together and to collide. Figure 6.16(d) illustrates that the drops start to reach together and to collide after 40 time steps, whereas in the highly concentrated 50/50 blend, we saw that this phenomena was observed after 10 time steps.

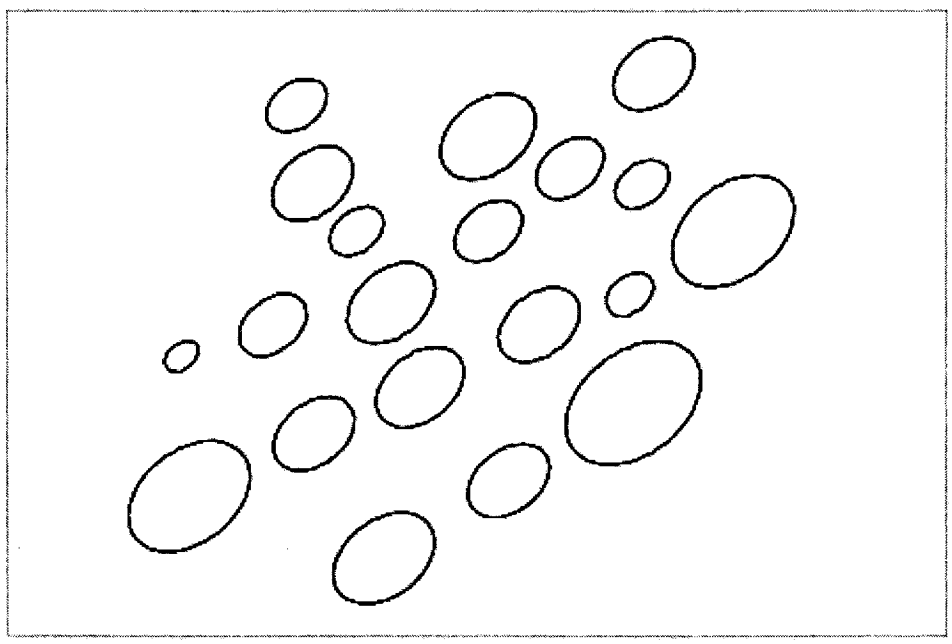

(a) After 10 time steps

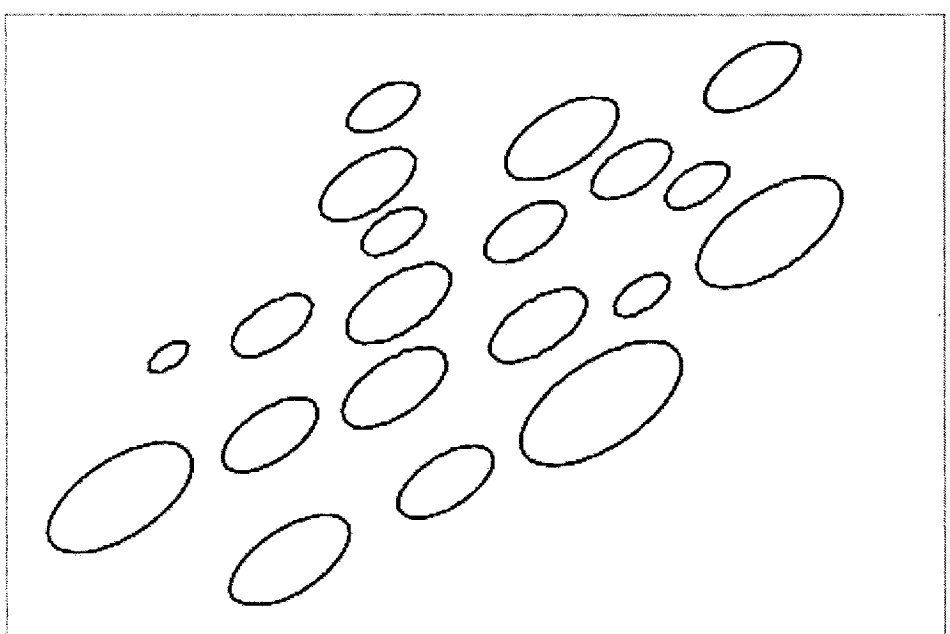

(b) After 20 time steps

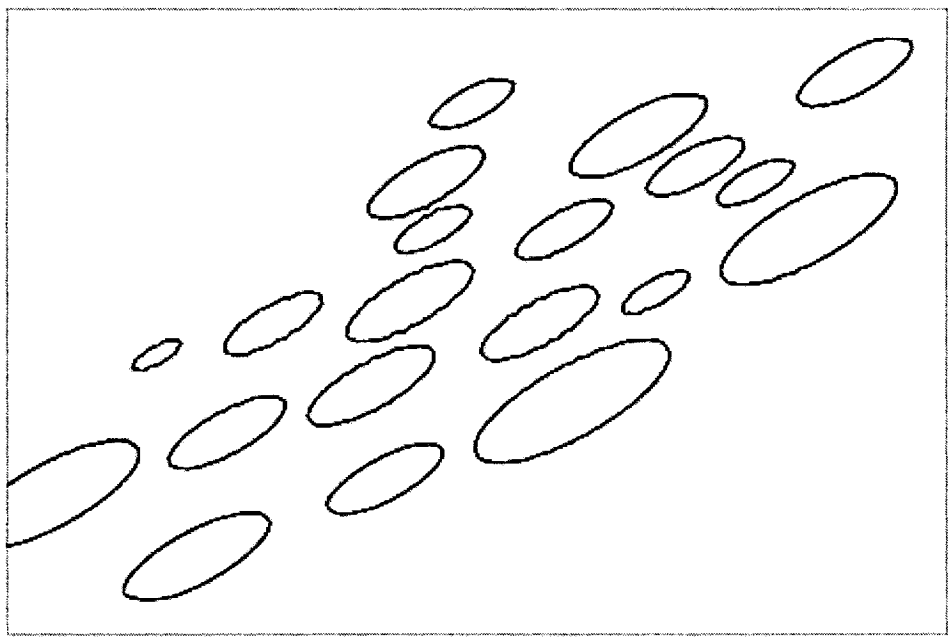

(c) After 30 time steps

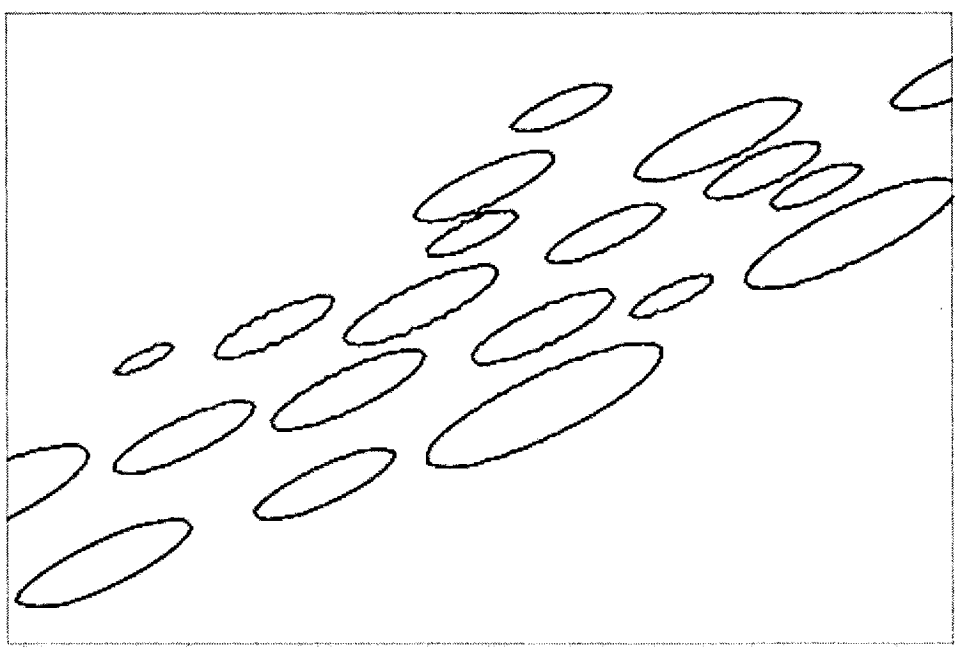

(d) After 40 time steps

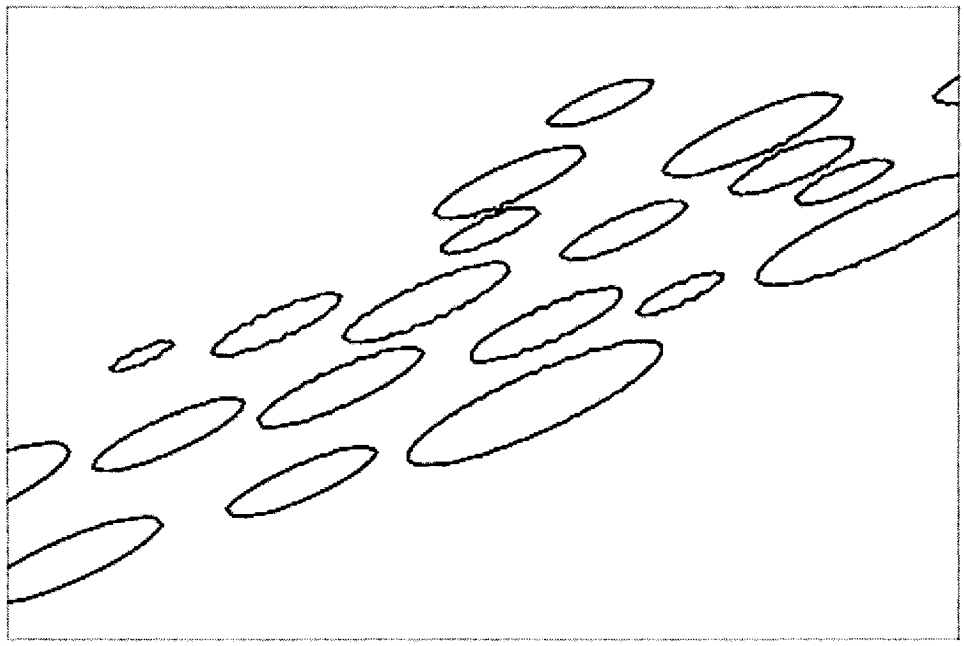

(e) After 45 time steps

Figure 7.12 Deformation of the Newtonian drops in a viscoelastic matrix (25/75 blend), at different time steps

Consequently, more rapid coalescence can be observed for highly concentrated blends. Lyu et al. [47] show experimentally that they can observe more rapid coalescence for highly concentrated blends than with low concentrated ones, which is in agreement with our numerical results. We investigated other factors that would influence the coalescence of the blend, such as the capillary number, the viscosity ratio and the shear rate, to name a few. But the concentration of the blend seems to be the main factor driving coalescence.

CONCLUSION

The *main objective* of this thesis was the numerical modeling of flow-induced morphological changes in immiscible polymer blends. In order to reach this goal, we proposed a transient numerical methodology, in the finite element framework.

The discretization of the conservation equations is performed using the Galerkin method. The transport equation of the pseudo-concentration is discretized using the SUPG method and the Oldroyd-B constitutive equations using the discontinuous Galerkin method.

Interfaces are captured using an Eulerian fixed mesh strategy. It is important to use an updating technique in order to have an accurate discretization of the pseudo-concentration function. Various techniques were studied, such as the local least-squares updating technique [39], the nonlinear absorption term of Layton and Polman [40], the filtering technique of Devals et al. [41] and finally convolution product smoothing [42]. We applied these techniques in order to improve the accuracy of the computed solution, and to eliminate the numerical oscillations and diffusion that are produce by the discretization of the hyperbolic transport equation. These techniques can remove most of the numerical oscillations. We observed that the technique of Devals et al. [41] produces a region of transition that is too sharp for the CSF model. This made us consider using a convolution product smoothing technique. We then observed that with this technique, there is a relationship between the radius of the support of the kernel and the size of the elements of the mesh. If we change the size of the elements, the radius of the support of

the kernel has to be changed in order to get accurate results. It is not clear how this can be determined automatically. In order to understand this relationship, more work has to be done in this area in the future. The approach of Layton and Polman [40] did not produce the expected results. We finally chose the local least-squares updating technique [39]. Even if it is not perfect, it gave us the best results for the problems studied. There is still a need for a local updating technique that performs better. This problem is still open.

Regarding the discretization of the constitutive equations, we focused our attention on the second mixed formulation (Brown et al. [19]). Results were obtained with relatively small values of the Deborah number. As it was mentioned previously (cf. chapter 4), the term $(\vec{u}\cdot\vec{\nabla})\dot{\bar{\bar{\gamma}}}$ must be computed with this formulation, which involves the computation of second order derivatives of the velocity. Therefore, this calculation must be performed with care. One way to circumvent this difficulty is to perform an integration by parts [38]. This can help to increase the values of the Deborah numbers. In order to obtain results with larger Deborah numbers, the Guénette and Fortin mixed formulation [20], could be implemented. We plan to use this formulation in the near future.

Interfacial tension was also included in the numerical model in order to study its influence on the topology of interfaces. Since modeling interfacial tension requires the computing of the derivatives of the pseudo-concentration, in order to obtain the normals and local curvature of the free surface, a sharp but smooth region of transition of the pseudo-concentration is needed. As a result, mesh adaptivity is required in order to perform an accurate modeling of interfacial physics, which will make it possible to use higher values of

interfacial tension in order to investigate its influence on the topology of the interfaces. Also, a better updating technique that reinitializes the pseudo-concentration as a sharp but smooth region of transition is still needed.

This research was verified by studying the Poiseuille flow of a viscoelastic fluid, and the transport of a single viscoelastic drop in a Poiseuille flow. The comparison between the stationary viscoelastic Poiseuille flow problem and the transient viscoelastic Poiseuille flow problem allowed us to verify our time integration schemes for discretizing the transient terms of the Stokes equations, of the transport equation of the pseudo-concentration and of the constitutive equations. The transport of a single drop allowed us to verify the transport of the pseudo-concentration and of the extra-stress components.

This work was validated by studying the deformation of a single drop, and multiple drops, in shear flow. Deformation of a single viscoelastic drop, immersed in a Newtonian fluid under shear flow, was studied. Using two different capillary numbers, we observed that larger values of the capillary number lead to a large deformation for the viscoelastic drop. Since, for this validation problem, we only considered the case where the viscosity of the fluids is equal to 1, the viscous force and the capillary force are of the same order of magnitude. Interfacial tension therefore influences the shape of the drop. Similar results are obtained by Yue et al. [46]. The extra-stress components were studied using two different relaxation times for the drop. We observed that larger values of the relaxation time produce larger extra-stress components in the drop. However, we did not observe a change in the shape of the drop when the viscoelasticity of the drop was modified. This is still under investigation. Finally, coalescence was investigated for two

different concentrations of polymer blends. We observed a larger coalescence rate in highly concentrated blends. Concentration seems to be the main factor driving coalescence rate. These results are in accordance with what is observed by Lyu et al. [47].

BIBLIOGRAPHY

[1] MARTIN, P., CARREAU, P.J., FAVIS, B.D. (2000). "Investigating the morphology/rheology interrelationships in immiscible polymer blends". *J. Rheol.* 44 : 3. 569 – 583.

[2] HOOPER, R., TOOSE, M., MACOSKO, C.W., DERBY, J.J. (2001). "A comparison of boundary element and finite element methods for modelling axisymmetric polymeric drop deformation". *Int. J. Numer. Meth. Fluids.* 37. 837 – 864. (DOI: 10.1002/fld.190)

[3] FAVIS, B.D. (1991). "Polymer alloys and blends: Recent advances". *Can. J. Chem. Eng.* 69 : 3. 619 – 625.

[4] UTRACKI, L.A. and SHI, Z.H. (1992). "Development of polymer blend morphology during compounding in a twin-screw extruder. Part I: Droplet dispersion and coalescence-A review". *Polym. Eng . Sci.* 32. 1824 – 1833.

[5] LACROIX, C., GRMELA, M., CARREAU, P.J. (1999). "Morphological evolution of immiscible polymer blends in simple shear and elongational flows". *J. Non-Newtonian Fluid Mech.* 86. 37 – 59.

[6] RISCANU, D., FAVIS, B.D., FENG, C., MATSUURA, T. (2004). "Thin-film membranes derived from co-continuous polymer blends: preparation and performance". *Polymer.* 45. 5597 – 5609.

[7] LI , J., FAVIS, B.D., (2002). "Strategies to measure and optimize the migration of the interfacial modifier to the interface in immiscible polymer blends". *Polymer.* 43 : 18. 4935 – 3945.

[8] BREZZI, F. (1974). "On the existence, uniqueness and approximation of saddle-point problems arising from Lagrangian multipliers". *R.A.I.R.O.* 8. 129 – 151.

[9] FORTIN, M. and PIERRE, R. (1989). "On the convergence of the mixed method of Crochet and Marchal for viscoelastic flows". *Comp. Methods Appl. Mech. Eng.* 73:3. 341 – 350.

[10] BROOKS, A.N. and HUGHES, T.J.R. (1981). "Streamline upwind /Petrov-Galerkin formulations for convection dominated flows with particular emphasis on the incompressible Navier-Stokes equations". *Comp. Methods Appl. Mech. Eng.* 32 : 1-3. 199 – 259.

[11] MARCHAL, J.M. and CROCHET, M.J. (1987). "A new mixed finite element for calculating viscoelastic flow". *J. Non-Newtonian Fluid Mech.* 26 : 1. 77 – 114.

[12] CROCHET, M.J. and LEGAT, V. (1992). "The consistent streamline-upwind /Petrov-Galerkin method for viscoelastic flow revisited". *J. Non-Newtonian Fluid Mech.* 42 : 3. 283 – 299.

[13] FORTIN, M. and FORTIN, A. (1989). "A New approach for the FEM simulation of viscoelastic flows". *J. Non-Newtonian Fluid Mech.* 32. 295 – 310.

[14] SUN, J., SMITH, M.D., ARMSTRONG, R.C., BROWN, R.A. (1999). "Finite element method for viscoelastic flows based on the discrete adaptive viscoelastic stress splitting and the discontinuous Galerkin method: DAVSS-G/DG". *J. Non-Newtonian Fluid Mech.* 86. 281 – 307.

[15] KING, R.C., APELIAN, M.R., ARMSTRONG, R.C., BROWN, R.A. (1988). "Numerically stable finite element techniques for viscoelastic calculations in smooth and singular geometries". *J. Non-Newtonian Fluid Mech.* 29 : 1-3. 147 – 216.

[16] RAJAGOPALAN, D., ARMSTRONG, R.C., BROWN, R.A. (1990). "Finite element methods for calculation of steady, viscoelastic flow using constitutive equations with a Newtonian viscosity". *J. Non-Newtonian Fluid Mech.* 36. 159 – 192.

[17] CHANG, P.W., PATTEN, T.W., FINLAYSON, B.A. (1979). "Collocation and Galerkin Finite Element Methods for Viscoelastic Fluid flow em dash 1. Description of Method and Problems with Fixed Geometry". *Comp. Fluids.* 7 : 4. 267 – 283.

[18] FORTIN, A., ZINE, A., AGASSANT, J.F. (1992). "Computing viscoelastic fluid flow problems at low cost". *J. Non-Newtonian Fluid Mech.* 45. 209 – 229.

[19] BROWN, R.A., SZADY, M.J., NORTHEY, P.J., ARMSTRONG, R.C. (1993). "On the numerical stability of mixed finite-element methods for viscoelastic flows governed by differential constitutive equations". *Theoret. Comput. Fluid Dynamics.* 5. 77 – 106.

[20] GUÉNETTE, R. and FORTIN, M. (1995). "A new mixed finite element method for computing viscoelastic flows". *J. Non-Newtonian Fluid Mech.* 60. 27 – 52.

[21] LIU, A.W., BORNSIDE, D.E., ARMSTRONG, R.C., BROWN, R.A. (1998). "Viscoelastic flow of polymer solutions around a periodic, linear array of cylinders: comparisons of predictions for microstructure and flow fields". *J. Non-Newtonian Fluid Mech.* 77. 153 – 190.

[22] BÉRAUDO, C., FORTIN, A., COUPEZ, T., DEMAY, Y., VERGNES, B., AGASSANT, J.F. (1998). "A finite element method for computing the flow of multi-mode viscoelastic fluids: comparison with experiments". *J. Non-Newtonian Fluid Mech.* 75. 1 – 23.

[23] LESAINT, P. and RAVIART, P.A. (1974). "On a finite element method for solving the neutron transport equations, in: C. de Boor (Ed.)". *Mathematical Aspects of Finite Elements in Partial Differential Equations.* Academic Press, New York, NY. 89 – 123.

[24] BAAIJENS, F.P.T. (1998). "Mixed finite element methods for viscoelastic flow analysis: a review". *J. Non-Newtonian Fluid Mech.* 79. 361 – 385.

[25] ZINE, A. (1991). *Méthode des Éléments Finis pour la Résolution de Problème d'écoulements de Fluides Viscoélastiques*. 136P. Thèse de Doctorat en Mathématique Appliquées, École Polytechnique de Montréal, Canada

[26] MCLEISH, T.C.B. and LARSON, R.G. (1998). "Molecular constitutive equations for a class of branched polymers: the pom-pom polymer". *J.Rheol.* 42. 81 – 110.

[27] DUFOUR, S. (1999). *Méthodes d'éléments Finis Adaptatives pour les Écoulements Multifluides*.181P. Thèse de Doctorat, École Polytechnique de Montréal, Canada.

[28] DUFOUR, S. and PELLETIER, D.(2001). "Computations of Multiphase Flows with Surface Tension Using an Adaptive Finite Element Method". *Numerical Heat Transfer, Part A* . 40. 335 – 362.

[29] BRACKBILL, J.U., KOTHE, D.B. and ZEMACH, C. (1992). "A continuum Method for Modeling Surface Tension". *J. Comput. Phys.* 100. 335 – 354.

[30] MALIDI, A., DUFOUR, S., N'DRI, D. (2000)."A study of time integration schemes for the numerical modelling of free surface flows". *Int. J. Numer. Meth. Fluids* . 00. 1 – 6.

[31] RAITHBY, G.D. (1976). "Skew upstream differencing schemes for problems involving fluid flow". *Comput. Mthods Appl. Mech. Engrg.* 9. 153 – 164.

[32] HUGHES, T.J.R. and BROOKS, A. (1979). "A multi-dimensional upwind scheme with no crosswind diffusion". *Finite Element Methods for Convection Dominated Flows*, T. J. R. Hughes, ASME, New York, tome 34. 19 – 35.

[33] BARANGER, J. and SANDRI, D. (1991). *C.R. Acad. Sci. ,Série* I. 541 – 544.

[34] SAAD, Y. and SCHULTZ, M.H. (1986). *SIAM J. Sci. Stat. Comput.* 7. 856.

[35] FORTIN, A. and FORTIN, M. (1990). "A preconditioned GMRES Algorithm for the Numerical Solution of Viscoelastic Fluid Flows". *J. Non-Newtonian Fluid Mech.* 36. 277 – 288.

[36] FORTIN, M. and GLOWINSKI, R. (1983). *Résolution Numérique de Problème aux Limites par des Méthodes de Lagrangien Augmenté*, Dunod.

[37] FORTIN, M., FORTIN, A. (1985) "A generalization of Uzawa's algorithm for the solution of the Navier-Stokes equations". *Communications in Applied Numerical Methods.* 1 : 5. 205 – 208.

[38] FORTIN, A. and ZINE, A. (1992). "Improved GMRES method for solving viscoelastic fluid flow problems". *J. Non-Newtonian Fluid Mech.* 42 : 1-2. 1 – 18.

[39] DUFOUR, S. and MALIDI, A. (2000). "A free surface updating methodology for marker function based Eulerian free surface capturing techniques on unstructured meshes". 00. 1 – 10.

[40] LAYTON, W. and POLMAN, B. (1996). "Oscillation absorption finite element methods for convection-diffusion problems". *SIAM J. Sci. Comp.* 17 : 6. 1328 – 1346.

[41] DEVALS, C., HENICHE, M., BERTRAND, F., TANGUY, P.A. and HAYES, R.E. (2004). "A filtering technique for solving the advection equation in two-phase flow problems". *12th Annual Conference of the CFD Society of Canada, Multiphase and Multi-Species Flows II.*

[42] WILLIAMS, M.W., KOTHE, D.B., PUCKETT, E.G. (1998). "Convergence and accuracy of kernel-based continuum surface tension models". *Technical Report LA-UR-98-2268, Los Alamos National Laboratory, Los Alamos, NM.*

[43] TAYLOR, G.I. (1932). "The viscosity of a fluid containing small drops of another fluid". *Proceedings of the Royal Society, A138.* 41 – 48.

[44] SHETH, K.S. and POZRIKIDIS, C. (1995). "Effects of inertia on the deformation of liquid drops in simple shear flow". *Computers & fluids.* 24 : 2. 101 – 119.

[45] TUCKER, C.L. and MOLDENAERS, P. (2002). "Microstructural evolution in polymer blends". *Annu. Rev. Fluid Mech.* 34. 177 – 210.

[46] YUE, P., FENG, J.J., LIU, C. and SHEN, J. (2005). "Viscoelastic effects on drop deformation in steady shear". *J. Fluid Mech.* 540. 427 – 437.

[47] LYU, S.P., BATES, F.S. and MACOSKO, C.W. (2000). "Coalescence in Polymer Blends During Shearing". *American Institute of Chemical Engineers. AIChE Journal.* 46 : 2. 229 – 238.